University of Miami
Scholarly Repository

Open Access Dissertations | Electronic Theses and Dissertations

2018-04-02

Fluorophores in Confined Spaces: From Targeting Molecular Transporters to Encapsulation by Organic Nanocontainers

Anthony Cauley
University of Miami, acauley18@gmail.com

Follow this and additional works at: https://scholarlyrepository.miami.edu/oa_dissertations

Recommended Citation
Cauley, Anthony, "Fluorophores in Confined Spaces: From Targeting Molecular Transporters to Encapsulation by Organic Nanocontainers" (2018). *Open Access Dissertations*. 2023.
https://scholarlyrepository.miami.edu/oa_dissertations/2023

This Open access is brought to you for free and open access by the Electronic Theses and Dissertations at Scholarly Repository. It has been accepted for inclusion in Open Access Dissertations by an authorized administrator of Scholarly Repository. For more information, please contact repository.library@miami.edu.

UNIVERSITY OF MIAMI

FLUOROPHORES IN CONFINED SPACES: FROM TARGETING MOLECULAR TRANSPORTERS TO ENCAPSULATION BY ORGANIC NANOCONTAINERS

By

Anthony Nolan Cauley

A DISSERTATION

Submitted to the Faculty
of the University of Miami
in partial fulfillment of the requirements for
the degree of Doctor of Philosophy

Coral Gables, Florida

May 2018

©2018
Anthony Nolan Cauley
All Rights Reserved

UNIVERSITY OF MIAMI

A dissertation submitted in partial fulfillment of
the requirements for the degree of
Doctor of Philosophy

FLUOROPHORES IN CONFINED SPACES: FROM TARGETING MOLECULAR TRANSPORTERS TO ENCAPSULATION BY ORGANIC NANOCONTAINERS

Anthony Nolan Cauley

Approved:

_____ James N. Wilson, Ph.D. Associate Professor of Chemistry	_____ Françisco M. Raymo, Ph.D. Professor of Chemistry
_____ Marc R. Knecht, Ph.D. Associate Professor of Chemistry	_____ Guillermo Prado, Ph.D. Dean of the Graduate School
_____ Ryan L. Karkkainen, Ph.D. Assistant Professor of Engineering	

CAULEY, ANTHONY NOLAN (Ph.D., Chemistry)
Fluorophores in Confined Spaces: From Targeting Molecular Transporters to Encapsulation by Organic Nanocontainers (May 2018)

Abstract of a dissertation at the University of Miami.

Dissertation supervised by Professor James N. Wilson.
No. of pages in text. (110)

Fluorescence is achieved by emission of electromagnetic radiation in the form of ultraviolet, visible, or infrared photons as a result of an electronic transition from singlet excited state to singlet ground state. Fluorescence spectroscopy is a widely utilized technique for studying the structure and dynamics of matter and living systems. It may come in many forms such as small organic fluorophores taking on a "drug-like" role in biological organisms as well as supramolecular host-guest complexes for applications in drug delivery and cellular imaging. Herein, two research projects at the interface of chemistry and biology will be fully discussed. Although the two ventures have different goals, the overarching theme is confining fluorescent molecules in a tight space, such as a transporter or organic nanoparticle, to enhance the optical properties by restricting motion and limiting solvent accessibility.

First, a series of stilbene derivatives were synthesized and investigated as substrates targeting monoamine transporters (MATs). The sensitivity of these fluorescent probes allows binding-induced fluorescence based on their ability to access a twisted intramolecular charge transfer (TICT) state. The photophysical properties of the dyes were studied in solvents differing in polarity and viscosity to model their response and translate this behavior to a binding event. The lack of specificity to the MAT target lead

to their use as generic cell membrane stains, comparable to that of a commercially available, widely used dye in biological laboratories.

Also, a library of functionalized lignins is reported to demonstrate their utility as nanocontainers for organic dyes in biologically relevant applications. Kraft lignin was modified via S_N2 reaction at the phenolic -OH group utilizing a mild base, potassium carbonate, and various alkyl halides, several bearing additional functionalities, with dimethylsulfoxide as solvent. The resulting phenoxy ethers were characterized by ^{1}H-NMR and IR spectroscopy, as well as DLS and SEM to evaluate their morphology and supramolecular organization. Lignin modified with long-chain hydrocarbon tails was found to effectively encapsulate DiD, a cyanine dye, decrease aggregation, enhance optical transitions, and exert a photoprotective effect. The dye-lignin assemblies were also examined as imaging agents, via confocal microscopy, and found to accumulate intracellularly with no leaching of the dye to hydrophobic subcellular components observed. Lignin functionalized with short chain carboxylic acids interacts with ligands directed at the norepinephrine transporter (NET), suggesting applications in sequestration of neuroactive compounds. Lignin nanocontainers can also be employed in other applications such as coatings for cell culture vessels, ion-sensitive cargo release, energy transfer between guest molecules, and specific drug delivery targeting the biotin transport system. This comprehensive list of applications utilizing lignin proves its worth as a nanomaterial in a biomedical setting.

To My Parents and Future Wife,
The Three Most Important People in My Life

ACKNOWLEDGMENT

First and foremost, I would like to thank my advisor Dr. James N. Wilson for his guidance throughout my graduate studies. His help both inside the lab and being down-to-earth outside have made my experience in graduate school a very enjoyable one. I also express my gratitude to Dr. Massimiliano Lamberto for sparking my interest in chemistry as an undergraduate at Monmouth University. Without his encouragement, I would have never pursued a higher degree in chemistry.

In addition, I would like to thank the members of my committee; Dr. Françisco M. Raymo, Dr. Marc R. Knecht, and Dr. Ryan L. Karkkainen for attending all of my qualifying exams and providing assistance and ideas pertaining to my projects. I would also like to thank the staff in the Department of Chemistry at the University of Miami for all of their help throughout my years in graduate school.

Thank you to my past group members, Dr. Demar R.G. Pitter and Dr. Jyothi Dhuguru, for helping me get started in the lab as well as my current labmates, Wesley Cunningham and Heajin Lee. I've been fortunate enough to work with very talented undergraduate students including Rachel Johnson, Irene Manning, Yuija Zhou, Grace Jean, and Izabela Sartori. I know they will all go on to be successful in either graduate or medical school.

Finally, I would like to thank my family and friends. My parents, Toni and Kevin, as well as my grandparents, Bud and Paula, have given me unwavering support and I cannot express how grateful I truly am. My fiancée, Samantha, supported me moving away to pursue my dream and has put up with long periods apart and traveling to spend time together. I cannot thank you enough. My friends, both old and new, were an integral part of me completing my studies. Thank you to all!

TABLE OF CONTENTS

Page

LIST OF FIGURES AND SCHEMES

slightly, there are conserved functional groups such as phenolic and aliphatic hydroxyl, methoxy, carbonyl, carboxylic, and cyclic ether substituents. (31)

Figure 3.4. Lignocellulosic biomass, such as wood and other dry plant matter, enters the pulping process to separate the components of the plant cell wall. Cellulose, a strong crystalline polymer, is used for paper production. Hemicellulose, made up of random sugars and more susceptible to hydrolysis, is used as an additive or feed stock. Lignin was once considered a waste material but is now used in synthesis of valuable materials. The lignin isolation process influences the final products, categorized as either sulfur or sulfur-free, both differing in structure and physical properties. (32)

Scheme 3.1. Reactions intended to further conjugate the lignin backbone or form fluorescent moieties were carried out revealing the low reactivity of the crowded aromatic rings. (From top, clockwise) Knoevenagel condensation, Pechmman condensation, alkylation, halogenation, oxidative cross coupling, and Friedel-Crafts acylation. (35)

Scheme 3.2. Bimolecular substitution reactions at the phenolic -OH position using an excess of alkyl halide, K_2CO_3 as a base, DMSO to solubilize all reaction components, and moderate heating allows for appending a diverse set of functional groups to the lignin backbone. (36)

Figure 3.5. ^{1}H-NMR of **L-Bu**, **L-HA**, and **L-PTMA** shows changes from the spectrum of unmodified lignin. Alkylation of the phenolic -OH groups produces three noticeable changes a) the addition of new methylene groups is apparent in the aliphatic region for longer alkyl chains. b) Expansion of the aromatic region reveals the appearance of a shoulder corresponding to the Ar-H of the newly formed phenyl ethers. c) The downfield

dye. In water, however, the complexes are very stable and do not show any dye release into the organic layer. This can be seen in the absorbance of the aqueous layer as it decreases in PBS but is consistent in H_2O (b). (59)

Figure 4.7. Multiple fluorescent cargo can be encapsulated within one modified lignin nanocontainer. The interaction can be followed by looking at the FRET between guest molecules. a) Binary mixture of DiO and DiI can be excited at 3 different wavelengths and show the same emission, regardless of the excitation wavelength. The same results can be seen when using two dyes that have a bathochromic shift in absorbance and emission, as with the DiI/DiD binary mixture (b). A ternary mixture (c) of fluorescent dyes can also participate in FRET where irrespective of excitation wavelength, the lowest energy emission of the reddest dye is observed. (62)

Figure 4.8. L-PA effectively sequesters a cationic inhibitor of the norepinephrine transporter (NET). a) The fluorescent ligand binds to the membrane bound transporter, b) but the addition of L-PA, at t = 60 s, results in a rapid decrease of the emission intensity as di-ASP^+ is encapsulated and removed from solution. c) Cartoon representation of di-ASP^+ binding to NET and encapsulation by L-PA. (64)

Scheme 4.1. Propargyl groups were appended to kraft lignin using S_N2 reaction conditions previously developed. This introduces a reactive handle for further modification via copper-catalyzed azide-alkyne cycloaddition (CuAAC) “click” chemistry. In this way, biologically relevant ligands can decorate the surface of the macromolecule for targeted delivery. (66)

LIST OF TABLES

LIST OF ABBREVIATIONS

1,1′-dioctadecyl-3,3,3′,3′-tetramethylindodicarbo-cyanine perchlorate (DiD C18 Cy5)

4-(4-(dimethylamino)-styryl)-N-methylpyridinium (ASP^+)

4-(4-(dimethylamino)phenyl)-1-methylpyridinium (APP^+)

Absorbance (λ_{max})

Allosteric binding site (S2)

Aluminum trichloride ($AlCl_3$)

Bacterial leucine transporter (LeuT)

Benzyl-modified lignin (L-Bn)

Bimolecular substitution reactions (S_N2)

Butyl-modified lignin (L-Bu)

Central nervous system (CNS)

Copper-catalyzed azide-alkyne cycloaddition (CuAAC)

Cyanine dyes (Cy)

Decyl-modified lignin (L-Dec)

Dimethyl formamide (DMF)

Dimethyl sulfoxide (DMSO)

Dopamine (DA)

Dopamine transporter (DAT)

Dynamic light scattering (DLS)

Electron donating group (EDG)

Electron withdrawing group (EWG)

Fluorescence resonance energy transfer (FRET)

Food and Drug Administration (FDA)

Fourier transform infrared spectroscopy (FT-IR)

Hexanoic acid lignin (L-HA)

Human Embryonic Kidney – 293 (HEK293)

Methanol (MeOH)

Michigan Cancer Foundation-7 (MCF7)

Monoamine transporters (MATs)

N,N,N-trimethyl ammonium lignin (L-PTMA)

Near-infrared region (NIR)

Neurotransmitter sodium symporter (NSS)

Norepinephrine (NE)

Norepinephrine transporter (NET)

Octanol/water partition coefficient (K_{ow})

Poly(amido amine) (PAMAM)

Poly(lactic acid) (PLA)

Poly(lactic-co-glycolic acid) (PLGA)

Polysialic acid (PSA)

Potassium carbonate (K_2CO_3)

Propanoic acid lignin (L-PA)

Proton nuclear magnetic resonance (^{1}H-NMR)

Ring-opening polymerization (ROP)

Scanning electron microscopy (SEM)

Self-assembled monolayers (SAMs)

Serotonin (5-HT)

Serotonin transporter (SERT)

Sodium dodecyl sulfate-cetyl trimethylammonium bromide (SDS-CTAB)

Sodium sulfide (Na_2S)

Sodium-dependent multivitamin transporter (SMVT)

Substrate binding site (S1)

Sulfur dioxide (SO_2)

Toluene ($PhCH_3$)

Twisted intramolecular charge transfer state (TICT)

Ultraviolet-visible spectroscopy (UV-vis)

CHAPTER 1

Introduction to Fluorescence Spectroscopy

1.1 Fundamentals in Fluorescence Spectroscopy

Luminescence is achieved by emission of electromagnetic radiation in the form of ultraviolet, visible, or infrared photons as a result of an electronic transition from excited state to ground state. One of the most notable forms of luminescence is fluorescence which is observed when the electronic transition is from the singlet excited state to singlet ground state. Optically exciting a molecule quickly populates the excited state (10^{-15} s) with an electron that is paired by opposite spin to the electron in the ground state. This can be achieved by irradiation with a continuous source of light, in the case of steady-state measurements, or with a pulse, in time-resolved fluorescence. The latter can provide more detailed molecular information however, the former is simple and most commonly used to obtain an emission spectrum. Once in the excited state, there are a number of processes, both radiative and non-radiative, that compete with returning to the ground state and emitting a photon if they take place on a timescale comparable to that of the time the molecule spends in the excited state, referred to as the fluorescence lifetime (τ, 10^{-9} s). Vibrational relaxation (10^{-10}-10^{-12} s) to the lowest vibrational state generates the emissive form of the molecule and accounts for the lower emission energy compared to the excitation energy, or the Stokes shift. Here, there are several de-excitation pathways that can be conveyed through a simple Jablonski diagram (Figure 1.1): internal conversion (transition between 2 electronic states with same spin multiplicity), intersystem crossing (potentially followed by phosphorescence), and fluorescence emission. There are also interactions in the excited state that compete with de-excitation

such as intramolecular charge transfer, conformational change, electron/proton/energy transfer, exciplex/excimer formation, or photochemical transformation. All of these processes make fluorescence a versatile and highly sensitive method that can report information on the microenvironment surrounding the fluorescent probe. It is especially useful when analyzing a biochemical system making fluorescence a widely utilized technique for studying the structure and dynamics of matter and living systems.

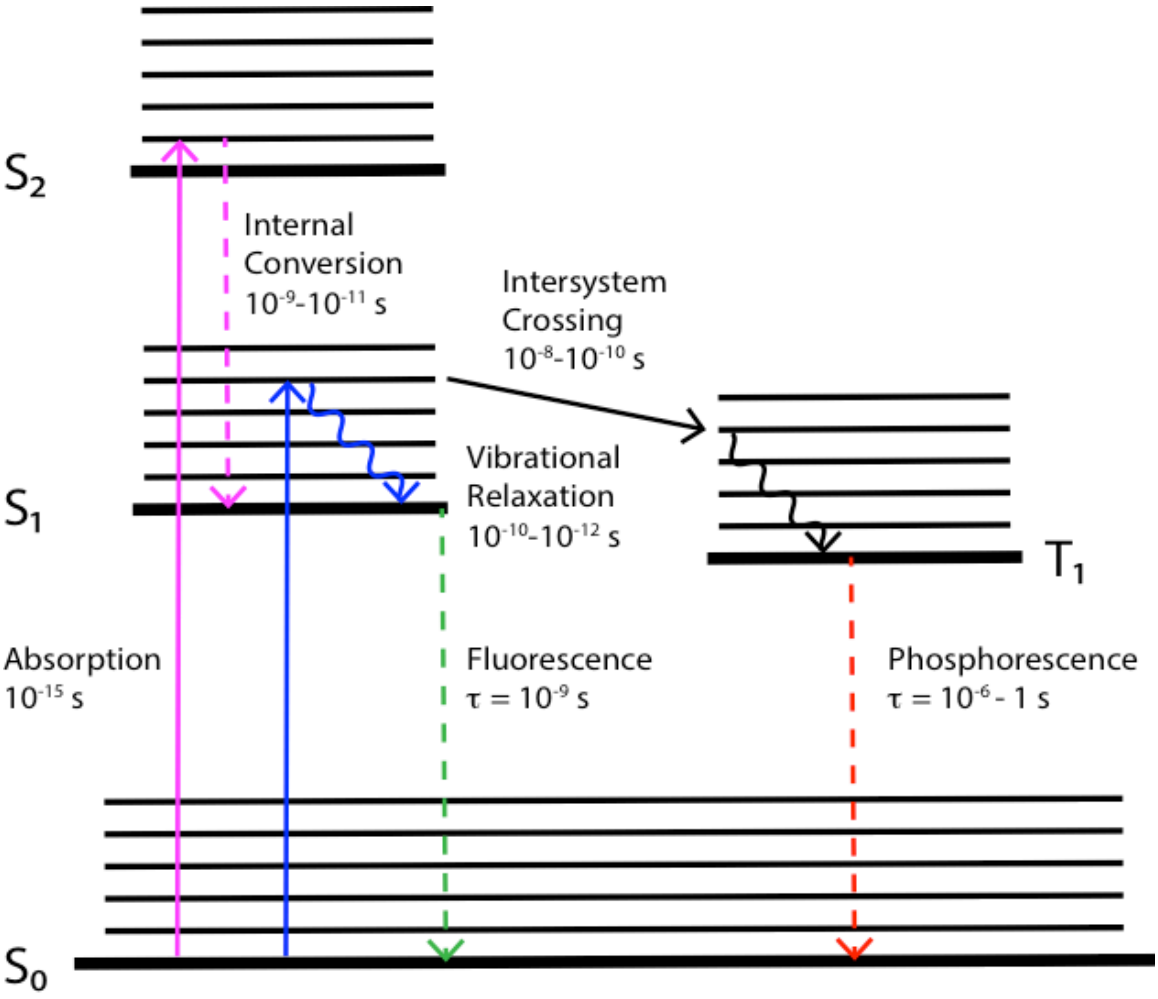

Figure 1.1. A simple Jablonski diagram shows competing de-excitation pathways and the relative time scales. Once promoted, there are many excited state interactions (not shown) that affect the fluorescence emission of a molecule.

Going forward, only essential fluorescence spectroscopy techniques and theory for understanding the scope of this thesis will be discussed. As listed above, there are many features that can be exploited to extract valuable information about a system using fluorescence. Herein, the tools used in studying fluorescent substrates of monoamine transporters and biomaterials for enhancing optical properties and cellular interactions of fluorescent dyes will be highlighted. The interested reader is referred to Valeur's *Molecular Fluorescence: Principles and Applications*[1] and Lakowicz's *Principles of Fluorescence Spectroscopy*[2] for all things fluorescence.

1.2 Steady-State Fluorescence Spectroscopy

The simplest and most popular method for measuring fluorescence is steady-state fluorescence spectroscopy. Excitation of a molecule is carried out by a continuous flow of photons at one energy that can be varied. The wavelength for excitation is typically at the absorbance maximum of the compound and the emission spectrum is recorded using a spectrofluorometer. Almost immediately, the steady-state is attained given the nanosecond timescale of fluorescence. The output gives the energy maximum and intensity of emission which can be influenced by a number of processes. This data is represented by a plot of fluorescence intensity versus wavelength (typically in nanometers) and can be normalized to qualitatively compared two or more fluorophores. Fluorescent molecules are sensitive to environmental parameters including pH, polarity, viscosity, presence of quenchers, and proximity to other molecules. Some of these factors will be discussed in more detail to explain the behavior of the probes used throughout this research. For example, the effect of polarity and viscosity on the intramolecular twisting of a probe plays a role in the "turn-on" properties of fluorescent substrates targeting

monoamine transporters. This can speak volumes to the localization of the probe in a complex environment such as the cell. In this work, steady-state fluorescence is the method of choice used to characterize the probes and complexes.

1.3 "Turn-on" Fluorescent Probes

Fluorescent probes come in many forms and the structural characteristics can be used to choose which fluorophore is best for a given application. Intrinsic fluorophores are fluorescent molecules that are already present in biological samples. These are difficult to utilize because of the high energy needed to excite them resulting in damage to the organism. Extrinsic fluorophores are added to biological samples and their fluorescence intensity, high wavelengths, and low energy can be used to study the system at hand. These can be in the form of fluorescent analogs of biomolecules. Fluorescent analogs take advantage of principles such as twisted intramolecular charge transfer, aggregation-induced emission, and excited-state intramolecular proton transfer to ensure that the fluorophores are "off" when unbound to the biological target and "on" when bound. This makes them excellent tools for highlighting events in the biological system of interest.

Fluorophores have been proven to be invaluable reporters in many chemical and biomedical systems. One criticism is the perturbation of the local environment produced by the probe itself. Examples of this include using pendant labels such as BODIPY, dansyl, coumarin, fluorescein, rhodamine, and 7-nitrobenzyl-2-oxa-1,3-diazole (NBD). To avoid this, a strategy can be employed to generate fluorescent mimics of substrates and ligands. Normally, natural substrates lack the properties needed to be useful in spectroscopy and modifications are needed to tune their properties. Preserving function is of utmost importance and can be done by maintaining the size, shape, and other

characteristics of nature's equivalent. If these strict qualifications are met, the term "probe" is acceptable but must not be confused with any fluorescent molecule, rather, a design that has the ability and sensitivity to report on a biologically relevant event with minimal disruption.[3]

1.4 Summary: Fluorescent Strategies Employed in Targeting Molecular Transporters and Encapsulation by Organic Nanocontainers

In this work, the following photochemical strategies were used and are explained in more detail in each of the corresponding sections. It is important for the reader to have a fundamental understand of the mechanisms involved to follow the flow and rationalization in each research project. First, twisted intramolecular charge transfer (TICT) was used in Chapter 2 – Fluorescent Substrates of Monoamine Transporters. These molecules, often referred to as molecular rotors, undergo a twisting motion in the excited state. At this point, the molecule can emit from the singlet excited state or twisted state (Figure 1.2). The energy gaps in these states are drastically different and emission from the twisted state has a characteristic red-shift or quenching of emission.[4] Molecular design and environmental effects of this mechanism can be found in Chapter 2, Sections 2.2 and 2.3. Next, molecular association through aggregation can quench the fluorescence emission of a molecule. This can be observed with cyanine dyes forming H-aggregates in aqueous solution as detailed in Chapter 4, Section 4.2. Finally, the mechanism involved in fluorescence resonance energy transfer (FRET), with chromophores in close proximity exchanging energy in the excited state, is described in full in Chapter 4, Section 4.6. Given the vast information in the field of fluorescence spectroscopy, this work is just a small glimpse into the phenomenon that is fluorescence. Hopefully, by the end, the reader

is convinced that fluorescence spectroscopy is a powerful tool for studying systems in bio-organic chemistry.

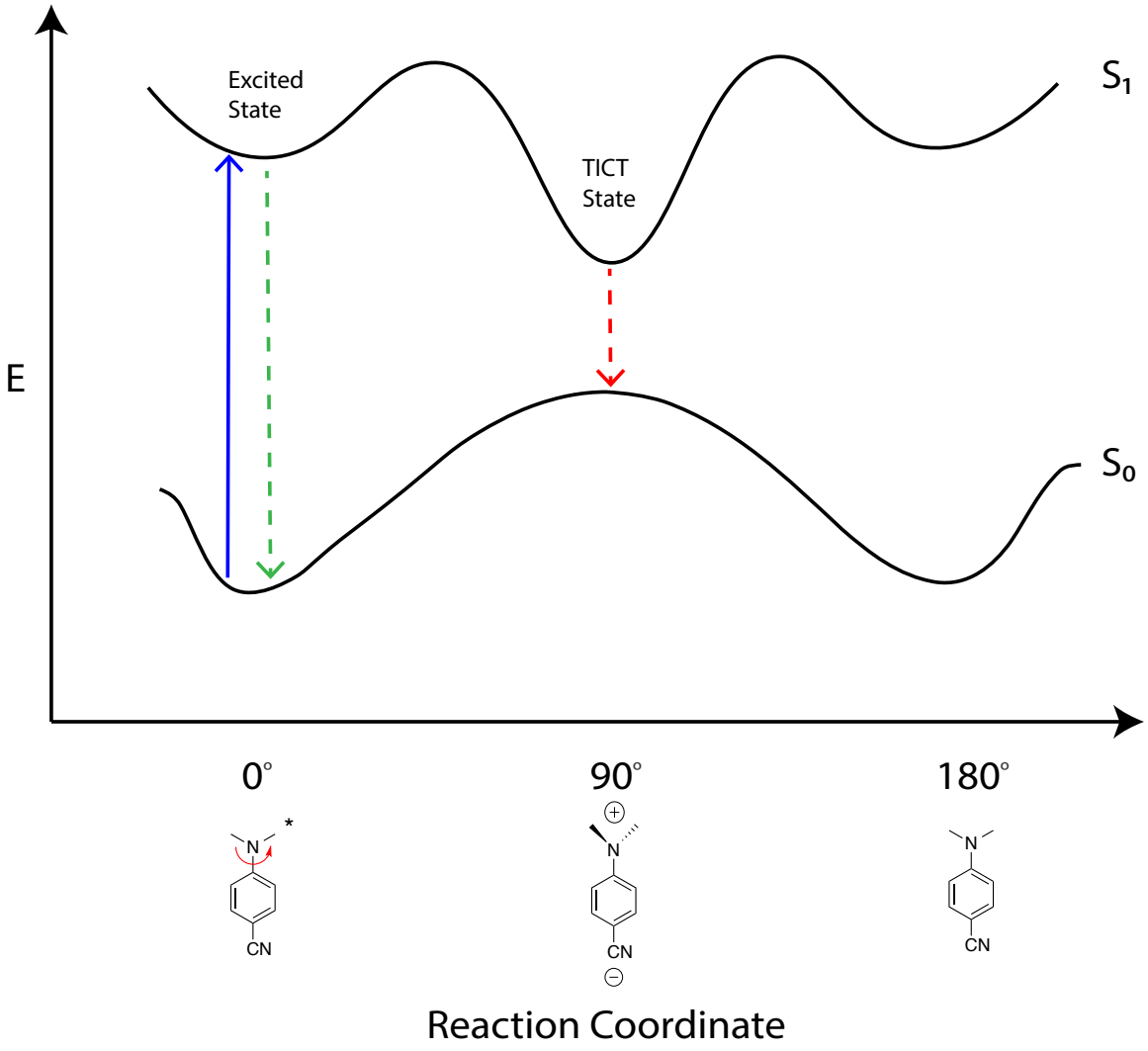

Figure 1.2. Potential energy diagram showing ground state and excited state energies of the planar and twisted configurations of a twisted intramolecular charge transfer (TICT) molecule, 4-(N,N-dimethylamino)benzonitrile (DMABN). Absorbing a photon elevates the molecule to the excited state where the angle of intramolecular rotation is zero. From there, the molecule can return to the ground state, emitting fluorescence, or twist to 90° accessing the TICT state. This intramolecular rotation drastically changes the energy gap, giving a lower energy emission or quenching of emission. As the molecule continues to rotate, it will once again reach the planar state (180°) and fluorescence emission is observed.

CHAPTER 2

Fluorescent Substrates of Monoamine Transporters

2.1 Overview: Structure and Function of Monoamine Transporters

Neurotransmitters are chemical messengers that play an important role in molding everyday life and function. They are simply categorized into three classes: amino acids, peptides, and monoamines. For monoamines, there are three main contributors including serotonin (5-HT), dopamine (DA), and norepinephrine (NE). Each of these are synthesized from readily available precursors, such as amino acids, and do not require a large number of biosynthetic steps for full conversion. After transformation, these biomolecules are distributed to nearly every part of the brain. They are released into the synaptic cleft between neurons (Figure 2.1) and travel to activate their respective receptors, setting off a cascade of events and inducing a specific response. Serotonin regulates appetite, sleep, mood, and behavior linked to the central nervous system (CNS). Norepinephrine is also related to the CNS, where it governs sleep patterns and alertness. Dopamine controls motor behavior such as pleasure and motivation, playing a critical role in the reward system. Though the main function is altering neurological processes, neurotransmitters affect the peripheral nervous system as well. Their influence over vital signs such as blood pressure and heart rate can lead to severe cardiac complications. The major role these signaling molecules play in the overall well-being of the human body make them a promising target to develop pertinent tools for new drug discovery.

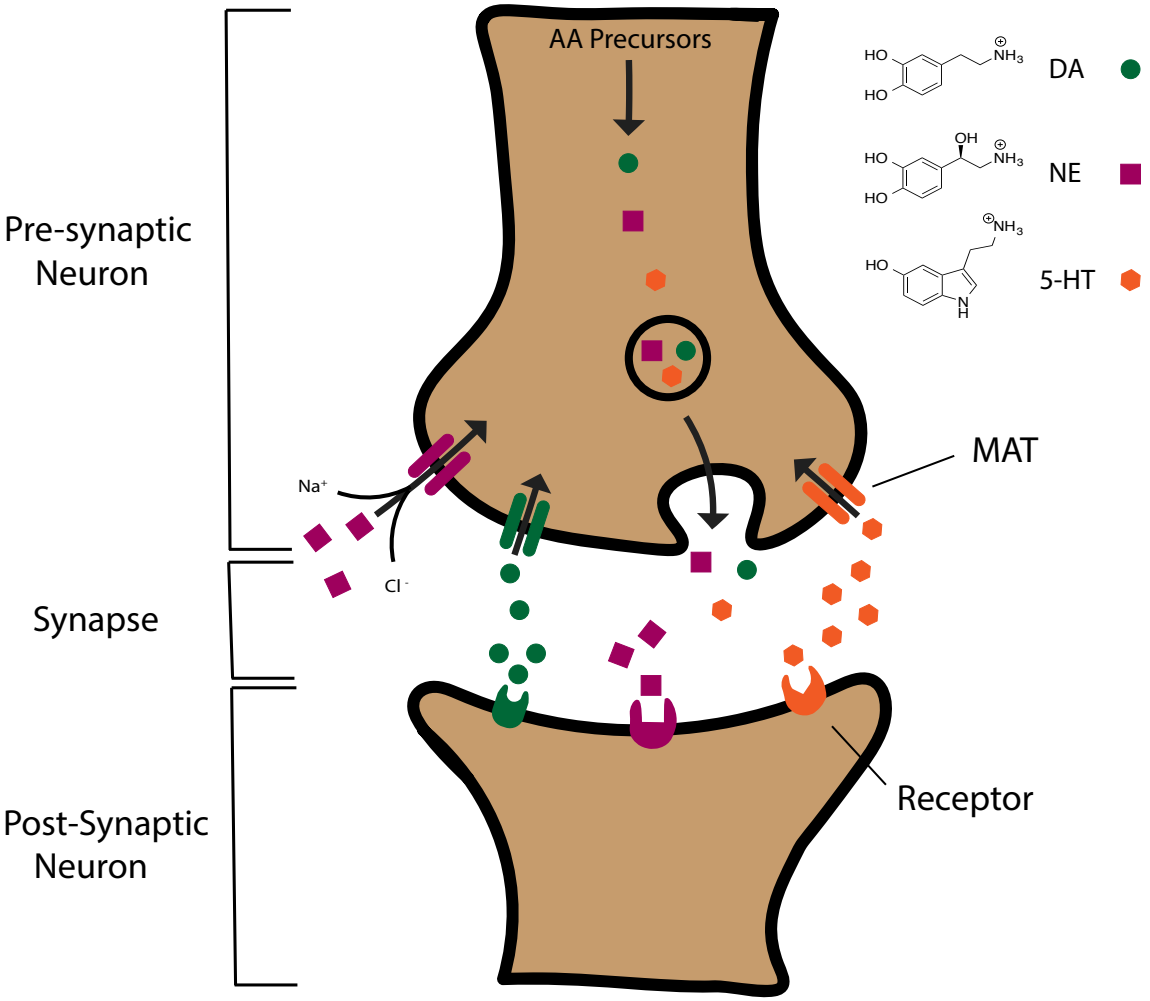

Figure 2.1. Neurotransmitters are biosynthesized from readily available precursors and released into the synapse via exocytosis by neurons. Once in the synapse, the concentration is regulated by reuptake into the presynaptic neuron carried out by MATs. The remaining neurotransmitters will bind and activate receptors on the postsynaptic neuron leading to a functional response.

Nature provides specificity and selectivity to allow neurotransmitters to recognize minuet differences between targets with similar functions. Release of monoamines into the presynaptic cleft is carried out by neurons and the concentration is then regulated by monoamine transporters (MATs), a subclass of the neurotransmitter sodium symporter (NSS) family of transporters. This sodium- and chlorine-dependent reuptake halts signaling of biogenic amines in the synapses. Each monoamine has its own transporter

including serotonin (SERT), dopamine (DAT), and norepinephrine (NET) transporters. These transporters have been targets of drugs of abuse, antidepressants or selective reuptake inhibitors, and tricyclic antidepressants. Traditionally, the function of MATs has been modeled after the bacterial leucine transporter (LeuT), with a sequence identity of approximately 20%, owing to the lack of knowledge on the exact structure of the transporters.[5] Recently, the first x-ray crystallographic structure of hSERT was reported (Figure 2.2), giving new insight on the structural determinants, allosteric mechanism, and important characteristics of human transporters.[6]

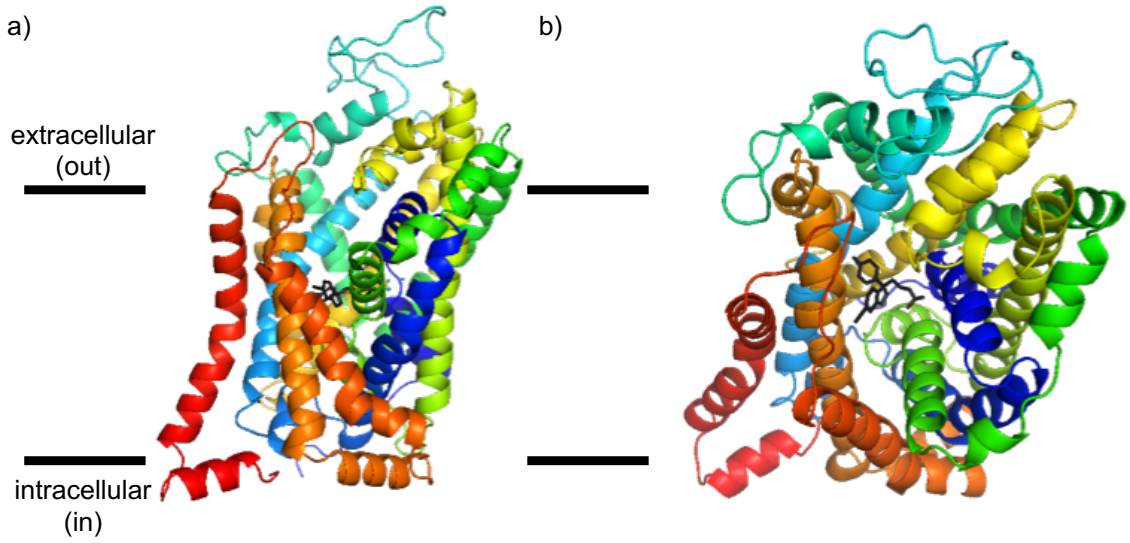

Figure 2.2. The x-ray crystal structure of human SERT bound to the antidepressant (S)-citalopram (PDB: 5I71) contains 12 transmembrane helices with both central and allosteric binding sites. The binding of the drug to the central site locks the transporter in the outward-open conformation, opening the allosteric binding site, and hindering ligand unbinding from the central site. This structure provides the mechanism of action for antidepressants towards hSERT. a) Structure of hSERT viewed parallel to the plasma membrane. b) View into the binding pocket from the extracellular side of the transporter.

Across the series, the transporters are made up of 12 transmembrane-spanning helices with 2 subunits, TM1-TM5 and TM6-TM10, related by a pseudo-two-fold axis. Within

the transporter, there are two ligand binding pockets. The substrate binding site (S1) is located centrally, about halfway across the membrane wedged between five helices. Upon substrate binding, the outward-open conformation is induced opening a second allosteric binding site (S2) in the extracellular vestibule that is oriented towards the aqueous, extracellular space. This provides a pathway for substrates, ions, and inhibitors to access the central binding site protected by a "gate" of amino acid residues. The extracellular vestibule contains both polar and nonpolar residues providing a low affinity binding site for small molecule inhibitors. This may explain the differences in selectivity of the natural substrates for their respective transporters and drugs of abuse, i.e. cocaine, which has similar binding affinities for all three MATs.[7]

Attempts have been made to study MAT function using immuno-histochemical assays[8] and radiolabeled high affinity antagonist displacement.[9] Fluorescence has emerged as a competing approach to assess MAT activity[10], distinguish binding and transport[11], visualize neurotransmitter release[12], and study binding and uptake kinetics.[13] This method relies solely on the availability of *truly* fluorescent substrates. There have been probes developed, along with natural substrates, that provide a starting point for the design of isomorphic inhibitors, incorporating new structural features to give desired photophysical characteristics without the loss of original function. A series of six fluorescent dyes targeting MATs is reported, featuring common structural characteristics of molecules accessing a twisted intramolecular charge transfer state (TICT). The fluorophores were found to have limited selectivity for MATs, however show promise as generic membrane stains for cellular imaging.

2.2 Fluorescent Probes Targeting Monoamine Transporters

Previously, new probe design for studying MAT function was explored in our group, focusing on the environmentally sensitive stilbazolium and 4-phenyl-1-methylpyridinium dyes (Figure 2.3). Differing only by the conjugation length between the aromatic rings, these dyes have been shown to be fluorescent MAT substrates with "turn-on" emission capabilities. "Turn-on" properties are associated with molecules that have weak or quenched fluorescence in bulk solvent, but experienced enhanced emission upon binding to a biomolecular target. Molecular design for such molecules begins with incorporating both an electron withdrawing group (EWG) and an electron donating group (EDG) separated by conjugation of varying length. This scaffold yields a structure that is highly polarized with strong charge-transfer character in the excited state. More polar solvents and environments can stabilize this state giving a bathochromic shift in wavelength to lower energies as well as emission quenching. These molecules also have the ability to twist, leaving the aromatic rings out of planarity and turning the emission of the probe "off". Viscose solvents and confined spaces such as a binding pocket can limit this twisting motion allowing the fluorescent substrates to highlight a binding or displacement event. The "on/off" capacity of these molecules provides a powerful tool for studying the function of MATs and gives potential to develop new fluorescent substrates.

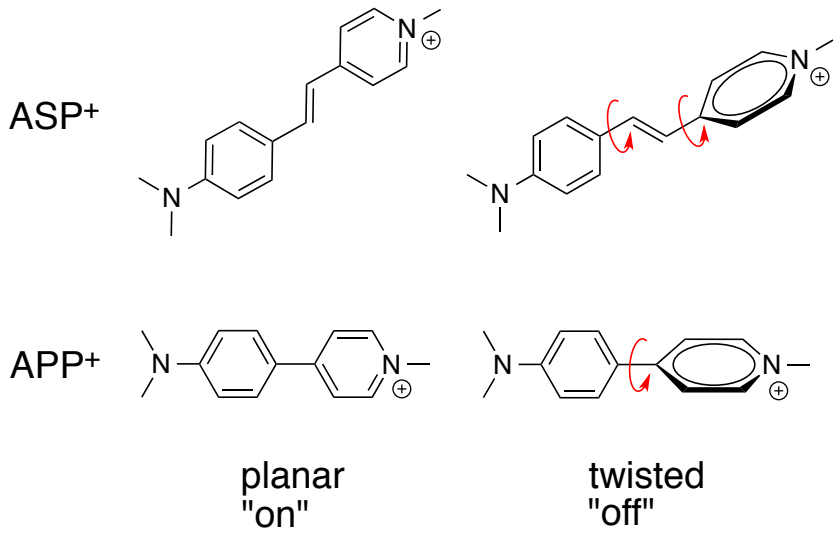

Figure 2.3. Environmentally sensitive fluorescent probes ASP^+ and APP^+ have the ability to twist out of planarity effectively turning the fluorescence emission "off". Preventing the molecule from twisting, either by nonpolar, viscose solvents or confined spaces such as a binding pocket, can switch the emission "on" and report a binding event or change in microenvironment.

One of the early fluorescent molecules, now the gold standard for probing MAT function, is 4-(4-(dimethylamino)-styryl)-N-methylpyridinium (ASP^+). This molecule enables visualization of binding and subsequent displacement in NET.[11] Analogues of ASP^+[14-15] and dimers[16] have been synthesized and were found to be highly selective for NET. Another fluorescent MAT substrate, 4-(4-(dimethylamino)phenyl)-1-methylpyridinium (APP^+), was found to exhibit "turn-on" emission when bound to SERT, but showed no activity towards DAT or NET.[17] These findings allow for differentiation between MATs and give structural insights for new probe design.

Both ASP^+ and APP^+ are modeled after the typical architecture for a molecule that can access a TICT state. They contain a highly electron withdrawing, cationic N-methylpyridinium opposite an electron donating (dimethylamino)phenyl group. The difference between the two is the length of conjugation, with ASP^+ having an addition

alkenyl group separating the aromatic rings. Modifications to the alkyl group appended to the heterocyclic pyridinium, termed the "tail", and diverse anilino substituents, or "head", have generated a library of fluorescent MAT substrates. Using these structural features as a guide, new fluorescent neurotransmitter mimics were developed to expand the archive.

2.3 Stilbene Dyes as Fluorescent MAT Substrates: Design and Synthesis

Design considerations for new fluorescent MAT substrates revealed stilbene and biphenyl dyes as potential lead hit compounds. With similar shape and size, the heterocycle was removed and replaced with a functionalized phenyl ring. Nitro- and cyano- substituents now act as powerful EWGs, replacing the N-methylpyridinium. The neighboring phenyl group contains a N-methyl piperazine moiety, similar to the dimethylamino group in the previous structures. This group not only preserves the "head" first binding mode, but also ensures aqueous solubility. The stilbene derivatives mirror ASP^+, with extended conjugation and potential for specific targeting of NET, while biphenyl products imitate the activity of APP^+ towards SERT.

Two stilbene dyes (**1** and **2**) were synthesized through the Horner-Wadsworth-Emmons reaction (Scheme 2.1) where the phenyl ring bearing the EWG was converted from the benzyl bromide to the diethyl phosphonate by treatment with triethyl phosphite ($P(OEt)_3$). This intermediate was then transformed into the phosphonate anion by sodium hydride (NaH) and reacted with an aldehyde containing the second aromatic ring and the EDG to give the final product in low to moderate yields. The biphenyl dyes (**3** and **4**) were synthesized in one step via a Suzuki coupling (Scheme 2.2). Commercially available 4-(4-methylpiperazin-1-yl)phenyl boronic acid was reacted with *p*-

functionalized bromobenzene under the palladium-catalyzed cross coupling conditions to afford the dyes in low yield.

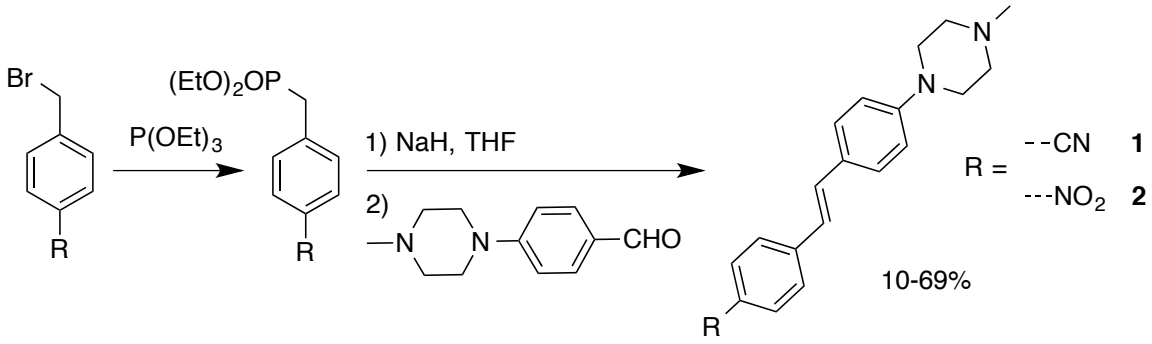

Scheme 2.1. Chemical synthesis of stilbene derivatives **1** and **2**.

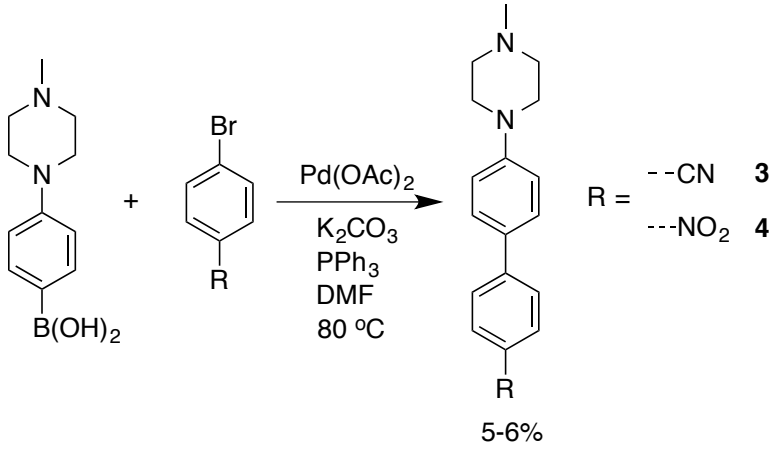

Scheme 2.2. Synthetic route to biphenyl dyes **3** and **4**.

2.4 Optical Properties of Stilbene Dyes

The photophysics of **1** and **2** (Figure 2.4) were studied in both methanol (MeOH) and toluene ($PhCH_3$). Solvents were chosen keeping in mind the hypothesis that these molecules can access a TICT state. The viscosity and polarity differences in the solvents will provide information about how the substrate will respond to changes in its microenvironment that can translate directly to a binding event. **1** exhibited a S_0-S_1 transition in MeOH, centered at 357 nm (ε = 17,310 M^{-1} cm^{-1}), with emission at 511 nm. The spectrum in $PhCH_3$ showed an increase in both absorbance (λ_{max}) at 375 nm, with ε =

32,030 M^{-1} cm^{-1}, and a blue-shifted emission at 454 nm. MeOH is more polar with the ability to stabilize the charge transfer state, giving a bathochromic shift in emission and lower intensity from the loss in energy. In comparison, $PhCH_3$ is less polar, more viscose (0.5520 mPa s vs 0.5445 mPa s), and participates in π-π stacking favoring fluorescence. Compound **2** displayed a λ_{max} = 400 nm with ε = 23,170 and quenched emission. The absorbance in $PhCH_3$ was similar with λ_{max} = 413 nm and ε = 22,350. The fluorescence emission at 555 nm was greatly enhanced in $PhCH_3$ given the destabilization of the twisted form. For both molecules, the increase in fluorescence intensity is expected in $PhCH_3$ following typical TICT behavior. However, the emission profiles in MeOH are intriguing. The lack of fluorescence of **2** in MeOH speaks to the ability of the nitro group to effectively separate charge in the excited state, ultimately producing a more sensitive fluorophore and offering better "turn-on" potential. HEK-293 cells overexpressing NET were treated with **2** and negligible binding was observed.

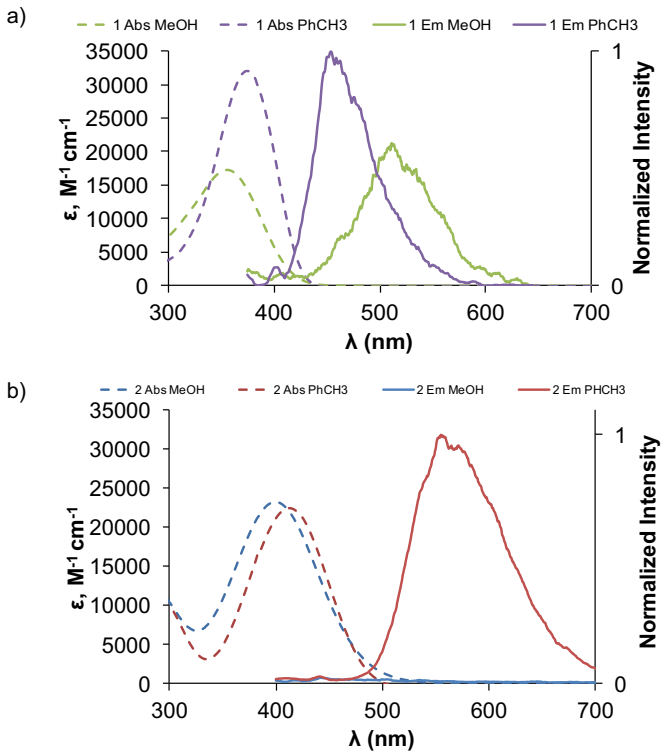

Figure 2.4. Excitation and emission spectra of a) **1** and b) **2** in MeOH and $PhCH_3$ show the effect of polarity and viscosity on fluorescence emission. Emission is enhanced in more viscose, nonpolar solvents that destabilize the twisted state. Polar solvents red-shift (emission from the twisted state) or quench fluorescence, giving desirable "turn-on" properties.

2.5 Re-evaluating Design of Stilbene Derivatives as Fluorescent MAT Substrates

After obtaining the cell imaging results for **1** and **2**, the structural features of the natural and fluorescent MAT substrates were analyzed again. Re-evaluation revealed a common characteristic within the bunch. At physiological pH (7.2-7.4), the three monoamines, 5-HT, DA, and NE, contain a protonated terminal amine group, with pK_as = 10.2[18], 8.9[19], and 8.6[20], respectively. ASP^+ and APP^+ bear a permanent positive charge on the heterocyclic pyridinium ring. Newly developed **1-4** do not contain this same cationic character. The N-methyl piperazine functional group has a pK_a of approximately 8.5-10, giving the potential for protonation at physiological pH, and the stilbene scaffold

does not exhibit a positive charge. With this in mind, **1** and **2** were treated with methyl iodide (MeI) in $PhCH_3$ to further methylate the terminal nitrogen of the piperazine ring, implementing a cationic charge (Scheme 2.3). Again, HEK-293 cells expressing NET were incubated with probe **2m**, showing increased binding but no selectivity. The fluorescence intensity in HEK-NET compared to native HEK cells is approximately the same, as seen in Figure 2.5. Also, when adding desipramine, a tricyclic antidepressant with high affinity for NET, no displacement was observed by loss of fluorescence intensity at the membrane. This is unfortunate for the probe's intended function, however, **2m** shows promise as a cell membrane stain.

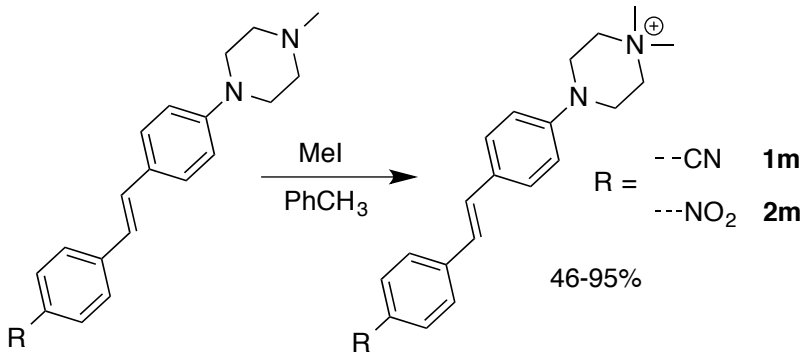

Scheme 2.3. Alkylation of **1** and **2** generate methylated derivatives bearing a permanent positive charge, similar to that of the natural and known substrates of MATs.

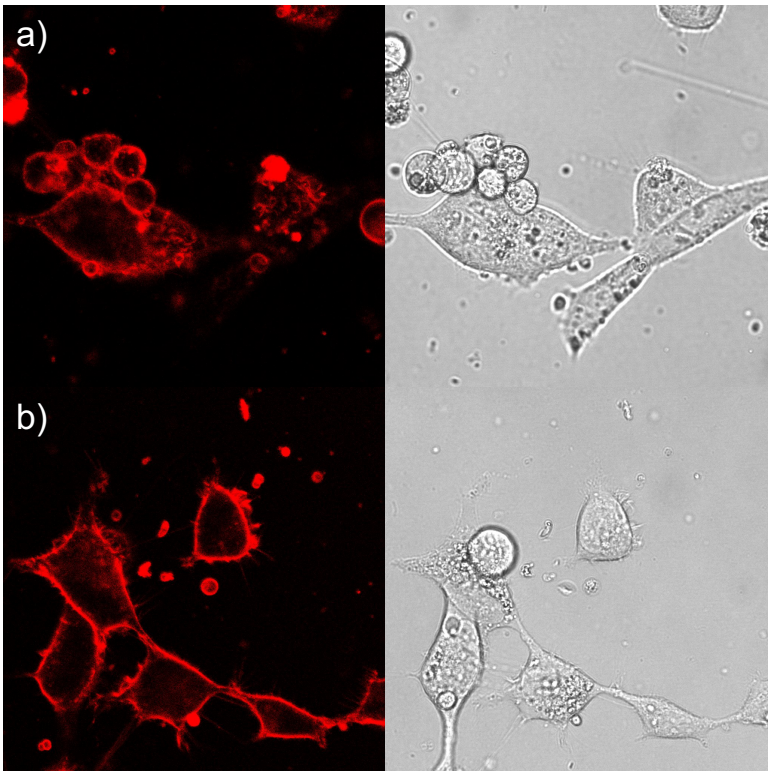

Figure 2.5. Compound **2m** shows little to no selectivity for NET when incubated in a) HEK-NET and b) HEK-293. The fluorescence intensity of the probe is identical at the membrane in both cell lines and no displacement is observed with the addition of a more potent inhibitor. These results make **2m** a promising cell membrane stain.

2.6 Cationic Stilbene Dyes as Generic Cell Membrane Stains

Once it was determined that compounds **1m** and **2m** were nonselective toward MATs, their use as a membrane stain was explored. The plasma membrane is the guardian of the cell, separating the interior components from the outside environment or extracellular space. It consists of a lipid bilayer embedded with proteins that selectively control the passage of ions and small organic molecules in and out of the cell and its organelles. Aside from protection, the cell membrane is involved in other processes such as adhesion and signaling. Fluorescent membrane stains are crucial for studying the structure and function of the plasma membrane. Molecular rotors have been used to quantify membrane viscosity and fluidity[21], visualize membrane microdomains or rafts[22],

and measure membrane integrity.[23] Stilbene derivatives **1m** and **2m** were studied in solution using a model membrane to assess their potential as cell membrane stains, followed by testing in live cell cultures.

2.7 Photophysical Characterization of Cationic Stilbene Dyes in a Model Phospholipid Bilayer

The photophysics of the doubly methylated stilbene dyes were studied in phosphate buffered saline (PBS), to mimic the cellular environment, and sodium dodecyl sulfate-cetyl trimethylammonium bromide (SDS-CTAB) acting as a model phospholipid bilayer. **1m** and **2m**, theoretically, will have increased mobility and rotation in PBS, but will be restricted from rotation in SDS-CTAB, effectively turning the emission "on". **1m** showed strange behavior in PBS with λ_{max} = 346 nm and ε = 44,494, emitting at 515 nm. With the addition of SDS-CTAB, there was a loss in absorbance (ε = 17,725) and a blue-shift in emission to 479 nm. The values match up well with the measurements of **1** in MeOH and $PhCH_3$, given the similar polarity to PBS and SDS-CTAB, respectively. However, these results do not confirm the hypothesis of free and restricted rotation. This may be due to the probe not being fully incorporated into the faux-membrane. On the contrary, **2m** exhibited definitive TICT characteristics with absorbance in PBS at 388 nm (ε = 26,815) and little to no emission. In SDS-CTAB, both the absorbance and emission were red-shifted to 399 nm and 557 nm, with a jump in intensity. The enrichment in fluorescence is due to the molecule having restricted rotation, destabilizing the twisted state, and favoring emission from the S_1 excited state. This further confirms the ability of the $–NO_2$ substituent to effectively separate charge in the excited state, generating a more

sensitive probe. With the promising optical data, **2m** was compared to a popular membrane stain used widely in biological laboratories.

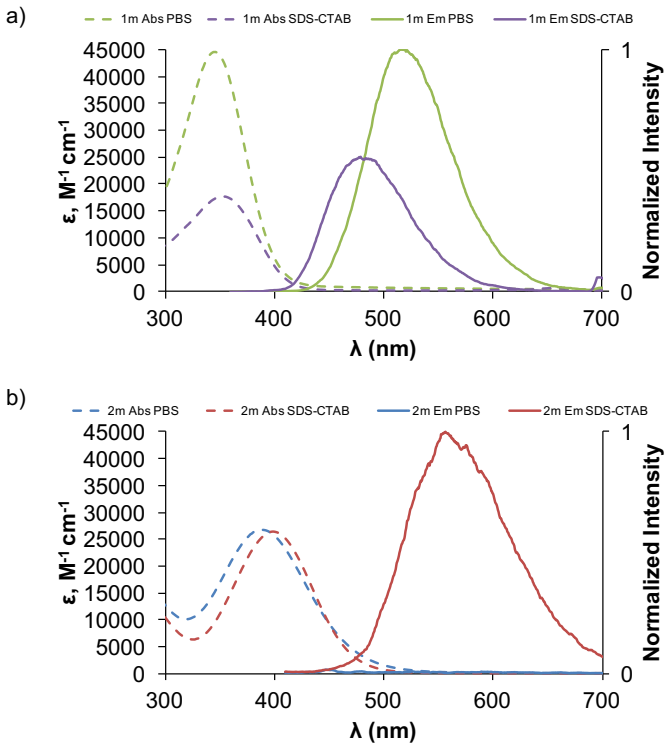

Figure 2.6. Absorption (dashed lines) and emission (solid lines) of a) **1m** and b) **2m** in the presence and absence of surfactant micelles acting as a model membrane. The nitrated **2m** exhibits more sensitivity than **1m** with quenched emission in PBS and greatly enhanced fluorescence when incorporated into the faux-membrane.

2.8 Comparison of Compound 2m to a Commercially Available Membrane Stain

With **2m** showing the best "turn-on" capabilities, its use as a membrane stain was compared to a commercially available cyanine dye, Cy5. Several derivatives of cyanine (Cy) dyes have been synthesized and are useful in biological applications. Structurally, the scaffold consists of two indole heterocycles separated by 2, 3, 5, or 7 methine groups. The conjugation length can tune the optical properties of the dye while the substitution pattern on the heteroatom of the indole ring can optimize interactions and solubility. For probing the cell membrane, octadecyl hydrocarbon chains are appended to the indole ring

yielding low water solubility and quenched emission. Upon binding to the membrane, there is an increase in emission, similar to the behavior of **2m**. Though the two dyes have some parallels, Cy dyes are slightly superior for visualizing the cell membrane.

Both **2m** and Cy5 have enhanced emission once incorporated into the cell membrane, showing the desirable "turn-on" property. When looking at the absorbance and emission profile of Cy5, in Figure 2.7, there are a few characteristics that stand out. The absorbance and emission bands are narrow, structured, and mirrored. This allows for selective excitation when imaging *in vitro*. The absorbance and emission are also red-shifted to the near-infrared (NIR) region of the electromagnetic spectrum, giving a spectroscopically distinct signal and eliminating background noise generated by the biological sample itself. The higher wavelength, lower energy radiation used to excite the molecule is also advantageous for lessening the damage to the cell and penetrating deeper into tissue. Cy dyes also have a small, polarity insensitive Stokes shift, high molar absorptivity coefficients, and moderate-to-high quantum yields when compared to dyes exhibiting charge transfer characteristics like **2m**.[24] Compound **2m**, in contrast, has a large Stokes shift and structure-less, broad optical bands. It also absorbs and emits at higher energy wavelengths rendering it less useful in that aspect. However, **2m** is capable of completing tasks, such as quantifying polarity and viscosity of the membrane, that a Cy dye cannot achieve. Figure 2.8a reveals the localization of **2m** exclusively at the cell membrane of HEK-293 cells. This has impeccable overlap with the Cy dye membrane stain shown in Figure 2.8b and the overlay in Figure 2.8c.

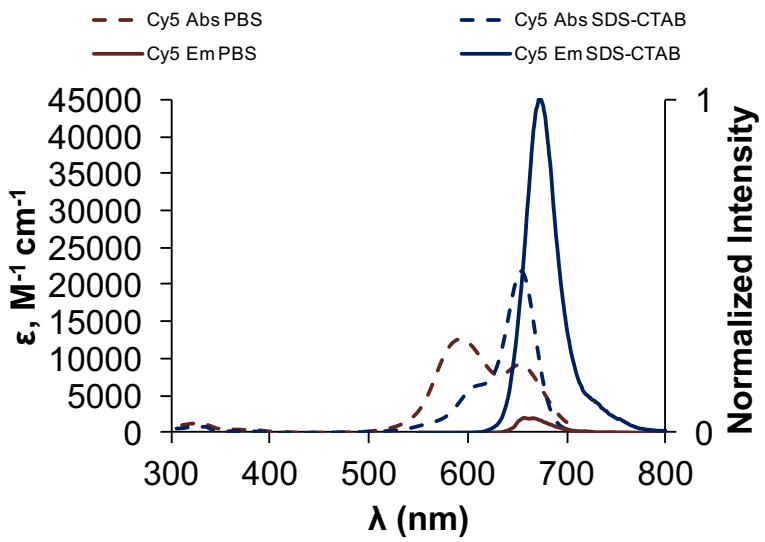

Figure 2.7. Optical spectra of commercially available 1,1′-dioctadecyl-3,3,3′,3′-tetramethylindodicarbo-cyanine perchlorate (DiD C18 Cy5) reveals a more desired spectral profile, however the behavior of the dye is not suitable for applications such as determining membrane polarity and viscosity.

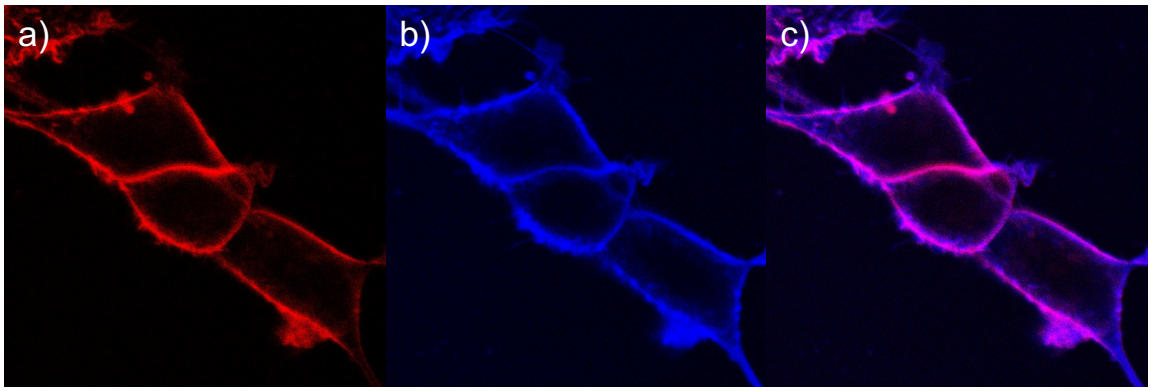

Figure 2.8. Cell imaging results of **2m** incubated in HEK-293 cells. a) Probe **2m** localizes in the cell membrane similar to that of the commercially available Cy dye (b). The overlay (c) shows great overlap proving that **2m** has potential as a charge-transfer dye highlighting the plasma membrane.

2.9 Summary: Stilbene Dyes Targeting the Cell Membrane

Six fluorescent candidates targeting MATs were synthesized based on past successful substrates. These molecules included structural features of common charge transfer dyes,

producing a "turn-on" effect to visualize binding. The length of conjugation, and subsequently the size, was used to differentiate between transporters and the functional groups maintained important interactions and improved solubility. The optical properties were studied in solvents differing in polarity and viscosity to determine behavior as a result of changes in the microenvironment. The unfortunate lack in specificity to MATs gave rise to one important structural change, and a new application, employing the dyes as generic cell membrane stains. One derivative, **2m**, showed promise owing to its wonderful "turn-on" emission when rotation within the molecule was limited. It was compared to a commercially available membrane stain where it was found to behave similarly. Although it lacked efficiency in certain aspects, it shows promise as a polarity and viscosity probe in the ongoing investigation of cellular membranes.

2.10 Experimental

***Representative Synthesis,* 4-(4-(cyano)styryl)-N-methylpiperazinyl benzene (1):** Diethyl (4-cyanobenzyl) phosphonate (760 mg, 3 mmol, 1 eq.), sodium hydride (180 mg, 7.5 mmol, 2.5 eq.), and dry THF (20 mL) were placed in an oven dried schlank flask with a stir bar under nitrogen purge. The solution was heated to 40 °C and 4-(4-methyl-1-piperazinyl) benzaldehyde in dry THF (20 mL) was added dropwise over approximately 1 hour. The reaction mixture was allowed to stir for an additional 24 hours. The reaction was quenched in water and extracted in chloroform (3 x 50 mL). The organic layer was dried over $MgSO_4$, concentrated until dryness, and the resulting solid was recrystallized in methanol to yield a yellow solid (629 mg, 69% yield); mp 236-238 °C; IR ν_{max} (cm^{-1}): 2798.0, 2216.9, 1593.5, 1447.3, 1141.6; ^1H NMR (400 MHz, $CDCl_3$): δ 2.37 (s, 3H), 2.59 (t, 4H, J = 10.4 Hz), 3.30 (t, 4H, J = 10.0 Hz), 6.93 (dd, 2H, J = 9.2 Hz), 6.95 (d, 1H,

J = 6.0 Hz), 7.16 (d, 1H, J = 16.4 Hz), 7.45 (dd, 2H, J = 8.8 Hz), 7.54 (dd, 2H, J = 8.4 Hz), 7.61 (dd, 2H, 8.4 Hz); ^{13}C NMR (500 MHz, $CDCl_3$): δ 46.2, 48.3, 55.0, 109.6, 115.5, 119.3, 123.5, 126.4, 127.3, 128.1, 132.2, 132.5, 142.5, 151.4; HR-ESI (Q-TOF) *m/z*: calcd. for $C_{20}H_{22}N_3^+$ $[M+H]^+$ calcd. 304.1800, found 304.1819.

4-(4-(nitro)styryl)-N-methylpiperazinyl benzene (2): Orange solid (80 mg, 10% yield); mp 245-248 °C; IR ν_{max} (cm^{-1}): 2942.8, 2829.4, 1584.0, 1505.9, 1142.90; ^{1}H NMR (500 MHz, $CDCl_3$): δ 2.38 (s, 3H), 2.60 (t, 4H, J = 10.0 Hz), 3.31 (t, 4H, J = 10.5), 6.93 (dd, 2H, J = 7.0 Hz), 6.99 (d, 1H, J = 16.5), 7.22 (d, 1H, J = 16.0 Hz), 7.47 (dd, 2H, J = 9.0 Hz), 7.58 (dd, 2H, J = 9.0 Hz), 8.20 (dd, 2H, J = 9.0 Hz); ^{13}C NMR (500 MHz, $CDCl_3$): δ 46.2, 48.2, 54.9, 115.4, 123.0, 124.2, 126.3, 127.1, 128.3, 133.2, 144.6, 146.1, 151.5; HR-ESI (Q-TOF) *m/z*: calcd. for $C_{19}H_{22}N_3O_2^+$ $[M+H]^+$ calcd. 324.1700, found 324.1719.

***Representative Synthesis,* 4-(4-(cyano)phenyl)-4,4-dimethylpiperazinyl benzene (3):** 4-(4-methylpiperazin-1-yl)phenyl boronic acid (220 mg, 1 mmol, 1.2 eq.), 4-bromobenzonitrile (152 mg, 0.8 mmol, 1 eq.), triphenylphosphine, potassium carbonate (excess), and DMF (10 mL) were added to a long schlenk flask. The mixture was frozen, pumped down by vacuum, and thawed until no more oxygen was present. Palladium (II) acetate was added and the reaction mixture was allowed to stir for 48 hours at 80 ^{o}C. The reaction was poured into 1M KOH and extracted into EtOAc (3 x 100 mL). The organic layer was dried over $MgSO_4$ and concentrated until dryness. The crude solid was purified through column chromatography with a gradient elution (DCM, EtOAc, MeOH) yielding a pale yellow solid (14 mg, 6% yield). ^{1}H NMR (500 MHz, DMSO-d_6): δ 2.21 (s, 3H), 2.46 (t, 4H), 3.23 (t, 4H), 7.04 (d, 2H), 7.61 (d, 2H), 7.80 (m, 4H).

4-(4-(nitro)phenyl)-4,4-dimethylpiperazinyl benzene (4): yellow-orange solid (12 mg, 5% yield); ^{1}H NMR (500 MHz, DMSO-d_6): δ 2.20 (s, 3H), 2.49 (t, 4H), 3.25 (t, 4H), 7.06 (d, 2H), 7.70 (d, 2H), 7.90 (d, 2H), 8.24 (d, 2H).

***Representative Synthesis,* 4-(4-(cyano)styryl)-4,4-dimethylpiperazinyl benzene (1m):** 4-(4-(cyano)styryl)-N-methylpiperazinyl benzene (200 mg, 0.6 mmol, 1 eq.) was dissolved in toluene (5 mL). Methyl iodide (228 mg, 2 mmol, 3 eq.) was added and the reaction was stirred at room temperature overnight. The resulting solid was collected by vacuum filtration and washed with toluene. The solid was then dried under vacuum to yield a bright yellow solid (202 mg, 95% yield); m.p. 293-296 ^{o}C; IR ν_{max} (cm^{-1}): 3005.1, 2226.1, 1590.9, 1171.0; ^{1}H NMR (500 MHz, DMSO-d_6): δ 3.19 (s, 6H), 3.57 (d, 8H, J = 12.7 Hz), 7.05 (d, 2H, J = 7.8 Hz), 7.18 (d, 1H, J = 16.6 Hz), 7.39 (d, 1H, J = 16.6 Hz), 7.57 (d, 2H, J = 7.3 Hz), 7.76 (dd, 4H, J = 18.7 Hz); ^{13}C NMR (500 MHz, DMSO-d_6): δ 41.9, 50.8, 60.5, 109.1, 115.8, 119.7, 124.2, 127.1, 128.2, 128.6, 132.5, 133.0, 142.9, 149.8; HR-ESI (Q-TOF) *m/z*: calcd. for $C_{21}H_{24}N_3^+$ $[M+H]^+$ calcd. 318.2000, found 318.2000.

4-(4-(nitro)styryl)-4,4-dimethylpiperazinyl benzene (2m): Orange solid (26 mg, 46% yield); m.p. 240-242 ^{o}C; IR ν_{max} (cm^{-1}): 3440.9, 3005.2, 1585.9, 1508.9, 1191.9; ^{1}H NMR (400 MHz, DMSO-d_6): δ 3.20 (s, 6H), 3.58 (d, 8H, J = 15.2 Hz), 7.07 (d, 2H, J = 8.4 Hz), 7.26 (d, 1H, J = 16.7), 7.47 (d, 1H, J = 16.4 Hz), 7.60 (d, 2H, J = 8.3 Hz), 7.80 (d, 2H, J = 8.6 Hz), 8.21 (d, 2H, J = 8.6 Hz); ^{13}C NMR (500 MHz, DMSO-d_6): δ 41.9, 50.8, 60.5, 115.7, 124.5, 127.2, 128.8, 133.6, 146.1, 150.0; HR-ESI (Q-TOF) *m/z*: calcd. for $C_{21}H_{24}N_3^+$ $[M+H]^+$ calcd. 338.1900, found 338.1881.

Optical Spectroscopy: UV-Vis spectra were acquired using a Perking Elmer Lambda 35 UV-Vis Spectrometer. Fluorescence spectra were obtained using a Perkin Elmer LS 55 Fluorescence Spectrometer. The final concentration of dye in solution was 10 μM for absorbance and 1 μM for fluorescence measurements.

Cell Culture. HEK293 and HEK-NET cells were maintained in DMEM (Dulbecco's Modification of Eagle's Medium with 4.5 g/L glucose, L-glutamine and sodium pyvuate) containing 10% dialyzed FBS, 2mM glutamine, 100 units/mL penicillin, 100 μg/mL streptomycin, and 250 μg/mL geneticin (in the case of HEK-NET) at 37 ^{o}C and 5% CO_2. Cells were seeded at a density of 10^5 cell/cm^2 in 96 microwell plates and incubated for atleast 48 hours until a visible monolayer was established. Prior to imaging, DMEM was removed and PBS was added to each well. Cells maintained a normal morphology during the course of the experiment (max. 1) and remained adhered to the imaging plate.

Confocal Microscopy. Imaging was performed on a Leica SP5 confocal microscope housed within the University of Miami Biology Imaging Core Facility. Excitation was achieved using the 405 nm laser. Images were analyzed using Fiji/ImageJA software.

CHAPTER 3

Functionalized Lignin Biomaterials: Design, Synthesis, and Structural Characterization

3.1 Motivation: Host-Guest Chemistry Utilizing Organic Polymers

Host-guest chemistry has begun to make a significant impact in medicine as a complimentary strategy to small molecule therapies. The use of a macromolecular host, to encapsulate and deliver a guest molecule to its physiological target, allows small molecules with poor solubility, permeability and oral bioavailability, to exhibit improved circulatory stability and prevents premature clearance. Typically, encapsulation is applied to large biomolecules such as peptides, proteins, and DNA, however, low molecular weight molecules i.e. hydrophobic drugs, fluorescent dyes[25-26], etc., can also benefit from supramolecular systems.

There are many examples of organic polymers suitable for drug delivery reported in the literature, spanning from linear homopolymers or block co-polymers to branched network and dendritic polymers. The substitution patterns, degree of crosslinking, and macromolecular organization govern the utility of the polymers as novel delivery systems and tune their physicochemical properties for desired performance. The ideal delivery vehicle should be on the nanoscale and be amphiphilic, composed of both a hydrophilic component for interacting with the surrounding aqueous environment, as well as a hydrophobic portion for non-covalently storing and protecting the guest molecule of interest.

Typically, polymer chains are either linear or branched, although other architectures do exist. Linear polymers employed as macromolecular hosts, such as poly(lactic acid) (PLA), poly(lactic-co-glycolic acid) (PLGA), and polysialic acid (PSA), are

biocompatible and have been approved by the Food and Drug Administration (FDA) for use in various therapeutic devices (Figure 3.1).[27] Although useful, these systems have drawbacks including complicated syntheses, low biodegradability, limited drug loading, and poor pharmacokinetic profile of complexed drugs.[28] Lactic acid and its copolymers can be synthesized through direct polycondensation or ring-opening polymerization (ROP). Direct condensation of the monomers is the preferred method, however generation of water creates competing side reactions, requires special procedures, such as melt or solution polymerization, and involves complicated distillation techniques for removal. ROP needs severe conditions including high temperatures (reaching 200 °C), low pressures, long reaction times, and metal catalysts.[29] PSA can be synthesized through carbodiimide crosslinking chemistry using organic catalysts which can persist through the purification process.[30] Given the disadvantages of linear polymers as drug delivery vehicles, development of systems utilizing branched polymers is a significant focus of researchers in this field.

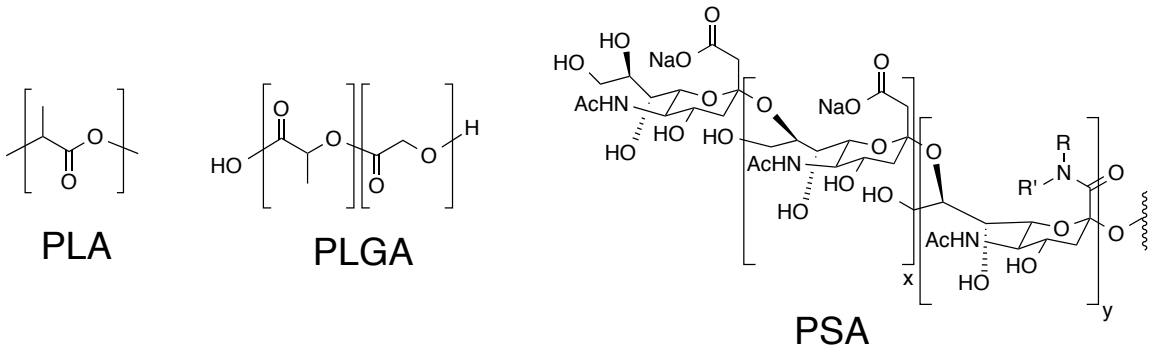

Figure 3.1. Representative chemical structures of traditional linear polymers used in drug delivery systems. PLA/PLGA has been approved by the FDA for use in several medical devices such as gels, injections, and oral tablets.

Branched or crosslinked polymers exhibit substantial improvements over their linear counterparts, most notably, dendrimers. Structurally, dendrimers consist of a

multifunctional central core, branched units, and surface functional groups. This construction makes dendrimers useful in many biomedical applications such as storage and delivery of guest molecules. The interior of a dendrimer, typically hydrophobic, provides efficient, non-covalent encapsulation of visiting molecules and enables their controlled release. Reactive handles on the surface of the dendrimer allow for incorporation of solubilizing groups or targeting moieties. Also, the heavily crosslinked and covalent network make dendrimer micelle organization more stable than other polymeric micelles. These advantages over conventional linear polymers caused a rise of interest in dendritic polymers for biological applications, though room for improvement still exists.

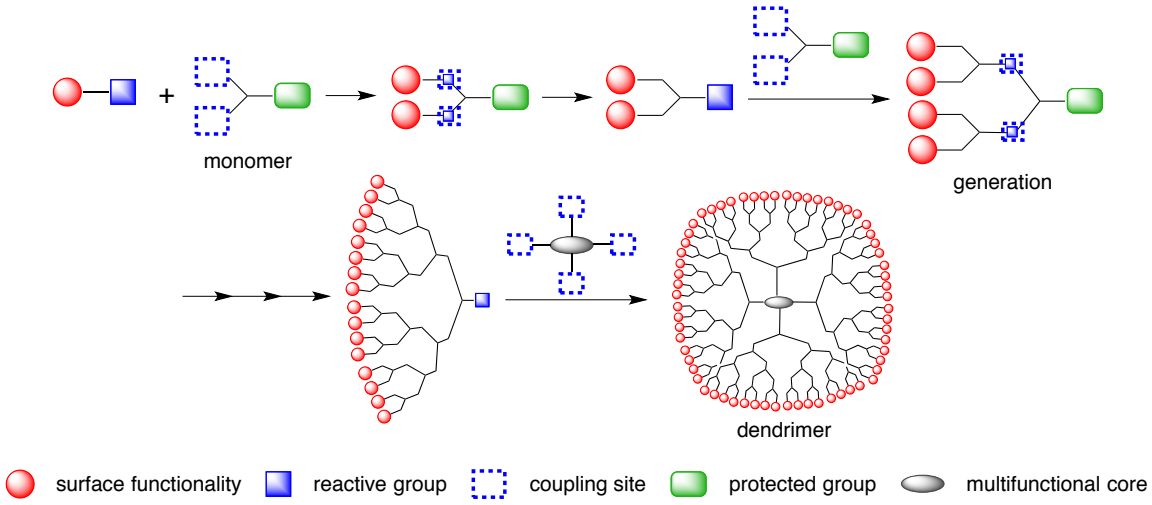

Figure 3.2. Convergent synthesis of dendrimers begins with some surface functionality tethered to a reactive group that can be coupled to a protected monomer. Deprotection yields a reactive group that is, again, coupled to a monomer creating generations within the dendrimer. This process is repeated until the desired number of generations are achieved. Finally, the generations are coupled to a multifunctional core giving the final macromolecule. This complicated growth approach can be avoided by using natural biomaterials with similar structure and function.

The synthetic procedure for dendrimers can be carried out in one of two ways 1) divergent growth from the inside-out or 2) convergent route from outside-in.[31] The divergent approach[32] begins with an initiator core reacting with a branched monomer through a Michael addition followed by repetitive amine couplings to give the desired number of generations. For convergent synthesis (Figure 3.2), the starting material will contain the surface functionality and a reactive group. The reactive point is condensed with a monomer bearing at least two coupling sites and a protected functional group. After deprotection to activate the group, repetitive reactions give one desired piece with a reactive handle that can be coupled to a multifunctional core resulting in the final macromolecule.[33] There are many dendrimers in the literature including the standard poly(amido amine) (PAMAM)[34], aromatic, aliphatic, etc. all requiring the same exhaustive syntheses. Nature provides us with a suitable biomaterial, in the form of lignin, that has similar structure and functionality as synthetic dendrimers, but removes the need for a complicated growth approach.

3.2 Lignin Chemical Structure, Isolation, Modification, and Primary Uses

Lignin is an organic substance found in plants that assists in the overall structure of the cell wall by controlling fluid flow and preventing against enzyme degradation. It is a byproduct of the paper, agricultural, and bio-refinery industries produced in large quantities only second to cellulose in bulk mass and first in aromatic subunits. Lignin, an aromatic, dendritic network polymer, is made up of phenyl propene base units. The base units are composed primarily of monolignols including p-coumaryl alcohol, coniferyl alcohol, and sinapyl alcohol (Figure 3.3). The polymeric structure is created through phenolic coupling reactions via radicals generated by peroxidase-H_2O_2 where monomer

units will add end to end through multiple linkages.[35] This introduces complexity and heterogeneity into its structure, leading to underutilization as a chemical resource. Though the structure of lignin is complex, it contains attractive structural features and comes as a biocompatible, renewable source. The polar aliphatic and phenolic hydroxyl, carbonyl, carboxylic, and methoxy substituents aid in its water solubility while the nonpolar backbone consisting of aryl propane units provides a lipophilic construct. The core is also extensively cross-linked which is required to maintain structural integrity and resist biochemical degradation in different environments.

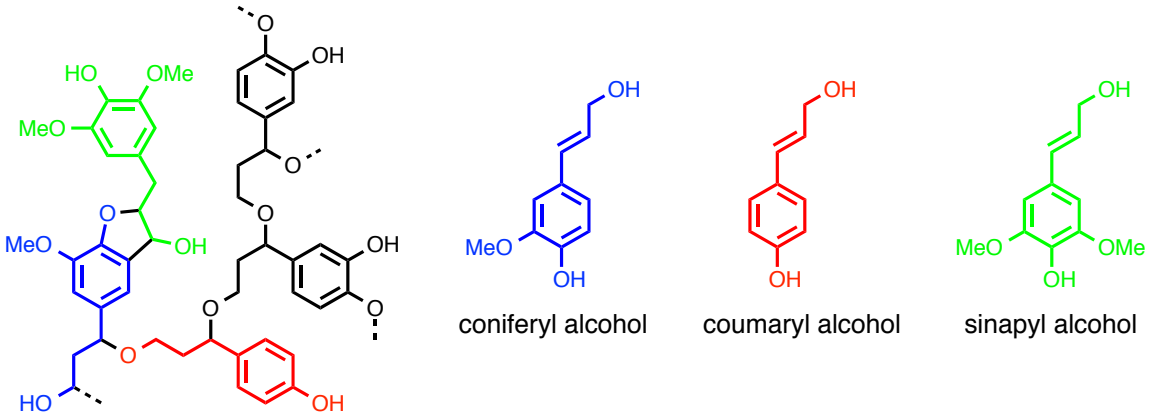

Figure 3.3. Lignin is an aromatic, dendritic network polymer composed mostly of 3 monolignols. The backbone is created by radical coupling reactions that give random linkages and no control over the final structure. Though each macromolecule differs slightly, there are conserved functional groups such as phenolic and aliphatic hydroxyl, methoxy, carbonyl, carboxylic, and cyclic ether substituents.

Extraction of lignin can be carried out by pulping processes that influence the structure and physical properties of the final product. Lignin was once considered a waste material, however, it should be noted that its recent popularity increase has deemed it a raw material with promising potential. Pulp mills are biorefineries, broadly defined as units converting biomass into bio-based products such as chemicals, materials, biofuels, etc., that transforms lignocellulosic biomass into its main constituents. The goal is to

separate 1) cellulose to make paper 2) valuable co-products such as lignin for material synthesis and 3) hemicellulose without completely degrading their functionality. After cleavage of ester and ether linkages in the *in planta* lignin, the isolated products can be broken down into 2 categories, sulfur and sulfur-free lignins (Figure 3.4).

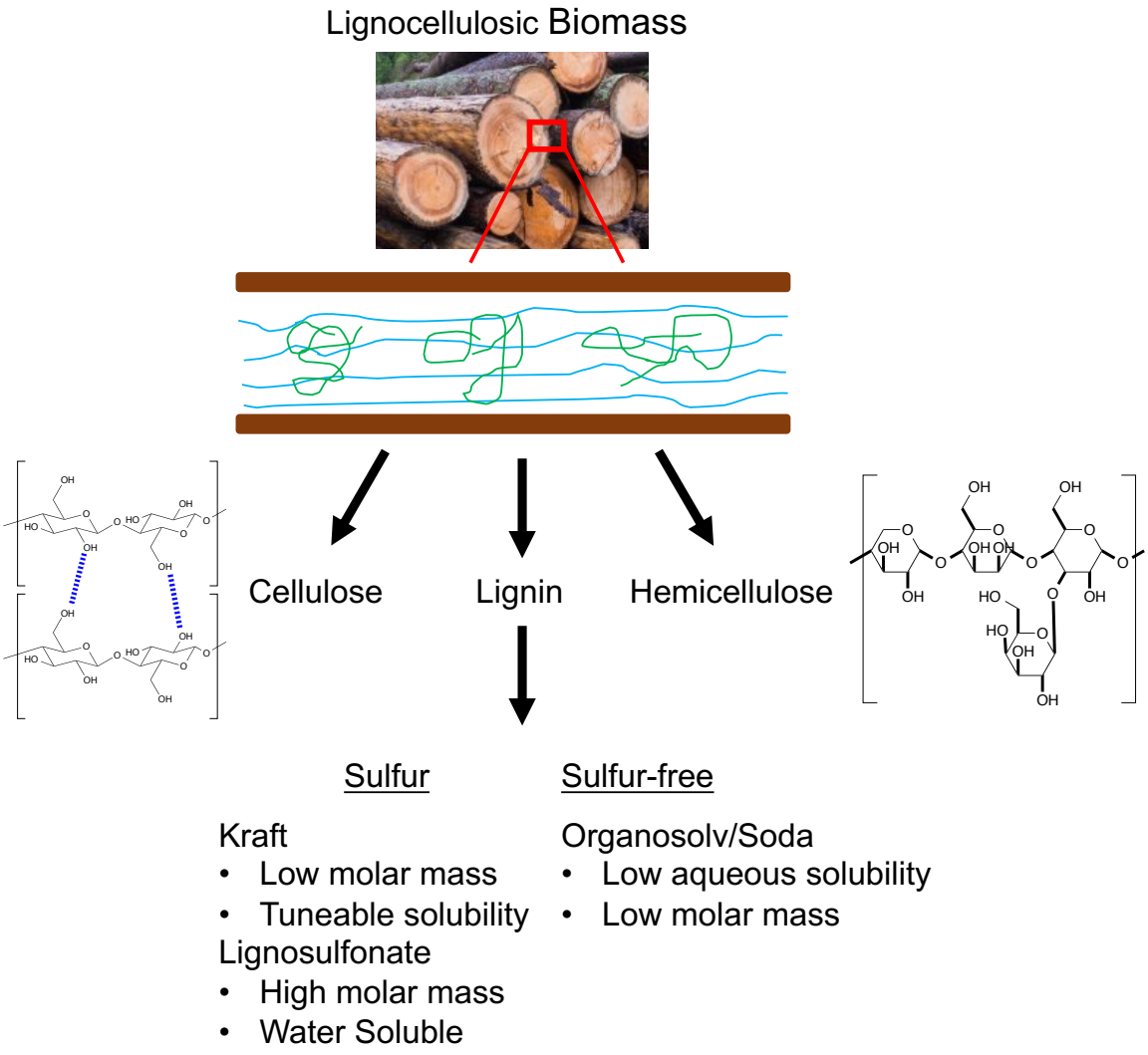

Figure 3.4. Lignocellulosic biomass, such as wood and other dry plant matter, enters the pulping process to separate the components of the plant cell wall. Cellulose, a strong crystalline polymer, is used for paper production. Hemicellulose, made up of random sugars and more susceptible to hydrolysis, is used as an additive or feed stock. Lignin was once considered a waste material but is now used in synthesis of valuable materials.

The lignin isolation process influences the final products, categorized as either sulfur or sulfur-free, both differing in structure and physical properties.

Organosolv and soda lignins are sulfur-free with small macromolecular size and poor aqueous solubility. Kraft and lignosulfonates are sulfur lignins and the primary isolates from the pulp and paper industries. These processes use a base along with other chemicals such as sodium sulfide (Na_2S) or sulfur dioxide (SO_2) to generate cellulose and "black liquor", containing the majority of lignin. After acidification, both lignins can be recovered. Lignosulfonates contain a high percentage of sulfur in the form of sulfate groups on the aliphatic chains, making them water-soluble with a higher average molar mass (>15,000 g/mol) and polydispersity index. Kraft lignin, on the other hand, contains only 1-2% sulfur content and a low molar mass (1,000-10,000 g/mol). More importantly, the high level of phenolic hydroxyl groups in kraft lignin are ideally suited as reactive handles for generating diverse materials.

Modification of lignin can be broken down into either fragmentation and depolymerization or functionalization to build up the structure and create new materials. Industrial-based chemical degradation of lignin breaks its structure down into small aromatic molecules for fine chemicals or burns it as a source of fuel. The growing need to find a replacement for fossil fuels is evident and biofuels offer desired benefits.[36] Given the complexity of its structure, the processing of lignin is a challenge and many groups are actively addressing it.[37-40] Modifications at the phenolic position have been done before including esterification,[41] alkylation, and oxypropylation.[42-43] For alkylation, the most common modification is methylating the phenolic –OH groups to enhance its mechanical properties as a thermoplastic or similar.[44] Long chain alkyl groups have received little attention with only one example of a dodecyl-modified lignin reported in

the literature.[45] Derivatives of lignin are also underutilized in a biomedical setting with only few groups exploring its potential.[46-47]

3.3 Exploring Reactivity: Attempts at Extended Conjugation

Considering the previous modifications to lignin and its aromatic structure, attempts were made to extend conjugation in the macromolecule generating a new class of fluorescent polymers (Scheme 3.1). Common reactions to link aromatic rings or produce fluorescent scaffolds were tested on the lignin backbone. Knoevenagel condensation using 4-picolinium iodide could react with aldehyde functionality in lignin to give stilbazolium moieties. Treatment with ethyl 4,4,4-trifluoroacetoacetate in the prescence of phosphoric acid, similar to the Pechmann condensation, can create courmarin rings after reacting with the phenolic -OH groups in lignin. Halogenation can impart halogen atoms in the place of hydrogens on the aromatic rings giving new reactive sites. Friedel-Crafts acylation using aluminum trichloride ($AlCl_3$) as a Lewis acid with a functionalized acid anhydride can also extend conjugation. Oxidative cross coupling reactions could further crosslink the structure of lignin, making extended pi-systems between the aromatic rings. After screening these reactions and isolating little to no product, it is apparent that the aromatic rings are inert, most likely due to the steric hindrance and substitution patterns on the phenyl rings. However, the high phenolic -OH content in kraft lignin allows for simple, facile bimolecular substitution reactions (S_N2) to impart new functionality to the native lignin structure.

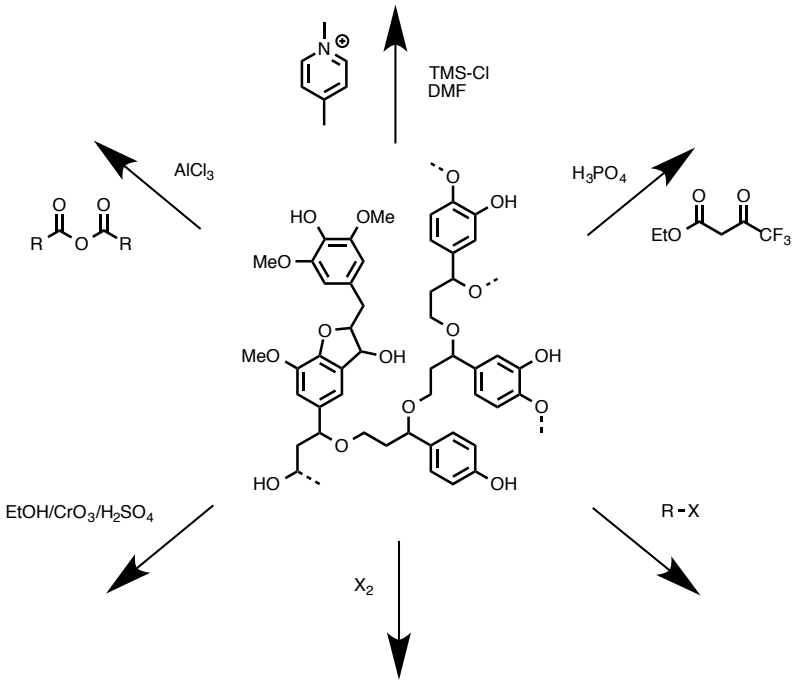

Scheme 3.1. Reactions intended to further conjugate the lignin backbone or form fluorescent moieties were carried out revealing the low reactivity of the crowded aromatic rings. (From top, clockwise) Knoevenagel condensation, Pechmman condensation, alkylation, halogenation, oxidative cross coupling, and Friedel-Crafts acylation.

3.4 Design and Synthesis of Lignin Derivatives via Substitution at the Phenolic Position

Hypothetically, incorporating alkyl chains, some bearing additional functionality, would give a library of lignin derivatives ranging from neutral to anionic to cationic. These modified lignins would then self-assemble into nanocontainers capable of storing and delivering suitable guest molecules in the cellular environment. For neutral derivatives, the increasing chain length of the alkyl group will impart a hydrophobic pocket for storing guest molecules, with a polarity similar to that of the cell membrane. This can be useful for hydrophobic dyes that have poor photophysical properties in aqueous solutions, as well as hydrophobic drugs with low solubility. Charged

derivatives, at physiological pH, can guide electrostatic interactions widening the potential applications.

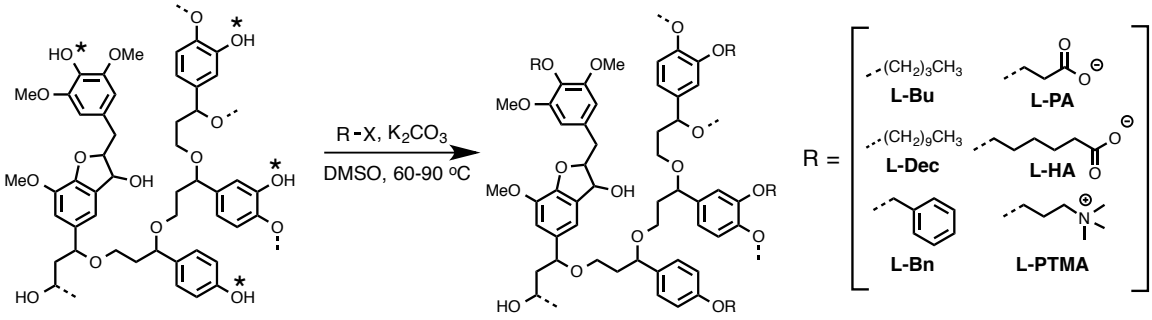

Scheme 3.2. Bimolecular substitution reactions at the phenolic -OH position using an excess of alkyl halide, K_2CO_3 as a base, DMSO to solubilize all reaction components, and moderate heating allows for appending a diverse set of functional groups to the lignin backbone.

Due to the nature of its structure and somewhat limited solubility, chemical transformation of lignin is typically carried out with the aid of surfactants, in biphasic reactions, emulsions, or under continuous ultrasonication.[48] Additionally, cross-linking of lignin is a frequent modification, despite the fact that the parent structure is already heavily cross-linked. Using a similar approach to previous lignin modification, a cohort of well-characterized lignin derivatives were developed using traditional substitution reaction conditions (Scheme 3.2) and without the need for additives or catalysts which can persist through purification.[49] The synthetic procedure allows for most alkyl halides to be appended to lignin using dimethyl sulfoxide (DMSO) as a nearly universal solvent, potassium carbonate (K_2CO_3) as a mild base, and moderate heating between 60-90° C. Good to excellent yields of conversion and mass yields were achieved after 48 h for most sterically unhindered substrates (Table 3.1). Even for reactions that required extended times, i.e. more sterically demanding or less reactive substrates, the mild conditions did not lead to any observable breakdown of the lignin backbone.

Table 3.1. Compound key and reaction yields for modified lignins.

Entry	*R =*	*Compound*	*Percent Conversion*	*Mass yield (%)*
1	$-CH_2CH_2CH_2CH_3$	L-Bu	100	74
2	$-(CH_2)_9CH_3$	L-Dec	95	60
3	$-CH_2Ph$	L-Bn	75	48
4	$-CH_2CH_2COO^-$	L-PA	65	40
5	$-(CH_2)_5COO^-$	L-HA	75	13
6	$-CH_2CH_2CH_2N(CH_3)_3^+$	L-PTMA	20	14

Purification of the modified lignins was achieved via precipitation into a non-solvent, such as ethyl acetate, followed by filtration and either rinsing with water or dialysis, to remove residual carbonate. Following lyophilization and ^{1}H-NMR spectroscopy, the products were found to be free of unreacted alkyl halides. The chemical functionality chosen each serves a different purpose. The methyl substitution was used to optimize reaction conditions with different equivalents of alkyl halide. It was found that the amount of methyl iodide would change the number of modified hydroxyl groups as shown through the amount of moderately water-soluble product obtained. Therefore, using a 1-3 equivalent excess of alkylating agent effectively masked the phenolic hydroxyl groups giving the most isolated product. After testing reaction conditions with methyl iodide, the scope of the substitution reactions was expanded to include longer chain alkyl groups, as well as water-soluble functionalities.

Butyl- (**L-Bu**), decyl- (**L-Dec**), and benzyl (**L-Bn**) alkyl chains were used to examine the effect of chain length on particle formation. Methyl substituents will mask the

phenolic hydroxyl groups but will not have the same hydrophobic effect driving particle formation as longer chain alkyl groups. Having synthesized particles with neutral substituents, the anionic and cationic counterparts were synthesized as water-soluble functionalites. Lignin can be anionic at pH greater than 10, where phenolic hydroxyl groups will be deprotonated, or depending on the amount of sulfonate groups in the structure. Taking into account the lower pKa, carboxylic acid moieties (**L-PA**, **L-HA**) were incorporated into the structure to give anionic derivatives at physiological pH. This can also give more reactive sites for further modification into esters and amides. Conversely, N,N,N-trimethyl (**L-PTMA**) substituents were used to produce a positively charged, cationic derivative. Lignin encompasses predominantly oxygen-containing functional groups. Introducing a quaternary amine into the structure not only gives it a useful positive charge, but also incorporates nitrogen, as a hydrogen bond acceptor, for added water solubility.

The products appeared to be light-brown to brown solids, which differed from the appearance of the dark-brown, natural lignin. The solubility of the products also differs from the natural lignin. Kraft lignin, with high phenolic hydroxyl group content, is freely soluble in aqueous solution. Upon modification, the products become moderately soluble in water and freely soluble in polar, organic solvents such as DMSO. This indicates partial masking of the hydrophilic groups in lignin. However, its moderate solubility in water can only be rationalized if the new alkyl chains are excluded from the aqueous solution. This behavior would lend itself to the alkyl chains oriented to the interior of the particle forming a hydrophobic pocket and the hydrophilic groups, such as the methoxy and cyclic ethers, facing the aqueous solution.

3.5 ^{1}H-NMR Spectroscopy of Modified Lignins

The structure of lignin is complex, and the ratio and composition of monomers can vary. Because of this, the proton nuclear magnetic resonance (^{1}H-NMR) spectrum of natural lignin displays broad peaks corresponding to distinguishable regions in its structure. The aromatic peak ranging from 6.5-7.5 ppm arises from overlap of multiple aromatic proton signals making each of them included in one broad signal. Similarly, a peak spanning from 3.5-4.0 ppm represents the methoxy substituents on the aromatic rings. In the aliphatic region from 1-3 ppm, there are no definitive peaks giving an opportunity to identify new peaks corresponding to the modifications in the lignin nanocontainers.

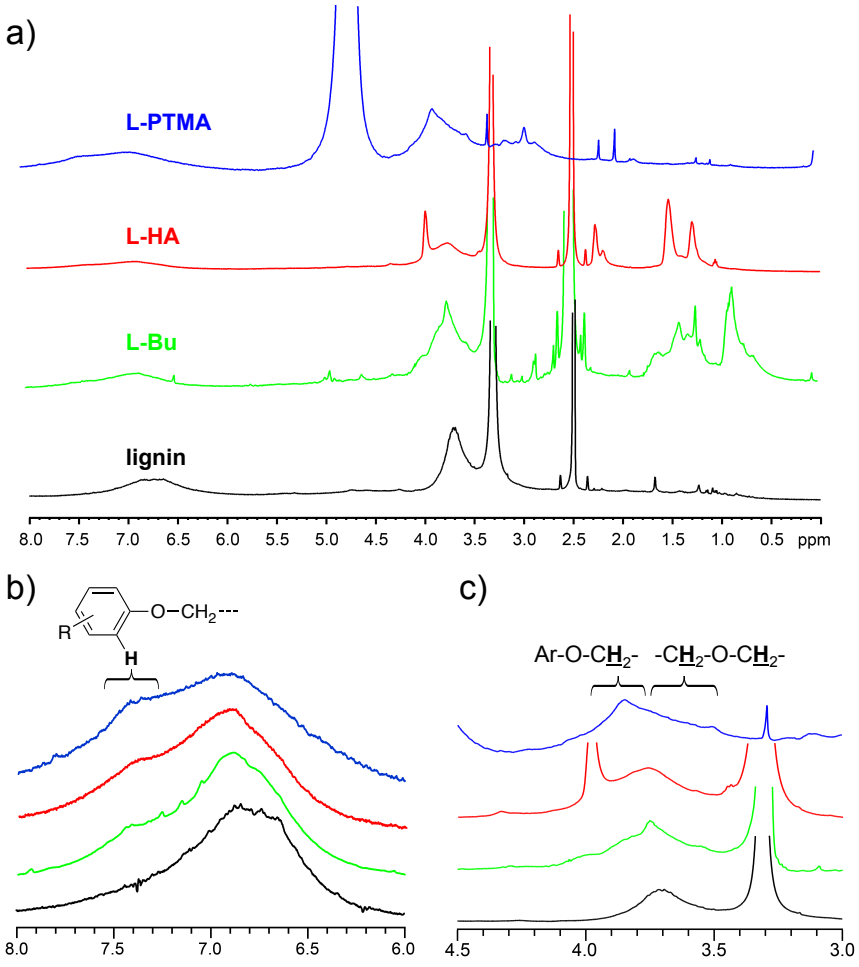

Figure 3.5. ^{1}H-NMR of **L-Bu**, **L-HA**, and **L-PTMA** shows changes from the spectrum of unmodified lignin. Alkylation of the phenolic -OH groups produces three noticeable changes a) the addition of new methylene groups is apparent in the aliphatic region for longer alkyl chains. b) Expansion of the aromatic region reveals the appearance of a shoulder corresponding to the Ar-H of the newly formed phenyl ethers. c) The downfield asymmetry in the ether region can be associated with the methylene of the alkyl group on the aromatic ether, which differs from aliphatic ethers.

^{1}H-NMR spectroscopy (Figure 3.5, also see Supporting Information Figures S11-S17) provides evidence of the chemical modifications. The formation of the phenolic ethers can be revealed both in the aromatic region, with a shoulder appearing at 7.4 ppm, and in the ether region, with prominent shoulders or peaks, corresponding to the alkyl -CH_2- appended to the phenoxy group, appearing from 3.8 to 4.1 ppm. These changes correlate very well with the spectroscopic features that differentiate the aromatic protons of phenol and anisole, as well as purely alkyl ethers from phenoxy-alkyl ethers. The aromatic protons of anisole are shifted downfield relative to phenol, and the alkylation of lignin matches this effect. Similarly, the appearance of features between 3.8 and 4.1 ppm, correlates well with the methyl peak of anisole, as opposed to the formation of aliphatic ethers, which typically appear between 3.4 and 3.6 ppm. Some evidence of aliphatic ether formation is evident in this region, but the asymmetry of the ether region, favoring the downfield side, suggests a predominance of alkylation at phenolic -OH groups. New peaks also appear in the aliphatic methylene region, most notably for the **L-Bu** and **L-Dec**, with other derivatives showing more moderate changes. By comparing the integration values for the aromatic and ether regions, the degree of functionalization of the lignins can be estimated from 100% for sterically unhindered substrates (**L-Bu**, **L-Dec**) to 20% for less reactive electrophiles (**L-PTMA**).

3.6 Infrared Spectroscopy of Modified Lignins

To further confirm the modification to the natural lignin, fourier transform infrared spectroscopy (FT-IR) spectra were obtained. Natural lignin exhibits a broad peak from 3000-3600 cm^{-1} representing the multiple phenolic and aliphatic hydroxyl groups in the structure. There is also a very weak signal at 2954 cm^{-1} corresponding to the C-H sp^3 stretch. The fingerprint region is relatively bare with no significant peaks, again, giving an opportunity to identify new functional groups introduced into the nanocontainers. For example, after modification with butyl- chains, the intensity of the C-H sp^3 peak increases indicating new vibrations in the structure. Similarly, the intensity of this peak drastically increases with addition of the decyl- substituent. Upon addition of benzyl groups, the area from 1450-1600 cm^{-1} sharpens to give distinct peaks corresponding to new benzyl vibrations. With the anionic derivatives, a peak develops at 1715 cm^{-1} that is in agreement with the frequency of the carbonyl in a carboxylic acid. For the N,N,N-trimethyl derivative, a peak appears at 1250 cm^{-1} indicating a C-N vibration. Also, the broad peak from 3100-3600 cm^{-1} narrows indicating less O-H stretching and rationalizing the modification of primarily phenolic hydroxyl groups.

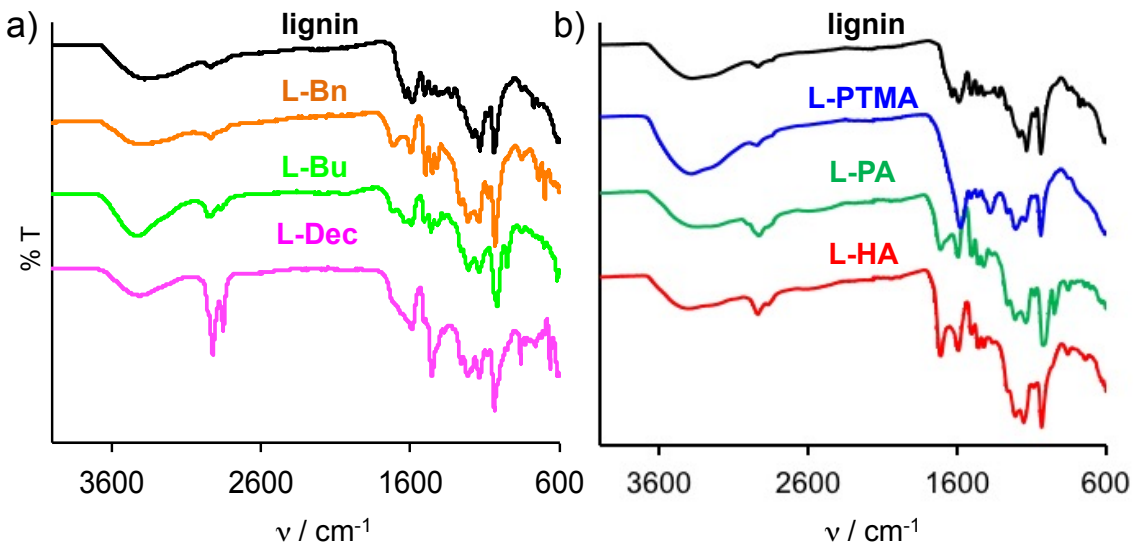

Figure 3.6. Comparison of the IR spectra of kraft and modified lignins a) neutral and b) ionic. Changes in the C-H, O-H, C=O, and benzyl regions of the spectrum show new vibrations and further confirm the modifications to the lignin structure. Conservation of the O-H stretch verifies predominant modification at the phenolic position, leaving the aliphatic -OH groups intact.

3.7 Size and Morphological Characterization of Lignin Nanocontainers

Organic nanoparticles, surfactants, and micelles are dynamic in nature where solvent and cargo are constantly and rapidly being exchanged.[50] For biomedical applications, it is desirable to have a defined size and stability so that early leakage of contents is not an issue. Conversion of a phenolic hydroxyl group in kraft lignin to a phenolic ether removes a hydrogen bond donor, while simultaneously introduces one or more hydrophobic methylene units. The net effect is that the lipophilic character of the modified lignin is increased with a concomitant change in aqueous solution behavior. The addition of alkyl chains to kraft lignin generates hydrophobic domains that self-assemble and these aggregates can be utilized to encapsulate hydrophobic cargo. The presence of ionic groups can also serve to guide interactions with various guest molecules or other targets. Aqueous solutions of all derivatives were prepared, and the

supramolecular structures were investigated by dynamic light scattering (DLS), to determine their hydrodynamic radius, and scanning electron microscopy (SEM), to explore their morphology.

Solutions of modified lignins were prepared by first dissolving in DMSO to produce stock solutions of 10 mg/mL which were passed through 0.2 μm PTFE filters, then diluted into deionized water for a final concentration of 10 μg/mL. The solutions appeared clear and were light brown in color. The sizes of 3 independent samples were taken over a period of 4 hours to ensure that, while dynamic, there was no drastic change in size through swelling or excessive particle aggregation. DLS of the modified lignins revealed particle sizes ranging from ~10 nm up to 1000 nm, with two or three discrete populations of different hydrodynamic radii for several of the compounds (see Supporting Information Figures S18-S24). Natural lignin shows high polydispersity, supporting the idea that the structure is not entirely optimized for self-assembly. A single lignin molecule should exhibit a radius on the order of 2 nm, thus even the smallest particles observed by DLS appear to be aggregates of ~15 individual lignin molecules. The larger particles can be formed by coalescence of the smaller particles,[51-53] which was confirmed by SEM. A "raspberry" morphology was observed similar to that reported in the literature, which supports the notion of hierarchal aggregates of lignin (Figure 3.7).[54]

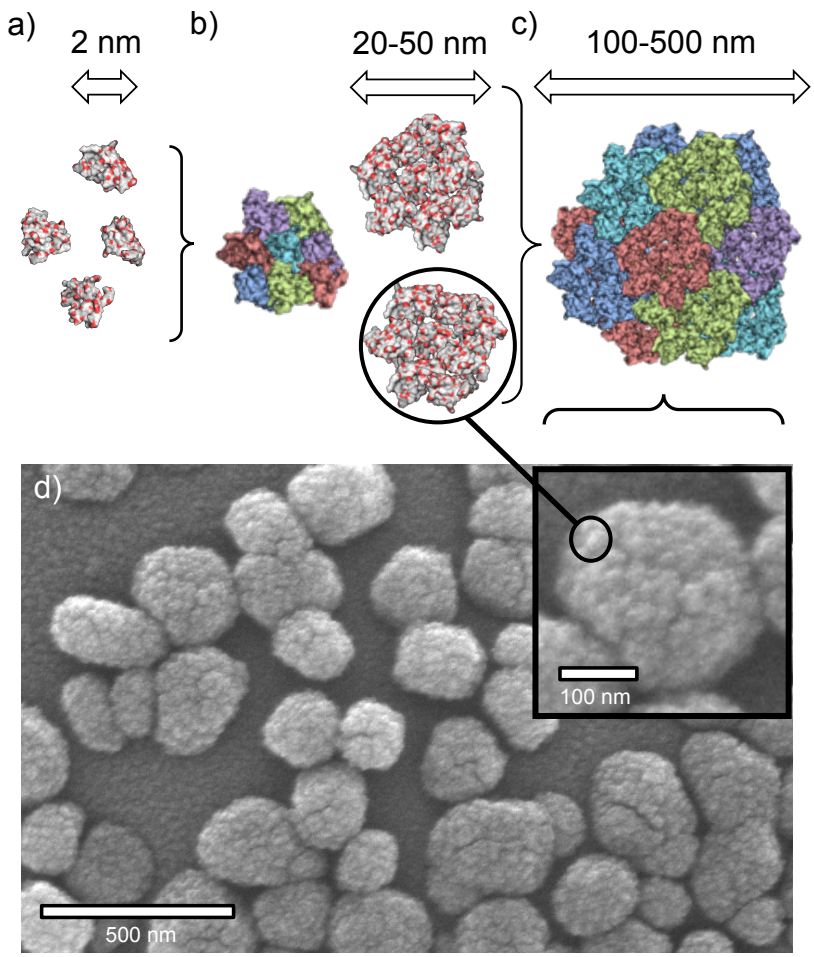

Figure 3.7. Comparison of the length scales and organization of **L-Bu** into supramolecular nanostructures. a) Individual lignin molecules with calculated radii of 1-2 nm assemble into (b) mesostructures with measured hydrodynamic radii of 20-50 nm. c) These can further assemble into larger nanoclusters with radii of 100-500 nm; the two larger assemblies are visible via SEM (d).

When extending the alkyl chain in **L-Bu** and **L-Dec**, a monodispersed behavior was observed with an average hydrodynamic radius of 24.03 ± 10.88 and 35.97 ± 11.59 nm, respectively. This is expected because hydrophobic interactions aid in stability of organic nanoparticles. In the case of lignin nanocontainers functionalized with carboxylic acid substituents, the sizes are slightly larger because of the hydrogen bonding associated with the functional group and the aqueous environment. The propyl and hexyl carboxylic

acid derivatives have diameters of 88.10 ± 20.74 nm and 164.39 ± 81.00 nm. This size difference is a direct effect of chain length rather than hydrophobic interactions driving the size. Likewise, nanocontainers functionalized with a terminal quaternary amine were 181.09 ± 57.07 nm due to the ion-dipole interactions with the aqueous environment causing larger particle size (Figure 3.8).

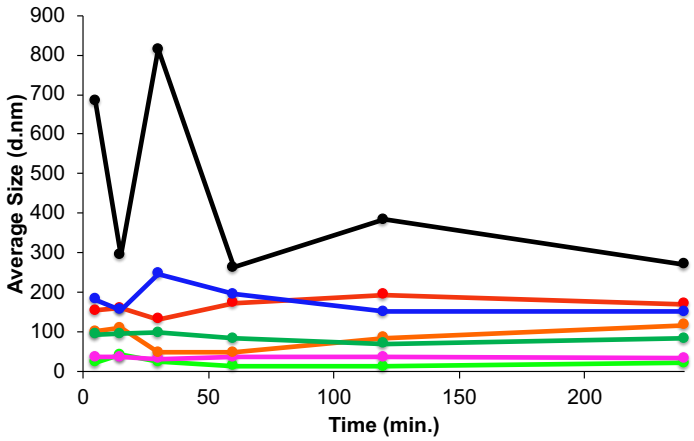

Compound	*Size (d.nm)*
Lignin	polydispersed
L-Bu	24.03 ± 10.88
L-Dec	35.97 ± 11.59
L-Bn	85.55 ± 50.08
L-PA	88.10 ± 20.74
L-HA	164.39 ± 81.00
L-PTMA	181.09 ± 57.07

Figure 3.8. The hydrodynamic radius of each modified lignin was measure over a period of 4 hours to ensure that, while dynamic, the system was stable with no extreme swelling or aggregation. Natural lignin shows high polydispersity, but when alkylated, a more uniform size is revealed.

3.8 Concluding Remarks on the Functionalization of Kraft Lignin

The cross-linked, amphiphilic structure of lignin makes this renewable biopolymer a versatile scaffold for chemical modification. Lignin avoids the pitfalls of traditional linear polymers and removes the complex syntheses associated with dendritic polymers. After exploring its reactivity, S_N2 reactions at the phenolic position of kraft lignin were exploited under mild conditions, to facilitate the addition of alkyl, carboxylate and tetraalkylammonium groups, allowing preparation of diverse lignin nanomaterials. The

chemical modifications were confirmed by ^{1}H-NMR and IR showing good conversion of phenolic hydroxyl groups to the corresponding phenoxy-alkyl ethers. SEM revealed clusters of individual lignin molecules on the order of 50-500 nm. DLS measurements were in close agreement and showed no drastic changes in size over a period of 4 hours. These materials were found to form hierarchal nanoassemblies, which facilitates the encapsulation of molecular cargoes, depending on the lignin modification. The idea of host-guest interactions can be applied to a variety of systems, proving the utility of lignin as a nanomaterial in a biomedical setting.

3.9 Experimental

Materials. Kraft lignin (alkali lignin, low sulfur content, CAS 8068-05-1), methyl iodide, 1-iodobutane, 1-iododecane, benzyl bromide, 3-bromopropanoic acid, 6-bromohexanoic acid, 3-bromo-N,N,N-trimethyl-1-propanaminium, sodium iodide, potassium carbonate and solvents were purchased from Sigma-Aldrich and used without further purification. Alkyl iodides were prepared via the Finklestein reaction.[55] Syringe filters (25 mm syringe filter with a 0.45 μm polytetrafluoroethylene (PTFE) membrane, 13 mm syringe filter with a 0.20 μm PTFE membrane).

L-Bu Synthesis. Lignin (0.2 g, 1.1 mmol, 1 eq.), 1-iodobutane (0.7 g, 3.7 mmol, 3 eq.), and K_2CO_3 (2.0 g) were dissolved in DMSO (1.0 mL) and the reaction was conducted at 90^{o} C for 48 h. The reaction mixture was allowed to cool to room temperature and isopropyl alcohol or ethyl acetate (0.2 L) was added. The resulting solid was collected via vacuum filtration and washed with ethyl acetate, water, and ether (0.2 L aliquots of each). The solid was collected and freeze dried for two days yielding a light brown solid (193 mg, 74% yield). IR ν_{max} (cm^{-1}): 3068.7-3700, 2965.1, 2881.1, 1728.9, 1647.7,

1600.0, 1513.9, 1466.3, 1434.6, 1222.1, 1145.7, 1025.3, 955.1; ^{1}H NMR (500 MHz, DMSO-d_6) δ 0.50-0.95, δ 1.05-1.80, δ 3.40-4.10, δ 6.50-7.60.

L-Dec Synthesis. Lignin (2.0 g, 11 mmol, 1 eq.) 1-iododecane (6.0 g, 23 mmols, 2 eq.), and K_2CO_3 (2.0 g) were dissolved in DMSO (5.0 mL) and the reaction was conducted at 90 ^{o}C for 48 h. The reaction mixture was allowed to cool to room temperature and ethyl acetate (0.2 L) was added. The resulting solid was collected via vacuum filtration and washed with ethyl acetate, water, and ether (0.2 L aliquots of each). The solid was collected and freeze-dried for two days yielding a light brown solid (2.146 g, 60% yield). IR ν_{max} (cm^{-1}): 3100.0-3700.0, 2926.5, 2856.0, 1594.6, 1459.1, 1266.7, 1221.9, 1142.8, 1039.8, 863.8; ^{1}H NMR (500 MHz, DMSO-d_6) δ 0.70-0.85, δ 0.86-1.45, δ 3.40-4.20, δ 6.50-7.60.

L-Bn Synthesis. Lignin (1.0 g, 5.6 mmol, 1 eq.), benzyl bromide (0.72 g, 4.2 mmol, 0.75 eq.), and K_2CO_3 (1.0 g) were dissolved in DMSO (2.0 mL) and heated at 60 ^{o}C for 48 h. The reaction was allowed to cool to room temperature and ethyl acetate (0.2 L) was added. The resulting solid was filtered and washed with ethyl acetate, water, and ether (0.2 L aliquots of each). The solid was collected and freeze-dried for two days yielding a light brown solid (541 mg, 48% yield). IR ν_{max} (cm^{-1}): 3074.6-3700, 2953.7, 1700.0, 1600.0, 1500.0, 1458.1, 1426.4, 1268.4, 1219.9, 1147.1, 1084.5, 1037.2, 859.4, 747.1, 700.0; ^{1}H NMR (500 MHz, DMSO-d_6) δ 3.00-4.00, δ 6.50-7.50 (broad), δ 7.05-7.40, δ 7.40-7.55 (within broad peak).

L-PA Synthesis. Lignin (1.0 g, 5.6 mmol, 1 eq.), 3-iodopropanoic acid (2.2 g, 10.6 mmol, 2.0 eq.), and K_2CO_3 (1.0 g) were dissolved in DMSO (6.0 mL) and heated to 90 ^{o}C for 48 h. The resulting reaction mixture was poured into 1M HCl (0.2 L). The solid

was then collected via vacuum filtration and washed with water. The solid was freeze-dried for two days yielding a brown solid (472 mg, 40% yield). IR ν_{max} (cm^{-1}): 3074.6-3690.2, 2947.1, 1719.2, 1598.9, 1500.0, 1464.8, 1430.6, 1267.9, 1217.7, 1144.8, 1029.3, 950.4; ^{1}H NMR (500 MHz, DMSO-d_6) δ 0.60-1.40, δ 3.30-4.20, δ 6.50-7.65.

L-HA Synthesis. Lignin (0.5 g, 2.8 mmol, 1 eq.), 6-iodohexanoic acid (1.3 g, 5.4 mmol, 1.9 eq.), and K_2CO_3 (1.0 g) were dissolved in DMSO (3.0 mL) and heated to 90 ^{o}C for 48 h. The reaction was allowed to cool to room temperature and ethyl acetate was added (0.2 L). The solid was collected via vacuum filtration and washed with ethyl acetate. The solid was then stirred in excess ethanol and acidified to approximately pH 4 with 1M HCl. The resulting solid was collected and washed with water. The solid was then dried under vacuum to give a brown solid (100 mg, 13% yield). IR ν_{max} (cm^{-1}): 3000-3685.2, 2949.3, 1714.9, 1597.2, 1500.0, 1464.5, 1424.9, 1200.0, 1159.6, 1036.9; ^{1}H NMR (500 MHz, DMSO-d_6) δ 1.05-1.35, δ 1.40-1.60, δ 2.10-2.45, δ 3.50-4.10, δ 6.50-8.00.

L-PTMA Synthesis. Lignin (1.0 g, 5.6 mmol, 1 eq.), 3-iodo-N,N,N-trimethyl-1-propanaminium (2.4 g, 6.7 mmol, 1.2 eq.), K_2CO_3 (1.0 g) were dissolved in DMSO and heated at 90 ^{o}C for 17 days. The reaction mixture was then distilled to remove DMSO and the resulting solid was dissolved in 0.1 L of deionized water and loaded into a Spectra/Por Dialysis Membrane with a 10 mm diameter and 100-500 molecular weight cutoff (MWCO). The dialysis water (2.0 L) was changed twice a day for 3 days. The resulting solution was freeze-dried to give a brown solid (229.5 mg, 14% yield). IR ν_{max} (cm^{-1}): 3053.7-3698.9, 2965.0, 1587.6, 1386.7, 1200.0, 1153.6, 1042.0, 800.0; ^{1}H NMR (500 MHz, D_2O) δ 2.60-3.20, δ 3.40-4.35, δ 6.20-7.80.

Nanoparticle Preparation. A stock solution of L-Dec in DMSO at a mass/volume ratio of 10 mg/mL was prepared. The solution was then filtered through a 25 mm syringe filter with a 0.45 μm PTFE membrane. The resulting solution was then filtered through a 13 mm syringe filter with a 0.20 μm PTFE membrane to give the final solution without further purification.

Dynamic Light Scattering (DLS) Analysis. DLS measurements were taken on a Malvern Zetasizer Nano – ZS. Three μL of the final particle solution was diluted into 3.0 mL of H2O and the resulting solution was used directly for the measurement. Three independent samples were made and sized over 4h to give an average size and standard deviation for each. All DLS measurements were taken at a scattering angle of 173^{o} and a temperature of 25 ^{o}C. Disposable cuvettes were used to contain each of the DLS samples.

Electron Microscopy Analysis. Scanning Electron Microscopy (SEM) images were obtained using a FEI XL-30 Field Emission ESEM/SEM. Aluminum Electron Microscopy mounts were purchased from VWR. 25 mg of L-Dec was dissolved in 500 μL of DMSO and heated slightly. The solution was pushed through a 13 mm syringe filter with a 0.20 μm PTFE membrane. One hundred μL of the resulting solution was diluted into 4.0 mL of H2O and ran through a 25 mm syringe filter with a 0.45 μm PTFE membrane to give the final solution. Ten μL of this solution was then drop-cast on aluminum studs and allowed to dry overnight in a desiccator. The samples were finally sputter-coated with palladium and used directly in the SEM for imaging.

CHAPTER 4

Lignin Nanocontainers for Enhancing Optical Properties and Cellular Interactions of Fluorescent Dyes

4.1 Introductory Remarks: Applying Functionalized Lignin to Biological Systems

The modification of kraft lignin, with high phenolic –OH content, was completed through facile S_N2 reactions to generate chemically diverse biomaterials that are readily assembled into nanocontainers. Several hydrophobic and hydrophilic moieties were introduced through the formation of phenolic ethers. In aqueous solutions under surfactant-free conditions, these modified lignins assemble into nanospheres with mean radii ranging from 24 to 180 nm, depending on the identity of the chemical modification.[56] Only a handful of research groups have investigated lignin as a nanomaterial in a biological setting. Crestini *et. al.* used ultrasonication to take advantage of the complex structure of lignin and introduce more crosslinking. These particles were then applied to cells for cytotoxicity studies showing the particles are non-toxic to cells.[57] Yiamsawas *et. al.* used additional crosslinking agents along with added surfactant to produce hollow lignin nanocontainers for potential agricultural applications.[58]

The utility of these supramolecular assemblies of modified lignins is demonstrated in several applications. First, lignin nanocontainers are useful as imaging agents through the encapsulation of Cy dyes as model lipophilic compounds. The dyes were found to have greater solubility and photostability when complexed with neutral lignin derivatives containing long hydrocarbon chains. The assemblies generate biocompatible, fluorescent nanoparticles that can be visualized in live cell cultures. Modified lignin itself is not only non-toxic to cells, but also promotes cell growth and adhesion in untreated cell culture vessels. No leaching of the dye to lipophilic cell compartments is observed, however, its

slow release can be shown in solution when looking at octanol/water partitioning. Then, multiple Cy dyes with fluorescence resonance energy transfer (FRET) capability can be loaded into lignin nanocontainers giving potential for multichannel cell imaging. Next, dynamic encapsulation with lignin as a host for neuroactive compounds reverses the binding of an inhibitor of a monoamine transporter. Finally, specificity can be introduced into the lignin structure producing polymer-bioconjugates for targeted drug delivery. As it is widely available as a by-product of the pulp industry, the ability to tune the chemical properties of this inexpensive, renewable polymer towards specific supramolecular assemblies, makes lignin an attractive biomaterial in a variety of biomedical applications.

4.2 Static Encapsulation of Model Lipophilic Dyes

For many applications, a fluorescent dye should be stable under relevant conditions such as the presence of other reagents, common temperatures, and excitation under light for typical detection times. To investigate the ability of the alkylated lignin nanocontainers to house hydrophobic guest molecules, a commercially available, lipophilic Cy dye was chosen. Typically, these dyes need an organic co-solvent such as dimethyl formamide (DMF) or DMSO when used in biological media so that the dye will interact with the biological target before precipitation or aggregation. At higher concentrations, even the co-solvent is not enough to solubilize the dyes in aqueous solution. These properties make 1,1′-dioctadecyl-3,3,3′,3′-tetramethylindodicarbo-cyanine perchlorate (DiD C18 Cy5) a good candidate for encapsulation in modified lignin nanocontainers.

Cy dyes form non-fluorescent or weakly emissive aggregates in aqueous solution. These dye-to-dye aggregates are most commonly stacked dimers.[59] Sulfonated

derivatives with a net negative charge may be used but can have unfavorable interactions with positively charged cell structures.[60] The optical properties of Cy dyes have been studied extensively[61] and their high sensitivity to their chemical microenvironment, electronic interactions, as well as aggregation state,[62] makes them ideal probes to explore encapsulation as they can report this information through their UV-vis and emission spectra. PBS solutions of Cy5 alone, unmodified lignin + Cy5, **L-Bu** + Cy5, and **L-Dec** + Cy5 were prepared at a molar ratio of 1:4 (or 1:20 by mass); higher dye loadings showed electronic coupling between individual dye molecules resulting in hypochromicity (see Supporting Information Figure S25). The particles were subject to ambient light for 24 hours and absorbance measurements were taken every 2 hours over that time period. Lignin, **L-Bu**, and **L-Dec** derivatives were examined in complexes with DiD to test the hypothesis that with increasing lipophilicity of the modification, comes efficient encapsulation of the hydrophobic guest molecule.

Ultraviolet-visible (UV-vis) spectroscopy revealed a significant effect of the lignins on the optical transitions of DiD compared with the aqueous solution (Figure 4.1), with the most pronounced changes observed for **L-Dec**. The UV-vis spectrum of the **L-Dec** encapsulated dye closely resembles DiD in organic solutions, where little to no aggregation is present: the 0-0 vibrational band of the S_0-S_1 transition, centered at 660 nm, is the most prominent band and the 0-1 vibronic shoulder at 615 nm is easily distinguishable, as well. In aqueous solution, the hydrophobic DiD molecules form H-aggregates, which can be observed via their unique spectroscopic features, namely the appearance of a broad, blue-shifted band, centered at 550 nm, as well as a loss in intensity of transition at 660 nm. The transition at 610 nm is the most prominent, with ε

= 5.4 x 10^4 M^{-1} cm^{-1}. DiD in the presence of unmodified lignin exhibits much lower intensity at 550 nm, but the spectrum still shows weakening of the 660 nm peak (ε = 7.5 x 10^4 M^{-1} cm^{-1}), while DiD with **L-Bu** more closely resembles **L-Dec**, with very moderate attenuation of the 660 nm peak (ε = 1.2 x 10^5 M^{-1} cm^{-1}). From these UV-vis spectra, it is clear that the presence of lignin, especially alkylated lignins, can effectively encapsulate DiD and preserve the high molar absorptivity of the dye in its monomeric form.

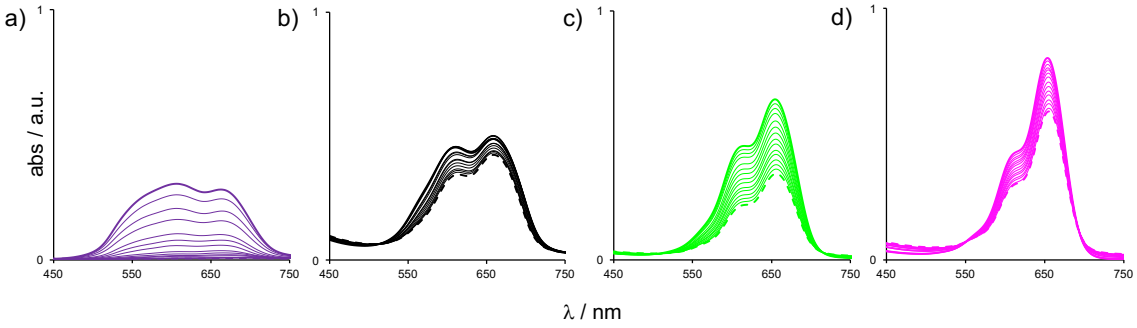

Figure 4.1. a) DiD in aqueous solution exists as H-aggregates as evidenced by the characteristic blue shift and broadening of the absorption spectrum. Rapid photobleaching of the H-aggregates occurs in solution. The addition of b) lignin, c) **L-Bu** and d) **L-Dec** shows less aggregation of the dye, with the H-band disappearing from the absorption spectrum across the lignin series.

The photosensitivity of Cy5 dyes has been described previously[63-64] and in the initial work with the encapsulated dye, some photobleaching was observed under ambient light. For example, after irradiation under 100-W mercury arc lamp for 95 seconds, Cy5 only retains 55% of its initial fluorescence. To obtain spectra of the unbleached, encapsulated dye, solutions were prepared and handled in low-light conditions and stored in the dark when not in use. With this in mind, the effect on the photostability of DiD after encapsulation in a lipophilic environment was studied (Figure 4.2). To determine the relative rates of bleaching of DiD, the solutions utilized for the UV-vis measurements

were allowed to sit under ambient light (fluorescent mercury vapor lamp, with a prominent 550 nm band) and the absorption values were taken at defined intervals. While DiD in aqueous solution saw 100% bleaching in 16 h, bleaching was limited to only 25% over 24 h in solution with **L-Dec**. DiD with **L-Bu** saw moderately increased bleaching (33%), while DiD with unmodified lignin was somewhat less. At 24 h, the ε values for DiD with **L-Bu** and unmodified lignin are the same, within experimental error ($\varepsilon = 6.6 \times 10^4$ and 6.1×10^4 M^{-1} cm^{-1}, respectively), while the **L-Dec** encapsulated dye showed approximately 50% higher ε value ($\varepsilon = 1.0 \times 10^5$ M^{-1} cm^{-1}). These results demonstrate that in addition to the effective encapsulation by lignin and alkylated lignins, the supramolecular assembly imparts a photoprotective effect on this Cy5 derivative.

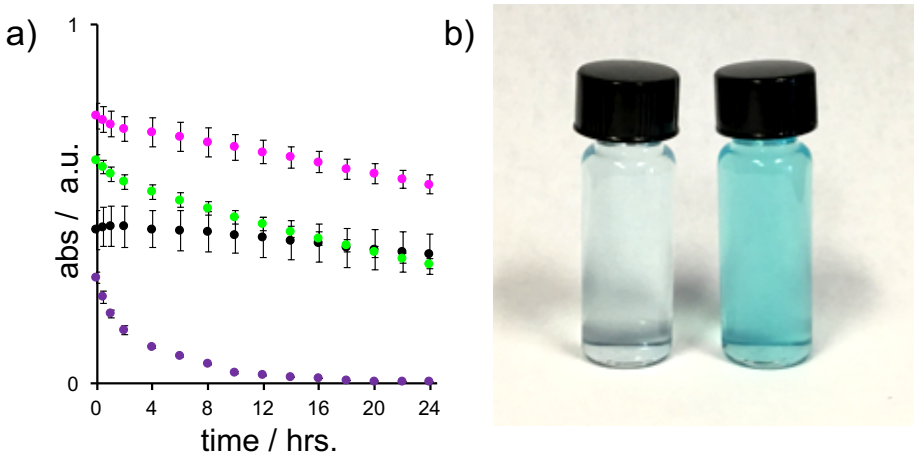

Figure 4.2. Along with decreased aggregation of the dye as shown by the absorbance spectra, photobleaching is markedly attenuated, demonstrating the photoprotective effect of the lignins (a). b) Comparison of DiD in aqueous solution (left) and with **L-Dec** (right) readily reveals the increased ε and stability of the encapsulated dye.

In addition to the enhanced molar absorptivity and photoprotective effects observed for DiD encapsulated in **L-Dec**, the lipophilic environment of the alkylated lignin also enhances the emission of DiD. Figure 4.3 shows the increase in fluorescence from DiD

moving from water alone, in which DiD is essentially non-emissive, to a ~2-fold increase with the addition of unmodified lignin, and more dramatic 35- and 75-fold in the presence of **L-Bu** and **L-Dec**, respectively. The attractive optical and physical properties of the L-Dec encapsulated DiD warranted further investigation of this supramolecular assembly as an imaging agent.

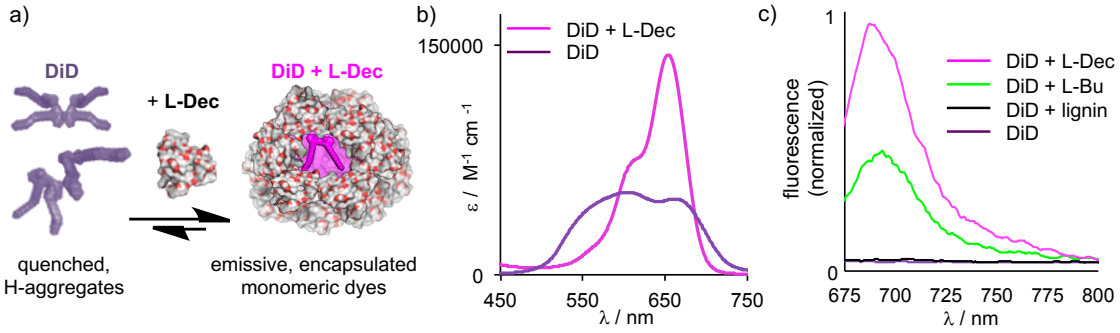

Figure 4.3. a) DiD, a hydrophobic cyanine dye, is effectively encapsulated in **L-Dec** nanocontainers with marked changes apparent in the optical spectra of the dye. b) H-aggregate formation in aqueous solution (purple line) results in diminished absorptivity and broadening of the UV-vis spectrum, however, encapsulation by **L-Dec** effectively insulates individual DiD molecules as the UV-vis spectrum reveals sharper and an increased S_0-S_1 optical transition. c) Increased emission intensity is also observed upon encapsulation in alkylated lignins.

4.3 Visualization of Modified Lignin-Dye Complexes in Live Cell Cultures

To evaluate the biocompatibility and stability of the assemblies, MCF-7 cells were exposed to solutions of **L-Dec**/DiD, then co-stained with Miami Green (nucleus)[65] and Cell Mask Deep Orange (cell membrane). The **L-Dec**/DiD assemblies were found to accumulate intracellularly, as shown in Figure 4.4, and showed no inhibition of cell growth or effect on cell morphology after 48 h of exposure, demonstrating the biocompatibility of the nanocontainers with cultured cells. Furthermore, even after prolonged staining times, the hydrophobic dye was not leached from the nanocontainers.

No dye was found to colocalize in the cell membrane, which could be expected given the lipophilic nature of DiD.

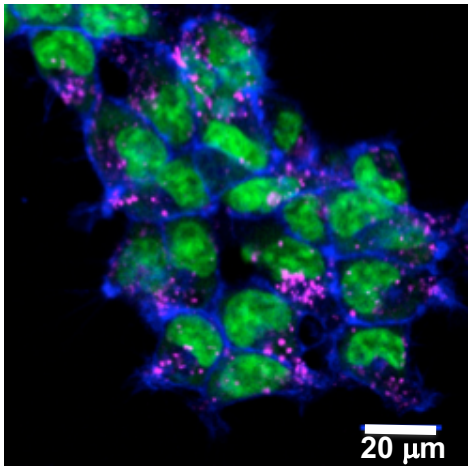

Figure 4.4. Increased emission intensity of Cy5 is observed upon encapsulation in modified lignin nanocontainers, which can be utilized to image the uptake of lignin nanoparticles in live MCF-7 cells. The complexes are internalized into cells and gather in the cytoplasm with no apparent cytotoxicity.

4.4 Cell Adherence and Growth in Modified Lignin-Coated Cell Culture Vessels

After imaging the uptake of lignin-dye complexes, no negative effect on cell growth, adhesion, or morphology was observed. Rather, these factors seemed to be promoted in the cell culture vessels containing modified lignin nanoparticles compared to the untreated flasks and plates. Historically, cell cultures were grown on glass surfaces such as glass flasks and petri dishes. Many cells experienced difficulty attaching to glass surfaces, specifically primary cell cultures or cells being recovered from frozen cultures. In addition, glass surfaces require extensive treatment to remove any unwanted residues that could interfere with essential cellular processes. This lead to the development of disposable cell culture vessels made from plastic in the form of flasks, dishes, and 96-well plates. Polystyrene was the popular choice because it can be easily molded,

sterilized by UV irradiation, and has optical clarity when imaging. However, the hydrophobic nature of the material and low "wettability" interferes with cell attachment and requires additional modification, i.e. oxidation, to produce a more hydrophilic surface.[66] This opened the door for researchers to expand the types of surfaces used in cell culture vessels to give the optimum conditions for culturing.

In the grand scope, understanding how tissues interact with biomaterials at the cellular level is important for the development of medical devices, implants, and biosensors. Polymers are the popular choice for fabricating these biomaterials owing to the ease of surface modification. The effect of wettability has been extensively studied by varying the surface functionality with hydroxyl, carboxylic acids, amines, esters, and other groups. The composition of functional groups can vary the charge and hydrophobicity/hydrophilicity which dictates the ability of cells to grow on that surface. Common polymers used are self-assembled monolayers (SAMs) of organosilanes[67], alkanethiols[68-70], conducting polymers[71], and linear polymers[72] with different terminal functional groups that can be extended from basic substituents to bioactive molecules such as nucleic acids, peptides, enzymes, and antibodies. Modified lignin becomes a viable option for surface coatings given its diverse chemical structure and ease of modification of the phenolic -OH position to tune wettability.

Four human cell lines; including HEK-293, MCF-7, BT-474, and HeLa, were grown in a 96-well, polystyrene, untreated plate. A 10 mg/mL solution of **L-Dec** was added to the cells in serum-free medium with final concentrations ranging from 100 ng/mL to 100 μg/mL. The cells were allowed to incubate for 24 hours before imaging on the confocal microscope. The increased stress on the cells should promote inhibition of cell growth,

and ultimately, apoptosis. However, the addition of **L-Dec** increases adherence and growth rate (Figure 4.5). In the absence of **L-Dec**, the cells do not grow to confluence, but at 1 μg/mL (1 μM) and 10 μg/mL (10 μM), coverage increases markedly. This demonstrates beyond a doubt that the modified lignins exhibit no toxicity and may actually promote cell growth through increased adhesion.

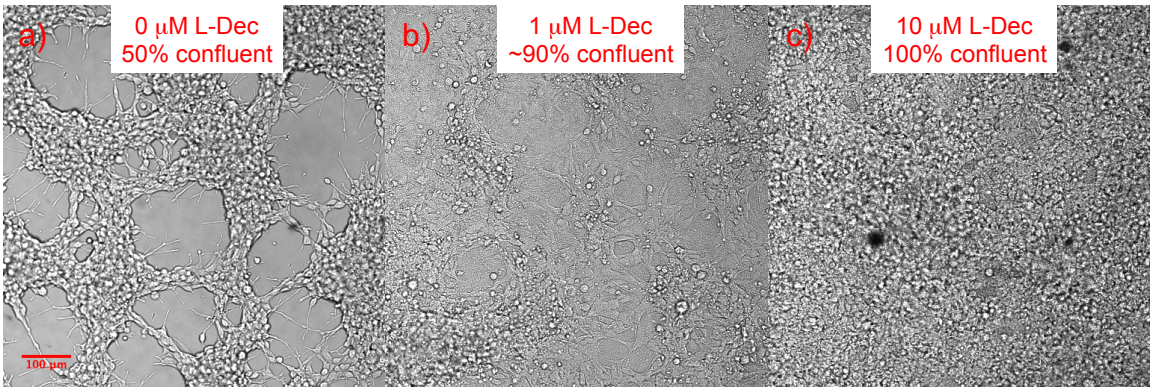

Figure 4.5. HEK-293 cells incubated in polystyrene, untreated cell culture vessels in serum-free medium have decreased cell adhesion and do not grow to confluence (a). With the addition of **L-Dec** at b) 1 μM and c) 10 μM, confluency noticeably increases proving that not only are modified lignins non-toxic to the organism but promote growth through increased adhesion to the vessel. This lack of inhibition is not surprising as lignin is an inert biopolymer with various functional groups that have been previously shown to promote cell growth and adhesion.

4.5 Octanol/Water Partitioning of Cy5 Loaded Lignin Nanocontainers

A partition coefficient is the ratio of concentration of a compound in two immiscible phases, ultimately a measure of solubility in those phases. For fluorescent dyes, the water solubility and octanol/water partition coefficient (K_{ow}) are important equilibrium constants and provide information on the affinity of the dyes to certain environments. This is useful in predicting the concentration and biodistribution of the dyes in an aqueous setting such as cell cultures or animal models.[73] For a hydrophobic dye such as

DiD Cy5 C18, the partition coefficient should be very high (>10^4) owing to its near insolubility in aqueous solution.[74] Cy5 loaded **L-Dec** nanoparticles show drastic changes in the release profile when going from a purely aqueous solution to a buffered solution (Figure 4.6). From the absorbance measurements in a buffered solution, the particles seem to be "flipping" to expose the lipophilic tails and moving from the aqueous to the organic phase along with the Cy5 dye. On the contrary, complexes in H_2O are highly stable and do not show any release of the dye into the octanol layer. This is certainly an effect of the ions in solution, however it is difficult to determine the exact ion producing this effect and it may be a combination of ions. Interestingly, the release to lipophilic compartments of the cell is not seen when incubating the particles in live cell cultures. This result suggests applications of the particles as stimulus-sensitive materials.

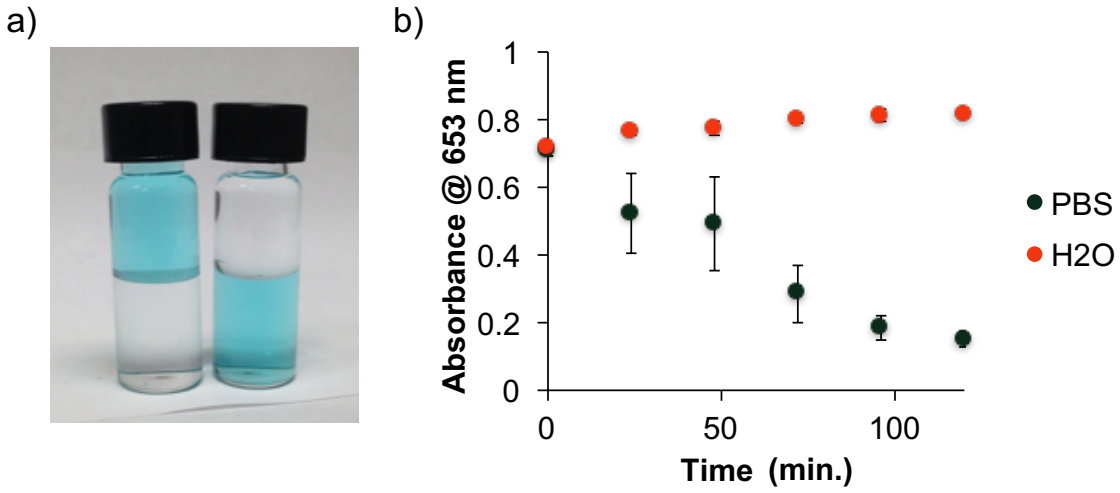

Figure 4.6. **L-Dec**/Cy5 complexes show severely different release profile in purely aqueous solution compared to a buffered solution (a). The complexes seem to invert, exposing the lipophilic decyl-substituents, moving to the octanol phase along with the dye. In water, however, the complexes are very stable and do not show any dye release

into the organic layer. This can be seen in the absorbance of the aqueous layer as it decreases in PBS but is consistent in H_2O (b).

4.6 Fluorescence Resonance Energy Transfer (FRET) Between Multiple Fluorophores Encapsulated in Modified Lignins

Previous encapsulation of hydrophobic fluorophores in the lipophilic cavity of modified lignins was successful with the host entrapping one guest molecule. This interaction can be expanded to capturing multiple guest species in one nanocontainer. A fluorescent molecule in the excited state can transfer its energy to a nearby molecule, non-radiatively deactivating the molecule. This molecule, the donor, will have no fluorescence emission, however, will populate the excited state of the proximal molecule, the acceptor. By transferring the excited state energy of the donor, the fluorescence emission of the acceptor will be observed. This process, referred to as fluorescence resonance energy transfer (FRET), can only be completed if there is significant overlap of the emission of the donor and absorbance of the acceptor. Also, the distance between the interacting fluorophores is very important where efficiency of energy transfer will decrease with increasing distance until the threshold is reached (~10 nm) and no energy transfer is observed. The idea of bringing two fluorescent probes in close promixity to one another by constricting their movement to the interior of a nanoparticle has been studied previously[75-76] and can assess the stability of the nanoparticle complex in a variety of conditions. This model can be applied to drug delivery for monitoring the release of hydrophobic drugs[77] or the conversion of prodrug to drug.[78]

L-Dec/dye complexes were prepared as described previously, but in either binary or ternary mixtures. Three Cy dyes; DiO, DiI, and DiD, have excellent spectral overlap and can participate in FRET (Figure 4.7d). The solutions were excited at wavelengths that

correspond to laser lines on a typical confocal microscope. In the binary **L-Dec**/DiO/DiI mixture (Figure 4.7a), excitation at 458 nm is within the absorbance band for DiO. After energy transfer, the emission of DiI at ~565 nm is observed. Exciting at 533 nm, within the absorbance of both molecules, or at 561 nm, promoting DiI, gives the same emission wavelength. Similar results are obtained with the **L-Dec**/DiI/DiD complex (Figure 4.7b) where the emission of DiD, with the lowest energy emission, is detected. Finally, the ternary mixture of **L-Dec**/DiO/DiI/DiD can be excited at 458 nm, well outside of the absorbance band of DiD, and the only emission produced is from DiD, emitting at ~660 nm (Figure 4.7c). The FRET between guest molecules in modified lignin is very efficient in solution but the same results are not obtained when moving into live cell cultures. This result gives insight into the stability of the superstructures in a complex environment such as the cell. The nanocontainers can encapsulate and protect a single guest species, as seen in the cell imaging of the **L-Dec**/DiD. However, these macromolecular architectures are not able to maintain their integrity and keep guest molecules in a tight space shown by the lack of FRET between molecules.

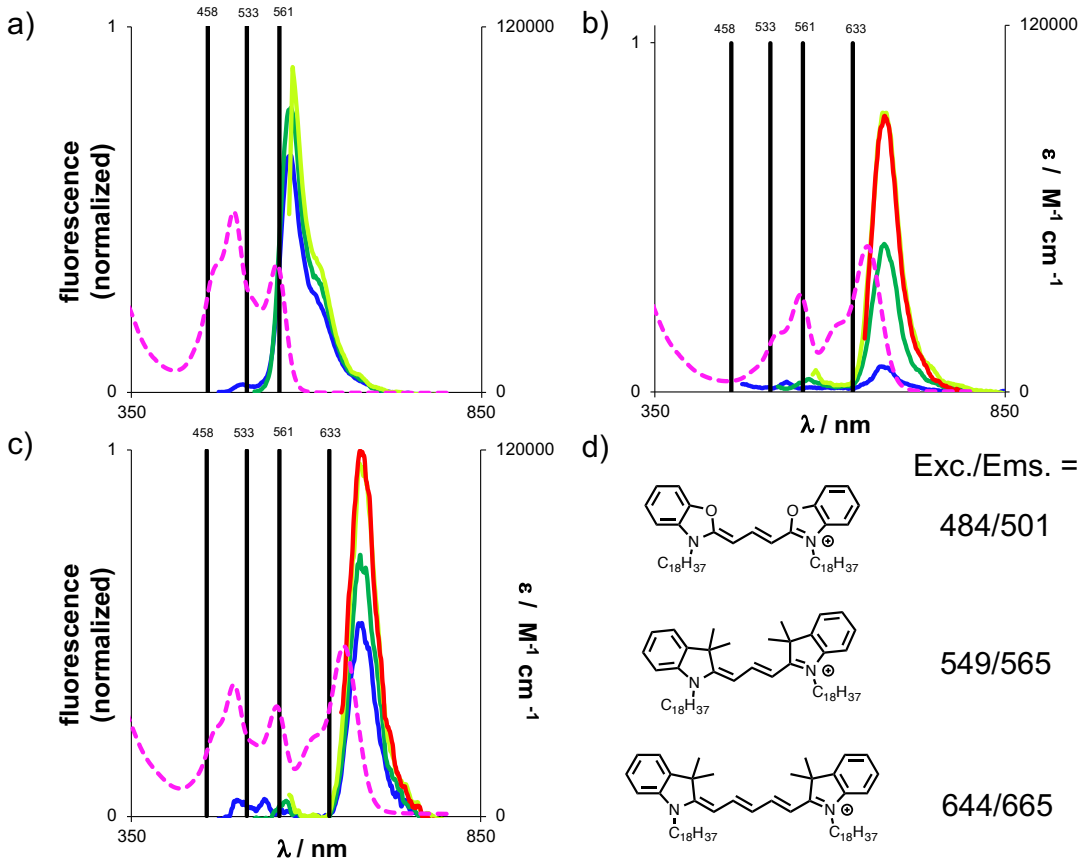

Figure 4.7. Multiple fluorescent cargo can be encapsulated within one modified lignin nanocontainer. The interaction can be followed by looking at the FRET between guest molecules. a) Binary mixture of DiO and DiI can be excited at 3 different wavelengths and show the same emission, regardless of the excitation wavelength. The same results can be seen when using two dyes that have a bathochromic shift in absorbance and emission, as with the DiI/DiD binary mixture (b). A ternary mixture (c) of fluorescent dyes can also participate in FRET where irrespective of excitation wavelength, the lowest energy emission of the reddest dye is observed.

4.7 Dynamic Encapsulation of Fluorescent NET Inhibitors

In addition to static encapsulation, the ability of a modified lignin to dynamically encapsulate guests in a biologically-relevant context in aqueous solution was investigated. While the stable **L-Dec**/DiD structures required the use of organic solvents to mix the lipophilic dye through dilution of the organic solution into aqueous media,

dynamic encapsulation of guest molecules in a purely aqueous system could prove useful for the removal of environmental contaminants, toxins or other bioactive molecules. Therefore, the interaction of the anionic **L-PA** with a cationic ligand for the norepinephrine transporter (NET), a transmembrane Na+/Cl-dependent transporter that is the target of both recreational and therapeutic drugs, was explored. To monitor binding to this important drugable target, several "turn-on" fluorescent dyes were developed that increase photoemission when bound to the active transport site of NET.[16-17] Treatment of NET-overexpressing HEK-293 cells with di-ASP$^+$ results in binding to NET at the cell membrane and concomitant turn-on emission,[17] visible in Figure 4.8. Subsequent treatment of the cells with a more potent NET inhibitor can result in displacement of the fluorescent reporter and subsequent loss of emission at the cell membrane. At physiological pH, the -COOH groups of **L-PA** should be deprotonated, resulting in an overall anionic structure that still possesses a relatively hydrophobic core. It was hypothesized that the amphiphilic nature of this macromolecule would allow it to interact with di-ASP$^+$, forming a supramolecular complex that would limit di-ASP$^+$ binding to NET-expressing cells. Indeed, addition of **L-PA** following di-ASP$^+$ treatment resulted in loss of emission at the cell membrane, demonstrating the ability of **L-PA** to effectively associate with di-ASP$^+$ and sequester it from solution. The formation of a supramolecular complex involving a neuroactive compound can be utilized in a biomedical context. The action of rocuronium, a muscle relaxant utilized during anaesthesia, can be reversed through the administration of sugammadex, a chemically modified γ-cyclodextrin. In this context, **L-PA** serves as a model compound for complexing NET-targeted drugs, such as cocaine and synthetic derivatives.

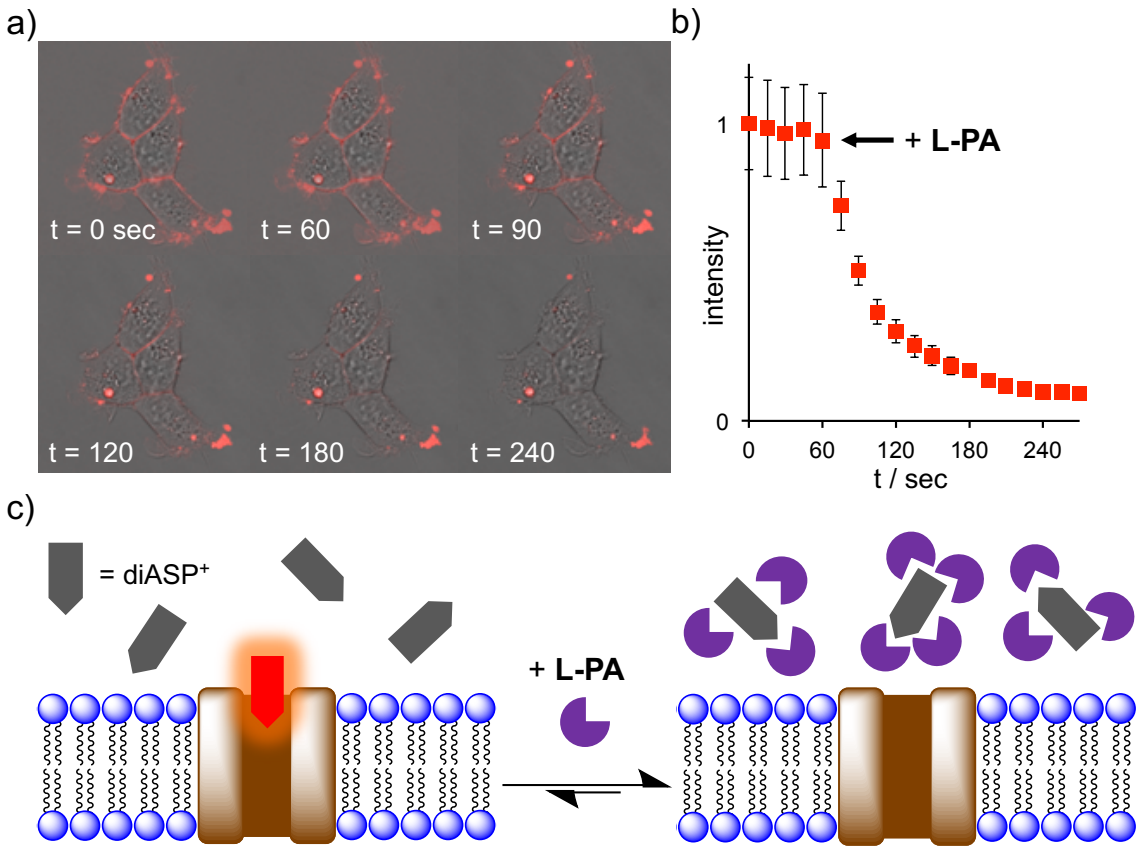

Figure 4.8. L-PA effectively sequesters a cationic inhibitor of the norepinephrine transporter (NET). a) The fluorescent ligand binds to the membrane bound transporter, b) but the addition of L-PA, at t = 60 s, results in a rapid decrease of the emission intensity as di-ASP$^+$ is encapsulated and removed from solution. c) Cartoon representation of di-ASP$^+$ binding to NET and encapsulation by L-PA.

4.8 Cell-Specific Targeting with Biotin-Conjugated Lignin

Target-specific drug delivery is a highly desired method in medicine to overcome the pitfalls of traditional therapies. By increasing therapeutic agent concentration through specific interactions in target tissues, drug efficacy is increased, normal cells remain intact, and side effects are reduced. There are many promising targets in anticancer therapies that take advantage of the physiological differences between healthy cells and tumor cells. One of which is the over-expression of biotin-selective transporters on the

surface of tumor cells.[79] Biotin, commonly known as vitamin-B_7, is an important molecule in cell processes such as growth, fatty acid production, and metabolism of amino acids. The biosynthetic pathway for biotin production is non-existent in mammals, therefore it must be acquired from outside sources such as peanuts, leafy-green vegetables, and egg yolks. There are two transport systems for biotin: a high-affinity biotin transporter (<10 nM) and a sodium-dependent multivitamin transporter (SMVT) (>10 μM). Given its low affinity for biotin along with high expression levels across many tissues and competitive uptake of other vitamins, SMVT is responsible for biotin uptake into cells. This is especially important because cancer cells have higher SMVT expression and biotin uptake ability.[79] By conjugating the biotin moiety onto a carrier molecule, as a biologically relevant ligand, a long sought-after target-specific drug delivery system is feasible.

After studying the reactivity of lignin, substitution reactions can tolerate the vast majority of functional groups. With this in mind, propargyl groups were introduced for further modification through copper-catalyzed azide-alkyne cycloaddition (CuAAC) reactions (Scheme 4.1).[80] This 1,3-dipolar cycloaddition, deemed "click chemistry", is a well-studied reaction that is high-yielding, wide in scope, easy to purify, and conducted in benign, environmentally friendly solvents. Though the synthesis has been known for over a decade, its use to modify lignin is relatively new. Chung and co-workers recently reported the extension of the lignin polymer through CuAAC to create a new mechanical polymer with self-healing properties.[81] The reaction was monitored through FT-IR tracking the disappearance of the typical azide band. ^{1}H-NMR was not reported for the final product following the cycloaddition reaction. Using these reaction conditions, with

slight adjustments, lignin derivatives with potential sensing molecules on the surface for biomedical applications can be synthesized and fully characterized.

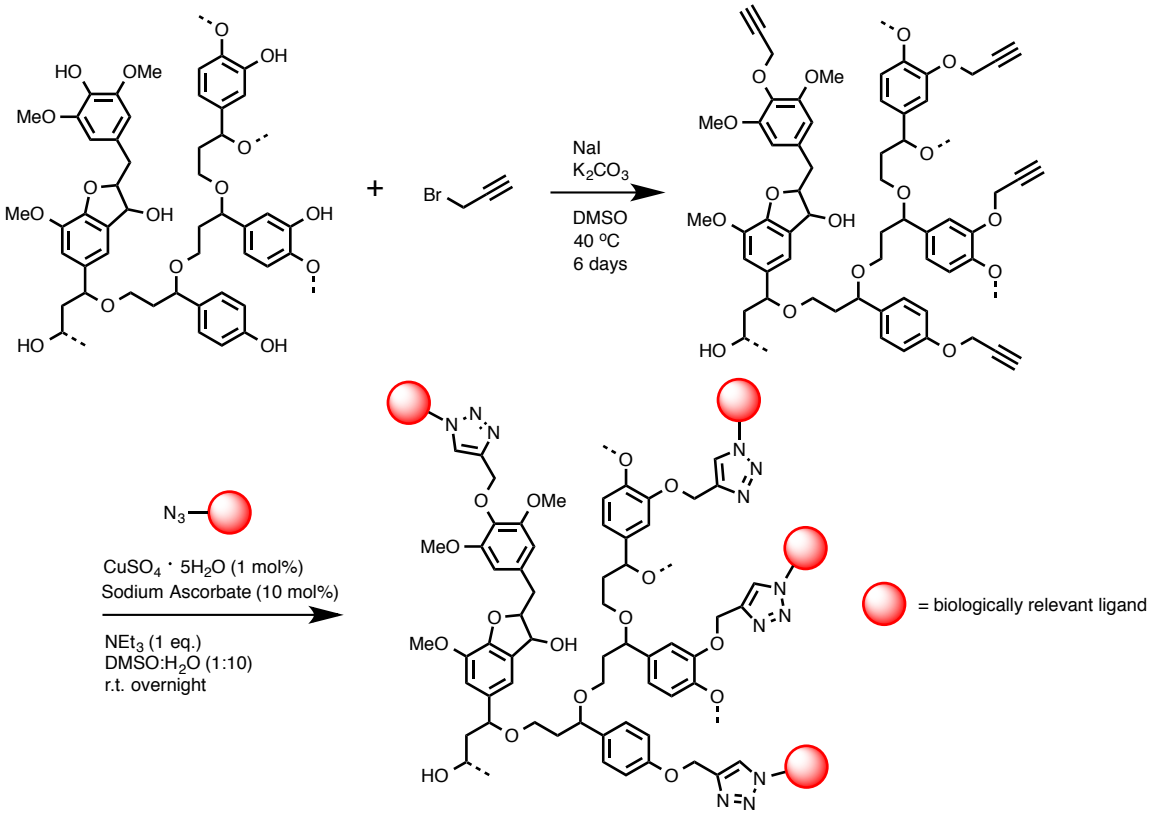

Scheme 4.1. Propargyl groups were appended to kraft lignin using S_N2 reaction conditions previously developed. This introduces a reactive handle for further modification via copper-catalyzed azide-alkyne cycloaddition (CuAAC) "click" chemistry. In this way, biologically relevant ligands can decorate the surface of the macromolecule for targeted delivery.

Currently, tailored reaction conditions and characterization of one lignin derivative with biotin as a promising sensing molecule on the surface for cell-specific targeting and delivery was completed. This is an improvement upon the earlier work where lignin nanoparticles non-specifically interacted with cells. Using developed methods, a terminal alkyne was successfully introduced into the lignin structure through substitution at the phenolic hydroxyl position. This modification was confirmed through multiple

spectroscopic techniques. ^{1}H-NMR clearly shows a new methylene peak at ~4.64 ppm and a peak at 2.54 ppm corresponding to the alkynyl proton (Figure 4.9). IR revealed a peak at 3309 cm^{-1} that is consistent with C-H sp stretching (Figure 4.11, red line). DLS was also conducted resulting in two particle size populations of 21.4 ± 6.50 nm and 278.2 ± 130.70 nm (see Supporting Information Figure S26).

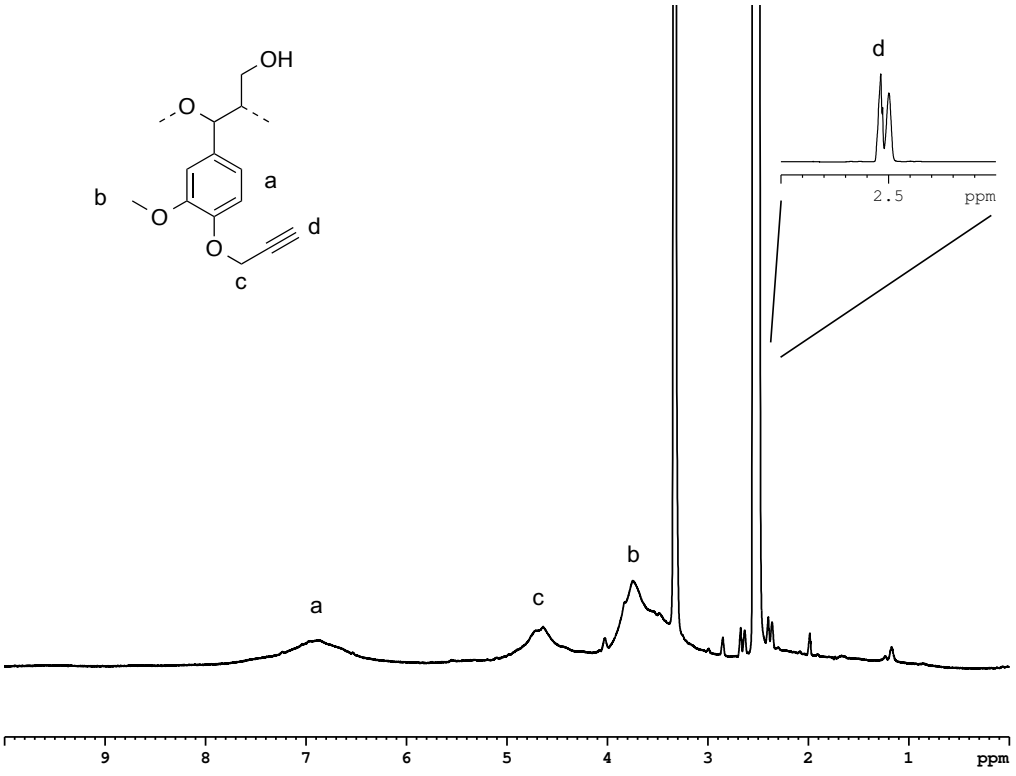

Figure 4.9. ^{1}H-NMR of propargylated lignin. The appearance of a peak at ~2.5 ppm represents the alkynyl proton and a new peak centered at ~4.6 ppm for the methylene group of the phenoxy ether confirm the structural change.

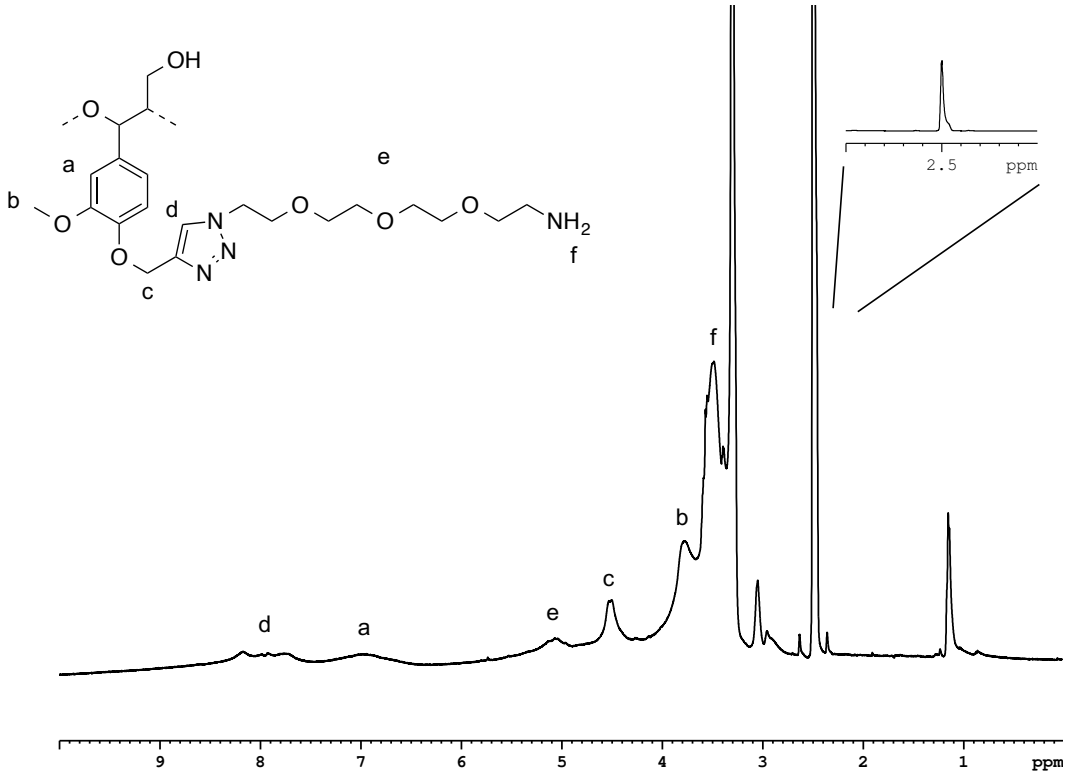

Figure 4.10. Cycloadduct of propargyl lignin and azido-PEG3-amine building block ^{1}H-NMR spectrum. The signal for the alkynyl proton has disappeared and new peaks corresponding to the free amine (3.6 ppm), PEG methylene groups (5.1 ppm), and triazole proton (7.6-8.3 ppm) prove a successful CuAAC reaction.

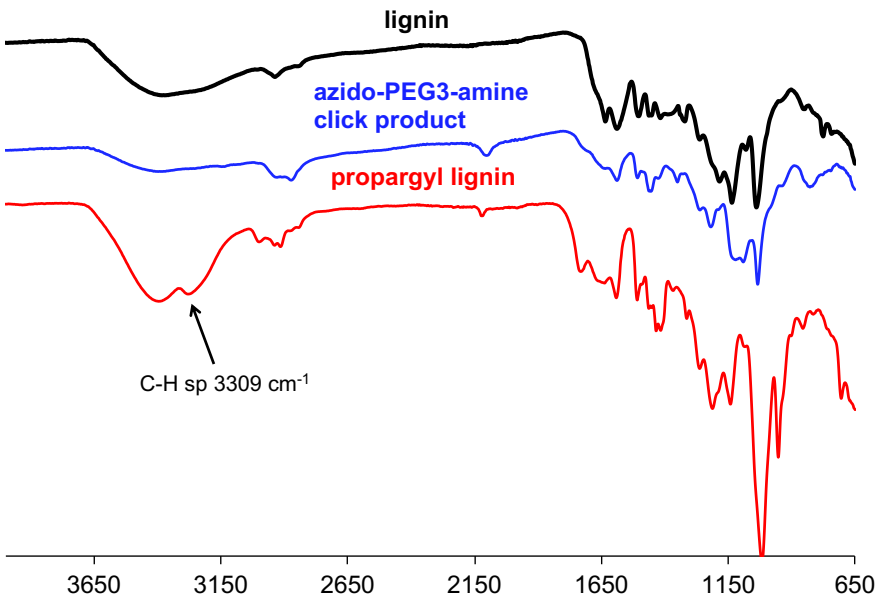

Figure 4.11. IR spectra of unmodified lignin (black), propargyl lignin (red), and the azido-PEG3-amine click product (blue). Upon modification, C-H sp stretching at 3309 cm^{-1} is clear and after the CuAAC reaction, the band vanishes.

Once the alkyne functional group was added to the native lignin structure, further modification was possible via CuAAC. As a starting point, a commonly used polyethylene glycol (PEG) spacer with a terminal azide and flanking amine was reacted with the alkynylated lignin. This product was fully characterized and new peaks in both the ^{1}H-NMR (Figure 4.10) and IR (Figure 4.11, blue line) proved that the CuAAC reaction was successful. The disappearance of the C-H sp proton in the NMR as well as the stretch in the IR confirmed the cyclization of the alkyne with the azide to give the triazole ring. There is also a new peak in the aromatic region, from 7.6-8.3 ppm, corresponding to the proton of the triazole ring. Other peaks matching the methylene groups of the PEG chain as well as the protons of the terminal amine are evident, centered at 5.1 and 3.6 ppm, respectively. These reaction conditions were then utilized with an azido-PEG3-biotin conjugate to functionalize the surface of the lignin

nanoparticle with biotin molecules. Again, ^{1}H-NMR was used to monitor the reaction and confirmed the presence of the biotin structure incorporated into lignin (Figure 4.12).

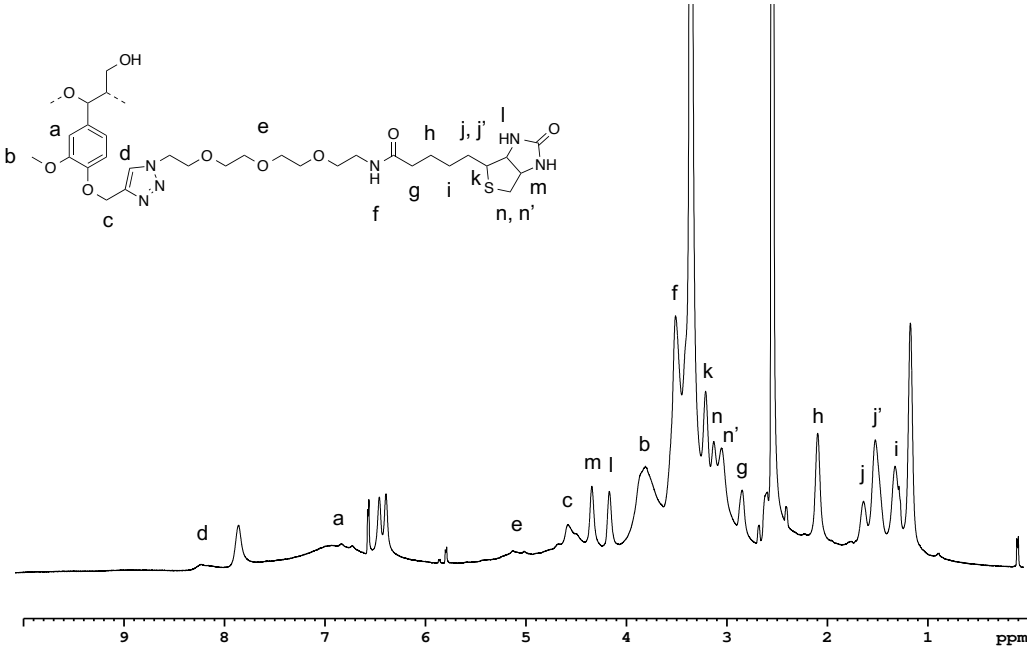

Figure 4.12. ^{1}H-NMR spectrum of biotin-conjugated lignin. Similar peaks from the azido-PEG3-amine click reaction (a-f) are also seen here and new peaks corresponding to the biotin moiety are evident in the aliphatic and ether region. Signals at 4-4.5 ppm represent the protons of the fused ureido (tetrahydroimidizalone) and tetrahydrothiophene rings. Protons on the tetrahydrothiophene ring can be seen from 3-3.3 ppm and methylene protons on the pentyl spacer are apparent from 1-3 ppm.

Cell lines that overexpress biotin receptors have not only been identified, but the degree of expression is also known. Two cell lines, MCF-7 and HEK-293, that are biotin positive and biotin negative, respectively, were used to determine the selectivity of the particles. Figure 4.13 shows biotinylated lignin nanoparticles loaded with Cy5 dye accumulating intracellularly in MCF-7 cells. This human breast cancer cell line is biotin receptor (+) with a high degree of expression compared to other cell lines expressing the

biotin receptor. In comparison, HEK-293 cells, a biotin receptor (-) cell line, does not uptake the same nanoparticles. These results are encouraging as a proof-of-concept system, although lacking in reproducibility. The modified lignin nanoparticles can be selective in target-specific delivery and this system can be optimized with a better targeting moiety that has a higher affinity for its receptor.

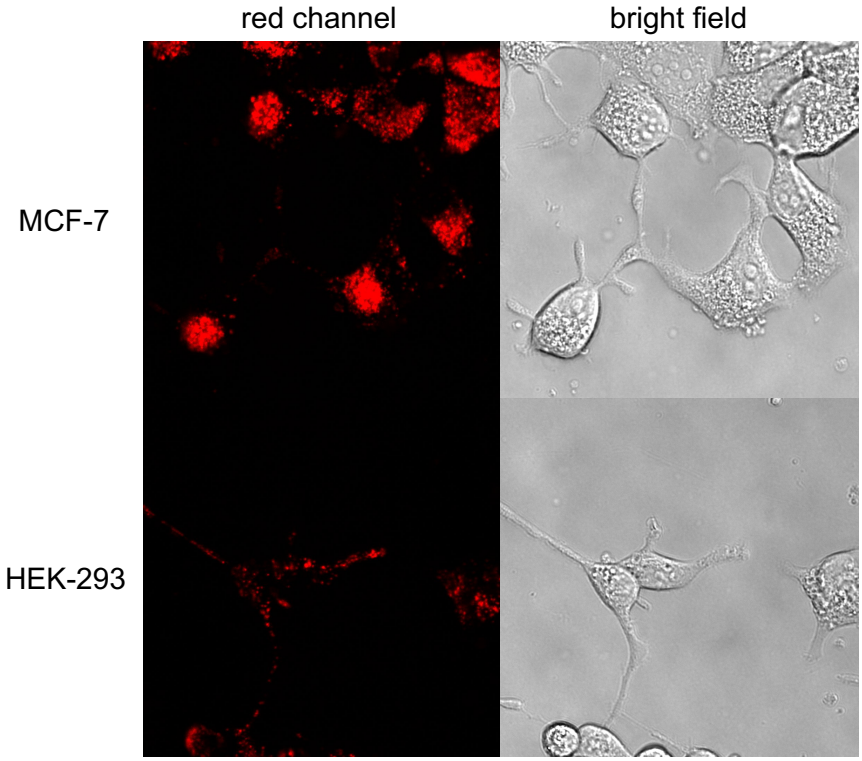

Figure 4.13. MCF-7 and HEK-293 cells incubated with dye-loaded biotin-conjugated lignin nanoparticles show modest differences in fluorescence intensity when visualized under the confocal microscope. MCF-7, with high biotin-receptor expression, readily uptakes the particles which accumulate in the cytoplasm and do not penetrate the nucleus. The same effect is not seen in HEK-293 cells with no biotin receptor expression. This is a promising result for the development of targeted lignin nanoparticles.

4.9 Conclusion

The utility of kraft lignin, as a highly crosslinked scaffold, with slight structural modifications was explored in a number of biological applications. It was demonstrated

that lignins possessing lipophilic groups exhibit a photoprotective effect on hydrophobic cyanine dyes, as well as enhance the overall brightness of the dyes in aqueous solution. The neutral derivatives complexed with the Cy dye can be imaged in live cell cultures, proving the biocompatibility of lignin as a nanomaterial. Not only is this inert polymer non-toxic to the organism, but it promotes cell growth through increased adhesion to the culture vessel. From the cell imaging results, the complexes are stable and do not release the dye to the lipophilic sub-compartments of the cell. This is not the case, however, when looking at the stability in purely aqueous solutions compared to buffered solutions. Leaching of the dye to the organic layer is increased in ionic solutions showing the potential as a slow-release delivery system. Mulitple guest molecules can be encapsulated by modified lignin and their interaction can be monitored by FRET. The nanoparticles are stable in solution but cannot maintain the close proximity of the fluorescent cargo in the complex cell environment. Dynamic encapsulation is also possible with ionic lignins which can be useful in sequestering toxins and bioactive molecules. In this sense, lignin with carboxylate moieties can interact with cationic ligands, effectively turning-off emission of fluorescent, NET-binding dye. Finally, specificity can be introduced into the lignin structure using developed syntheses. “Click” chemistry is an efficient way to decorate the lignin nanoparticles with targeting moieties for site-specific drug delivery, with one example being biotin. These applications speak to the potential of modified lignins as functional biomaterials with tunable properties for imaging and biomedical applications.

4.10 Experimental

Materials. Reagents and solvents were purchased from Sigma-Aldrich and used without further purification. Cyanine dyes, 1,1′-dioctadecyl-3,3,3′,3′-tetramethylindodicarbocyanine perchlorate (Cat. D307, 'DiD′ oil; $DiIC_{18}(5)$ oil), (Cat. D282, 'DiI'; $DiIC_{18}(3)$), and 3,3'-dioctadecyloxacarbocyanine perchlorate (Cat. D275, 'DiO';$DiOC_{18}(3)$) were purchased from Life Technologies. Syringe filters (25 mm syringe filter with a 0.45 μm polytetrafluoroethylene (PTFE) membrane, 13 mm syringe filter with a 0.20 μm PTFE membrane).

Nanoparticle Preparation. A stock solution of L-Dec in DMSO at a mass/volume ratio of 10 mg/mL was prepared. The solution was then filtered through a 25 mm syringe filter with a 0.45 μm PTFE membrane. The resulting solution was then filtered through a 13 mm syringe filter with a 0.20 μm PTFE membrane to give the final solution without further purification.

Optical Spectroscopy. UV-Vis spectra were acquired using a Perking Elmer Lambda 35 UV-Vis Spectrometer. The final concentration of polymer and dye in each solution was 100 μg/mL and 50 μg/mL, respectively. Fluorescence spectra were obtained using a Perkin Elmer LS 55 Fluorescence Spectrometer. At a dye:polymer ratio of 1:2, the 10 mg/mL stock solution of polymer (~2 mM, based on reported MW of kraft lignin) and the 1 mg/mL stock solution of dye (1 mM) were mixed and heated slightly. The solution was diluted with PBS and brought to a final volume of 4 mL.

Propargyl Lignin Synthesis. Lignin (1.06 g, 5.8 mmol, 1 eq.), propargyl bromide (1.33 g, 11.2 mmol, 2 eq.), NaI (0.45 g, 3 mmol, 0.5 eq.), and K_2CO_3 (0.5 g) were dissolved in DMSO (3.0 mL) and the reaction was conducted at 40^{o} C for 6 days. The reaction

mixture was allowed to cool to room temperature and ethyl acetate (0.2 L) was added. The resulting solid was collected via vacuum filtration and washed with ethyl acetate and water (0.2 L aliquots of each). The solid was collected and dried under vacuum for two days yielding a light brown solid (1.209 g, 93% yield). IR ν_{max} (cm^{-1}): 3647-3291, 3288-3061, 2987-2803, 2118; ^1H NMR (500 MHz, DMSO-d_6) δ 2.51, δ 3.5-4.0, δ 4.4-5.0, δ 6.50-7.60.

Lignin-triazolyl-PEG3-amine Synthesis. Propargyl lignin (2.5 mg, 0.046 mmol, 1 eq.) was dissolved in DMSO:H_2O (1:10 by volume). Azido-PEG3-amine (12 mg, 0.055 mmol, 1.2 eq.) and NEt_3 (6 μL) were added. Sodium ascorbate (228 mg, 0.012 mmol, 25 mol%) was next added followed by $CuSO_4$ ($5H_2O$) (30 mg, 0.0012 mmol, 2.5 mol%). The reaction was allowed to stir slowly overnight at room temperature. The resulting mixture was diluted into DI H_2O (<20% DMSO) and added to dialysis tubing (MWCO 100-500 Da). Dialysis was conducted for 3 days with more frequent changing of the dialysis water on day 1 (~every 2 hours), then changing twice a day. The solution was then freeze-dried for 2 days yielding a light-brown solid (120 mg, 48% yield). ^1H NMR (500 MHz, DMSO-d_6) δ 3.35-3.6, δ 3.6-4.1, δ 4.25-4.7, δ 4.9-5.35, δ 6.5-7.5, δ 7.5-8.4.

Lignin-triazolyl-PEG3-biotin Synthesis. Propargyl lignin (10 mg, 0.0450 mmol, 1 eq.) was dissolved in DMSO:H_2O (1:3 by volume). Azido-PEG3-biotin (10 mg, 0.0225 mmol, 0.5 eq.) and NEt_3 (6 μL) were added. Sodium ascorbate (~1 mg, 10 mol%) was next added followed by $CuSO_4$ ($5H_2O$) (~1 mg, 1.0 mol%). The reaction was allowed to stir slowly overnight at room temperature. The resulting mixture was diluted into DI H_2O (<20% DMSO) and added to dialysis tubing (MWCO 100-500 Da). Dialysis was conducted for 3 days with more frequent changing of the dialysis water on day 1 (~every

2 hours), then changing twice a day. The solution was then freeze-dried for 2 days yielding a light-brown solid (4.4 mg, 30% yield). ^{1}H NMR (500 MHz, DMSO-d_6) δ 1.29, δ 1.50, δ 1.61, δ 2.05, δ 2.84, δ 3.05, δ 3.15, δ 3.20, δ 3.50, δ 3.6-4.0, δ 4.1, δ 4.3, δ 4.35-4.7, δ 4.8-5.2, δ 6.5-7.5, δ 7.5-8.4.

Cell Culture. HEK293, HEK-NET, MCF7, BT474, and HeLa cells were maintained in DMEM (Dulbecco's Modification of Eagle's Medium) or RPMI (Roswell Park Memorial Institute) with 4.5 g/L glucose, L-glutamine and sodium pyvuate containing 10% dialyzed FBS, 2mM glutamine, 100 units/mL penicillin, 100 µg/mL streptomycin, and 250 µg/mL geneticin (in the case of HEK-NET) at 37 ^{o}C and 5% CO_2. Cells were seeded at a density of 10^5 cell/cm^2 in 96 microwell plates and incubated for atleast 48 hours until a visible monolayer was established. Prior to imaging, DMEM was removed and PBS was added to each well. Cells maintained a normal morphology during the course of the experiment (max. 1) and remained adhered to the imaging plate.

Confocal Microscopy. Imaging was performed on a Leica SP5 confocal microscope housed within the University of Miami Biology Imaging Core Facility. Excitation was achieved using 405, 458, 533, 561, or 633 nm lasers. Images were analyzed using Fiji/ImageJA software.

REFERENCES

1. Valeur, B. *Molecular Fluorescence: Principles and Applications*. Wiley-VCH: Weinheim. **2002**.

2. Lakowicz, J.R. *Principles of Fluorescence Spectroscopy*. Springer: New York. **2006**.

3. Sinkeldam, R.W.; Greco, N.J.; Tor, Y. Fluorescent Analogs of Biomolecular Building Blocks: Design, Properties, and Applications. *Chem. Rev.*, **2010**, 110, 2579-2619.

4. Haidekker, M.A.; Nipper, M.; Mustafic, A.; Lichlyter, D.; Dakanali, M.; Theodorakis, E.A. Dyes with Segmental Mobility: Molecular Rotors. *Advanced Fluorescence Reporters in Chemistry and Biology I: Fundamentals and Molecular Design*. **2010**, 8, 267-308.

5. LeVine, M.V.; Cuendet, M.A.; Khelashvili, G.; Weinstein, H. Allosteric Mechanisms of Molecular Machines at the Membrane: Transport by Sodium-Coupled Symporters. *Chem. Rev.* **2016**, 116, 6552-6587.

6. Coleman, J.; Green, E.M.; Gouaux, E. X-ray Structures and Mechanism of the Human Serotonin Transporter. *Nature* **2016**, 532, 334-339.

7. Gabrielsen, M.; Sylte, I.; Dahl, S.G.; Ravna, A.W. A Short Update on the Structure of Drug Binding Sites on Neurotransmitter Transporters. *BMC Res Notes* **2011**, 4, 559-563.

8. Blakely, R.D.; DeFelice, L.J.; Hartzell, H.C. Molecular Physiology of Norepinephrine and Serotonin Transporters. *J. Exp. Biol.* **1994**, 196, 263-281.

9. Arango, V.; Underwood, M.D.; Boldrini, M.; Tamir, H.; Kassir, S.A.; Hsiung, S.; Chen, J.J.; Mann, J.J. Serotonin 1A Receptors, Serotonin Transporter Binding and Serotonin Transporter mRNA Expression in the Brainstem of Depressed Suicide Victims. **2001**, 25, 892-903.

10. Beikmann, B.S.; Tomlinson, I.D.; Rosenthal, S.J.; Andrews, A.M. Serotonin Uptake is Largely Mediated by Platelets Versus Lymphocytes in Peripheral Blood Cells. **2013**, 4, 161-170.

11. Schwartz, J.W.; Blakely, R.D.; DeFelice, L.J. Binding and Transport in Norepiephrine Transporters: Real-time, Spatially Resolved Analysis in Single Cells Using a Fluorescent Substrate. *J. Biol. Chem.* **2003**, 278, 9768-9777.

12. Gubernator, N.G., Zhang, H.; Staal, R.G.; Mosharov, E.V.; Pereira, D.B.; Yue, M.; Balsanek, V.; Vadola, P.A.; Mukherjee, B.; Edwards, R.H.; Sulzer, D.; Sames, D. Fluorescent False Neurotransmitters Visualize Dopamine Release from Individual Presynaptic Terminals. *Science* **2009**, 324, 1441-1444.

13. Schwartz, J.W.; Novarino, G.; Piston, D.W.; DeFelice, L.J. Substrate Binding Stoichiometry and Kinetics of the Norepinephrine Transporter. *J. Biol. Chem.* **2005**, 280, 19177-19184.

14. Brown, A.S.; Bernal, L.; Micotto, T.L.; Smith, E.L.; Wilson, J.N. Fluorescent Neuroactive Probes Based on Stilbazolium Dyes. *Org. Biol. Chem.* **2011**, 9, 2142-2148.

15. Wilson, J.N.; Brown, A.S.; Babinchak, W.M.; Ridge, C.D.; Walls, J.D. Fluorescent Stilbazolium Dyes as Probes of the Norepinephrine Transporter: Structural Insights into Substrate Binding. *Org. Biol. Chem.* **2012**, 10, 8710-8719.

16. Smith, E.L.; Brown, A.S.; Adjaye-Mensah, E.; Wilson, J.N. Probing the Functional Limits of the Norepinephrine Transporter with Self-reporting, Fluorescent Stilbazolium Dimers. *Org. Biol. Chem.* **2012**, 10, 1493-1496.

17. Wilson, J.N.; Ladefoged, L.K.; Babinchak, W.M.; Schiott, B. Binding-Induced Fluorescence of Serotonin Transporter Ligands: A Spectroscopic and Structural Study of 4-(4-(dimethylamino)phenyl)-1-methylpyridinium (APP^+) and APP^+ Analogues. *ACS Chem. Neurosci.* **2014**, 5, 296-304.

18. Chattopadhyay, A.; Rukmini, R.; Mukherjee, S. Photophysics of a Neurotransmitter: Ionization and Spectroscopic Properties of Serotonin. *Biophys. J.* **1996**, 71, 1952-1960.

19. Borstnar, R.; Repic, M.; Kamerlin, S.C.L.; Vianello, R.; Mavri, J. Computational Study of the pK_a values of Potential Catalytic Residues in the Active Site of Monoamine Oxidase B. *J. Chem. Theory Comput.* **2012**, 8, 3864-3870.

20. Armstrong, J.; Barlow, R.B. The Ionization of Phenolic Amines, Including Apomorphine, Dopamine, and Catecholamines and an Assessment of Zwitterion Constants. *Br. J. Pharmacol.* **1976**, 57, 501-516.

21. Haidekker, M.A.; Ling, T.; Anglo, M.; Stevens, H.Y.; Frangos, J.A.; Theodorakis, E.A. New Fluorescent Probes for the Measurement of Cell Membrane Viscosity. *Chem. Biol.* **2001**, 8, 123-131.

22. Klymchenko, A.S.; Kreder, R. Fluorscent Probes for Lipid Rafts: From Model Membranes to Living Cells. *Chem. Biol.* **2014**, 21, 97-113.

23. Tashyreva, D.; Elster, J.; Billi, D. A Novel Staining Protocol for Multiparameter Assessment of Cell Heterogeneity in *Phormidium* Populations (Cyanobacteria) Employing Fluorescent Dyes. *PLoS ONE* **2013**, 8, 1-12.

24. Resch-Genger, U.; Grabolie, M.; Cavaliere-Jaricot, S.; Nitschke, R.; Nann, T. Quantum Dots Versus Organic Dyes as Fluorescent Labels. *Nature Methods* **2008**, 5, 763-775.

25. Pansare, V.J.; Hejazi, S.; Faenza, W.J.; Prud'homme, R.K. Review of Long-Wavelength Optical and NIR Imaging Materials: Contrast Agents, Fluorophores, and Multifunctional Nanocarriers. *Chem. Mater.* **2012**, 24, 812-827.

26. Auger, A.; Samuel, J.; Poncelet, O.; Raccurt, O. A Comparative Study of Non-Covalent Encapsulation Methods for Organic Dyes into Silica Nanoparticles. *Nanoscale Res. Lett.* **2011**, 6, 328-340.

27. Wischke, C.; Schwendeman, S.P.; Principles of Encapsulating Hydrophobic Drugs in PLA/PLGA Microparticles. *Int. J. Pharm.* **2008**, 364, 298-327.

28. Ahmed, S.; Vepuri, S.B.; Kalhapure, R.S.; Govender, T. Interactions of Dendrimers with Biological Drug Targets: Reality or Mystery – A Gap in Drug Delivery and Development Research. *Biomater. Sci.*, **2016**, 4, 1032-1050.

29. Masutani, K.; Kimura, Y. Chapter 1. PLA Synthesis. From the Monomer to the Polymer. In *PLA Synthesis and Polymerization*, ed. 1; Jimenez, A.; Peltzer, M; Ruseckaite, R., Eds.; Royal Society of Chemistry, 2014, 12, 3-36.

30. Bader, R. A.; Silvers, A. L.; Zhang, N. Polysialic Acid-Based Micelles for Encapsulation of Hydrophobic Drugs. *Biomacromolecules*, **2011**, 12, 314-320.

31. Hecht, S. Functionalizing the Interior of Dendrimers: Synthetic Challenges and Applications. *J. Polym. Sci. Part A: Polym. Chem.* **2003**, 41, 1047-1058.

32. Tomalia, D.A.; Baker, H.; Dewald, J.; Hall, M.; Kallos, G.; Martin, S.; Roeck, J.; Ryder, J.; Smith, P. Dendritic Macromolecules: Synthesis of Starburst Dendrimers. *Macromolecules* **1986**, 19, 2466-2468.

33. Hawker, C.J.; Frechet, J.M.J. Preparation of Polymers with Controlled Molecular Architecture. A New Convergent Approach to Dendritic Macromolecules. *J. Am. Chem. Soc.* **1990**, 112, 7638-7647.

34. Lee, J.W.; Kim, J.H.; Kim, B.; Kim, J.H.; Shin, W.S.; Jin, S. Convergent Synthesis of PAMAM Dendrimers Using Click Chemistry of Azide-functionalized PAMAM Dendrons. *Tetrahedron* **2006**, 62, 9193-9200.

35. Laurichesse, S.; Avérous, L. Chemical Modifications of Lignin: Towards Biobased Polymers. *Prog. Polym. Sci.* **2014**, 39, 1266-1290.

36. Ten, E.; Vermerris, W. Recent Developments in Polymers Derived from Industrial Lignin *J. Appl. Polym. Sci.* **2015**, 132, 42069-42082.

37. Nguyen, J.D.; Matsuura, B.S.; Stephenson, C.R.J. A Photochemical Strategy for Lignin Degradation at Room Temperature *J. Am. Chem. Soc.* **2014**, 136, 1218-1221.

38. Deuss, P.J.; Scott, M.; Tran, F.; Westwood, N.J.; deVries, J.G.; Barta, K. Aromatic Monomers by in Situ Conversion of Reactive Intermediates in the Acid-Catalyzed Depolymerization of Lignin. *J. Am. Chem. Soc.* **2015**, 137, 7456-7467.

39. Brown, M.E.; Walker, M.C.; Nakashige, T.G.; Iavarone, A.T.; Chang, M.C.Y. Discovery and Characterization of Heme Enzymes rom Unsequenced Bacteria: Application to Microbial Lignin Degradation. *J. Am. Chem. Soc.* **2011**, 133, 18006-18009.

40. Rahimi, A.; Azarpira, A.; Kim, H.; Ralph, J.; Stahl, S.S. Chemoselective Metal-Free Aerobic Alcohol Oxidation in Lignin. *J. Am. Chem. Soc.* **2013**, 135, 6415-6418.

41. Thielemans, W.; Wool, R.P. Lignin Esters for Use in Unsaturated Thermosets: Lignin Modification and Solubility Modeling. *Biomacromolecules* **2005**, 6, 1895-1905.

42. Duval, A.; Lange, H.; Lawoko, M.; Crestini, C. Modification of Kraft Lignin to Expose Diazobenzene Groups: Towards pH- and Light-Responsive Biobased Polymers. *Biomacromolecules* **2015**, 16, 2979-2989.

43. Duval, A.; Lange, H.; Lawoko, M.; Crestini, C. Reversible Crosslinking of Lignin via the Furan-Maleimide Diels-Alder Reaction. *Green Chem.* **2015**, 17, 4991-5000.

44. Sadeghifar, H.; Cui, C.; Argyropoulos, D.S. Towards Thermoplastic Lignin Polymers. Part 1. Selective Masking of Phenolic Hydroxyl Groups in Kraft Lignin via Methylation and Oxypropylation Chemistries. *Ind. Eng. Chem. Res.* **2012**, 51, 16713-16720.

45. Ren, W.; Pan, X.; Wang, G.; Cheng, W.; Liu, Y. Dodecylated Lignin-g-PLA for Effective Toughening of PLA. *Green Chem.* **2016**, 18, 5008-5014.

46. Jiang, S.; Kai, D.; Dou, Q.; Loh, X.J. Multi-arm Carriers Composed of an Antioxidant Lignin Core and Poly(glycidyl methacrylate-co-poly(ethylene glycol)methacrylate) Derivative Arms for Highly Efficient Gene Delivery. *J. Mater. Chem. B* **2015**, 3, 6897-6904.

47. Kai, D.; Tan, M.J.; Chee, P.L.; Chua, Y.K.; Yap, Y.L.; Loh, X.J. Towards Lignin-based Functional Materials in a Sustainable World. *Green Chem.* **2016**, 18, 1175-1200.

48. Caicedo, H.M.; Dempere, L.A.; Vermerris, W. Template-Mediated Synthesis and Bio-Functionalization of Flexible Lignin-Based Nanotubes and Nanowires. *Nanotechnology* **2012**, 23, 105605-105617.

49. Nevarez, L.A.M.; Casarrubias, L.B.; Celzard, A.; Fierro, V.; Munoz, V.T.; Davila, A.C.; Lubian, J.R.T.; Sanchez, G.G. Biopolymer-Based Nanocomposites: Effect of Lignin Acetylation in Cellulose Triacetate Films. *Sci. Technol. Adv. Mater.* **2011**, 12, 045006-045022.

50. Zhao, Y. Surface-Cross-Linked Micelles as Multifunctionalized Organic Nanoparticles for Controlled Release, Light Harvesting, and Catalysis. *Langmuir* **2016**, 32, 5703-5713.

51. Sarkanen, S.; Teller, D.C.; Hall, J.; McCarthy, J.L. Lignin. 18. Associative Effects Among Organosolv Lignin Components. *Macromolecules* **1981**, 14, 426-434.

52. Sarkanen, S.; Teller, D.C.; Abramowski, E.; McCarthy, J.L. Lignin. 19. Kraft Lignin Component Conformation and Associated Complex Configuration in Aqueous Alkaline Solution. *Macromolecules* **1982**, 15, 1098-1104.

53. Sarkanen, S.; Teller, D.C.; Stevens, C.R.; McCarthy, J.L. Lignin. 20. Associative Interactions Between Kraft Lignin Components. *Macromolecules* **1984**, 17, 2588-2597.

54. Hong, N.; Li, Y.; Zeng, W.; Zhang, M.; Peng, X.; Qiu, X. Ultrahigh Molecular Weight, Lignosulfonate-Based Polymers: Preparation, Self-Assembly Behaviors and Dispersion Properties in Coal-Water Slurry. *RSC Adv.* **2015**, 5, 21588-21595.

55. Finkelstein, H. Darstellung Organischer Jodide aus den Entsprechenden Bromiden und Chloriden. *Ber. Dtsch. Chem. Ges.* **1910**, 43, 1528-1532.

56. Cauley, A.N.; Wilson, J.N. Functionalized Lignin Biomaterials for Enhancing Optical Properties and Cellular Interactions of Dyes. *Biomater. Sci.* **2017**, 5, 2114-2121.

57. Tortora, M.; Cavalieri, F.; Mosesso, P.; Ciaffardini, F.; Melone, F.; Crestini, C. Ultrasound Driven Assembly of Lignin into Microcapsules for Storage and Delivery of Hydrophobic Molecules. *Biomacromolecules* **2014**, 15, 1634-1643.

58. Yiamsawas, D.; Baier, G.; Thines, E.; Landfester, K.; Wurm, F.R. Biodegradable Lignin Nanocontainers. *RSC Adv.*, **2014**, 4, 11661-11663.

59. Randolph, J.B.; Waggoner, A.S. Stability, Specificity and Fluorescence Brightness of Multiply-Labeled Fluorescent DNA Probes. *Nucleic Acids Res.* **1997**, 25, 2923-2929.

60. Panchuk-Voloshina, N.; Haugland, R.P.; Bishop-Stewart, J.; Bhalgat, M.K.; Millard, P.J.; Mao, F.; Leung, W.; Haugland, R.P. *J.* Alexa Dyes, a Series of New Fluorescent Dyes that Yield Exceptionally Bright, Photostable Conjugates. *J. Histochem. Cytochem.* **1999**, 47, 1179-1188.

61. Berlier, J.E.; Rothe, A.; Buller, G.; Bradford, J.; Gray, D.R.; Filanoski, B.J.; Telford, W.G.; Yue, S.; Liu, J.; Cheung, C.; Chang, W.; Hirsch, J.D.; Beechem, J.M.; Haugland, R.P. Quantitative Comparison of Long-wavelength Alexa Fluor Dyes to Cy Dyes: Fluorescence of the Dyes and Their Bioconjugates. *J. Histochem. Cytochem.* **2003**, 51, 1699-1712.

62. Berlepsch, H.; Bottcher, C. H-Aggregates of an Indocyanine Cy5 Dye: Transition from Strong to Weak Molecular Coupling. *J. Phys. Chem. B* **2015**, 119, 11900-11909.

63. Eggeling, C.; Widengren, J.; Brand, L.; Schaffer, J.; Felekyan, S.; Seidel, C.A.M. Analysis of Photobleaching in Single-Molecule Multicolor Excitation and Forster Resonance Energy Transfer Measurements. *J. Phys. Chem. A* **2006**, 110, 2979-2995.

64. van Hal, N.L.W.; Vorst, O.; van Houwelingen, A.M.M.L.; Kok, E.J.; Peijnenburg, A.; Aharoni, A.; van Tunen, A.J.; Keijer, J. The Application of DNA Microarrays in Gene Expression Analysis. *J. Biotechnol.* **2000**, 78, 271-280.

65. Pitter, D. R. G.; Wigenius, J.; Brown, A. S.; Baker, J. D.; Westerlund, F.; Wilson, J. N. Turn-on, Fluorescent Nuclear Stains with Live Cell Compatibility. *Org. Lett.* **2013**, *15*, 1330-1333.

66. Ryan, J.A. Evolution of Cell Culture Surfaces. *BioFiles*. **2008**, 3.8, 21-27.

67. Faucheux, N.; Schweiss, R.; Lutzow, K.; Werner, C.; Groth, T. Self-assembled Monolayers with Different Terminating Groups as Model Substrates for Cell Adhesion Studies. *Biomaterials*. **2004**, 25, 2721-2730.

68. Arima, Y.; Iwata, H. Effect of Wettability and Surface Functional Groups on Protein Adsorption and Cell Adhesion Using Well-defined Mixed Self-assembled Monolayers. *Biomaterials*. **2007**, 28, 3074-3082.

69. Barbosa, J.N.; Barbosa, M.A.; Aguas, A.P. Adhesion of Human Leukocytes to Biomaterials: An in vitro Study Using Alkanethiolate Monolayers with Different Chemically Functionalized Surfaces. *J Biomed Mater Res A*. **2003**, 65A,429-434.

70. Tidwell, C.D.; Ertel, S.I.; Ratner, B.D. Endothelial Cell Growth and Protein Adsorption on Terminally Functionalized, Self-Assembled Monolayers of Alkanethiolates on Gold. *Langmuir*. **1997**, 13, 3404-3413.

71. Oyman, G.; Geyik, C.; Ayranci, R.; Ak, M.; Demirikol, D.O.; Timur, S.; Coskunol, H. Peptide-modified Conducting Polymer as a Biofunctional Surface: Monitoring of Cell Adhesion and Proliferation. *RSC Adv.* **2014**, 4, 53411-53418.

72. Bhattacharyya, D.; Xu, H.; Deshmukh, R.R.; Timmons, R.B.; Nguyen, K.T. Surface Chemistry and Polymer Film Thickness Effects on Endothelial Cell Adhesion and Proliferation. *J Biomed Mater Res A*. **2010**, 94A, 640-648.

73. Baughman, G.L.; Weber, E.J.; Estimation of Water Solubility and Octanol/Water Partition Coefficient of Hydrophobic Dyes. Part I: Relationship Bewteen Solubility and Partition Coefficient. *Dyes Pigm.* **1991**, 16, 261-271.

74. Hughes, L.D.; Rawle, R.J.; Boxer, S.G. Choose Tour Label Wisely: Water-Soluble Fluorophores Often Interact with Lipid Bilayers. *PloS ONE* **2014**, 9, 87649-87657.

75. Swaminathan, S.; Garcia-Amoros, J.; Fraix, A.; Kandoth, N.; Sortino, S.; Raymo, F.M. Photoresponsive Polymer Nanocarriers with Multifunctional Cargo. *Chem. Soc. Rev.* **2014**, 43, 4167-4178.

76. Swaminathan, S.; Fowley, C.; McCaughan, B.; Cusido, J.; Callan, J.F.; Raymo, F.M. Intracellular Guest Exchange Between Dynamic Supramoleculat Hosts. *J. Am. Chem. Soc.* **2014**, 136, 7907-7913.

77. Chen, H.; Kim, S.; Li, L.; Wang, S.; Park, K.; Cheng, J. Release of Hydrophobic Molecules from Polymer Micelles into Cell Membranes Revealed by Forster Resonance Energy Transfer Imaging. *PNAS* **2008**, 105, 6596-6601.

78. Nicolas, J. Drug-Initiated Synthesis of Polymer Prodrugs: Combining Simplicity and Efficacy in Drug Delivery. *Chem. Mater.* **2016**, 28, 1591-1606.

79. Ren, W.X.; Han, J.; Uhm, S.; Jang, Y.J.; Kang, C.; Kim, J.; Kim, J.S. Recent Developments of Biotin Conjugation in Biological Imaging, Sensing, and Target Delivery. *Chem. Commun.* **2015**, 51, 10403-10418.

80. Han, Y.; Yuan, L.; Li, G.; Huang, L.; Qin, T.; Chu, F.; Tang, C. Renewable Polymers from Lignin via Copper-free Thermal Click Chemsitry. *Polymer* **2015**, 83, 92-100.

81. Liu, H.; Chung, H. Self-Healing Properties of Lignin-Containing Nanocomposite: Synthesis of Lignin-graft-poly(5-acetylaminopentyl acrylate) via RAFT and Click Chemistry. *Macromolecules* **2016**, 49, 7246-7256.

SUPPORTING INFORMATION

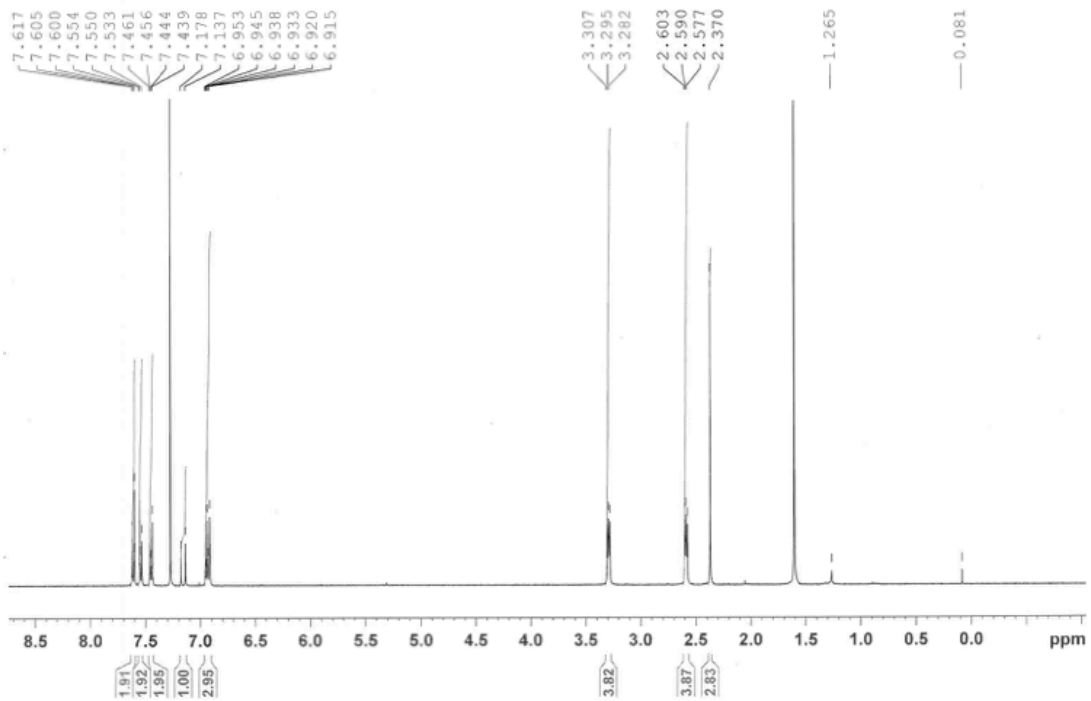

Figure S1. ^{1}H-NMR of **1**

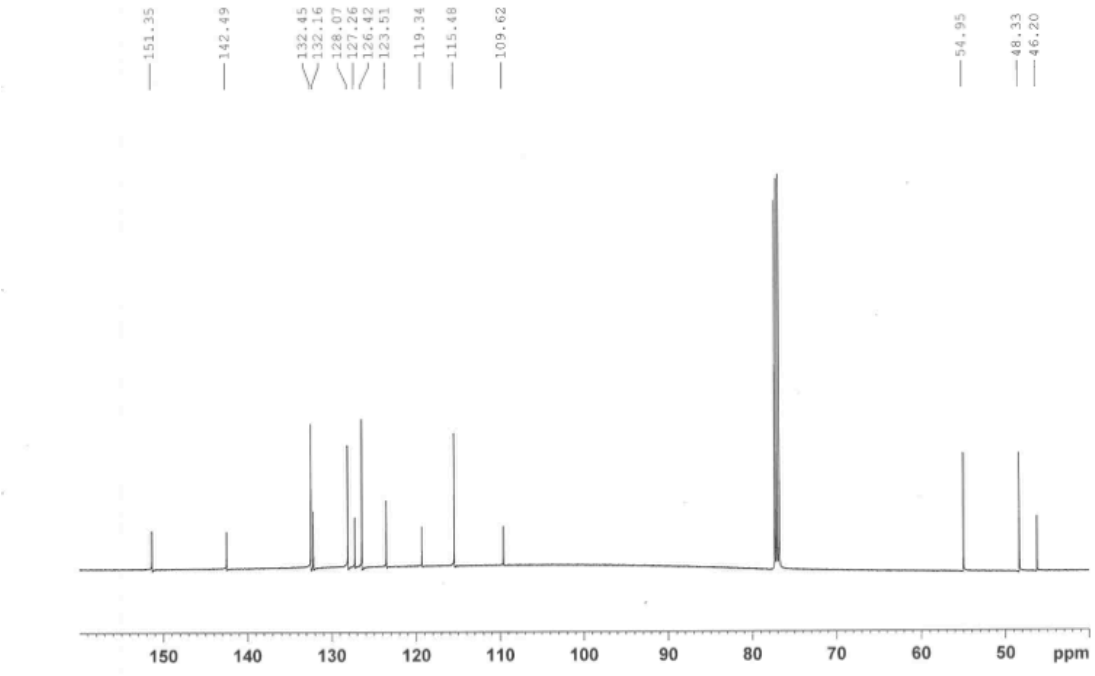

Figure S2. ^{13}C-NMR of **1**

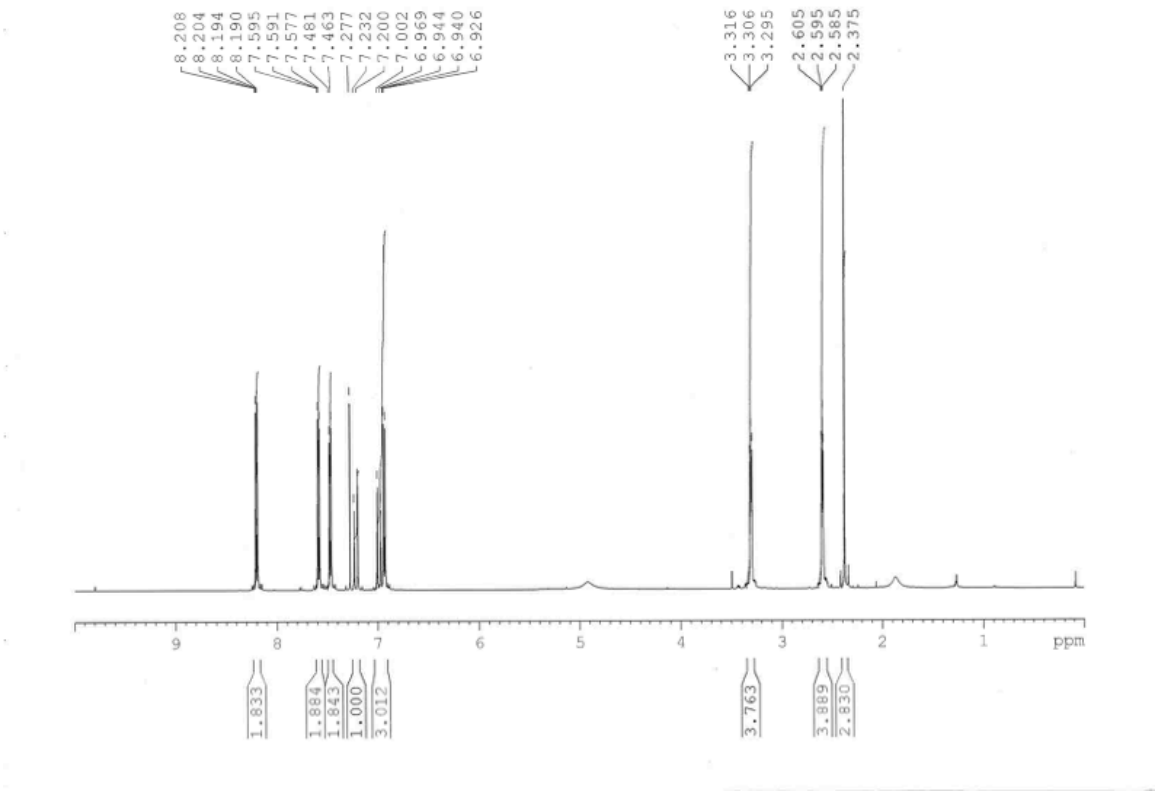

Figure S3. ^{1}H-NMR of **2**

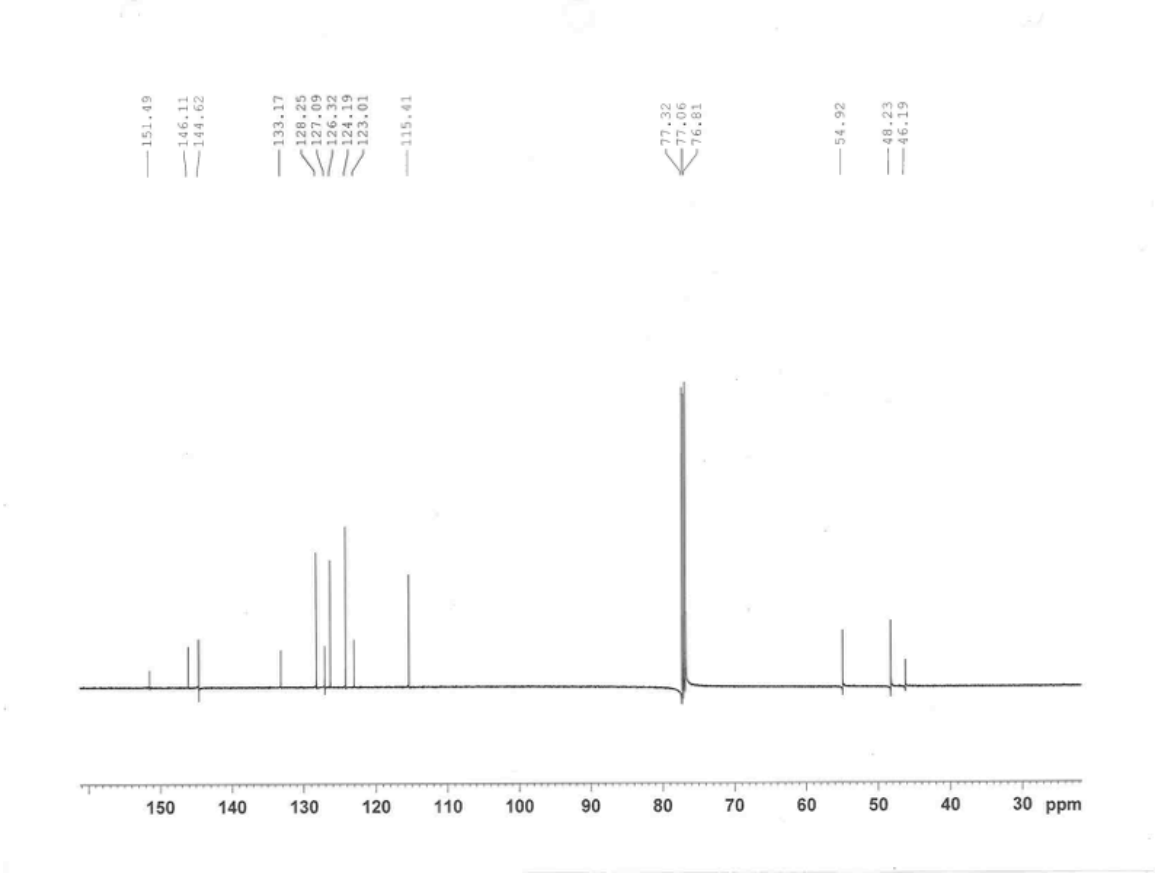

Figure S4. ^{13}C-NMR of **2**

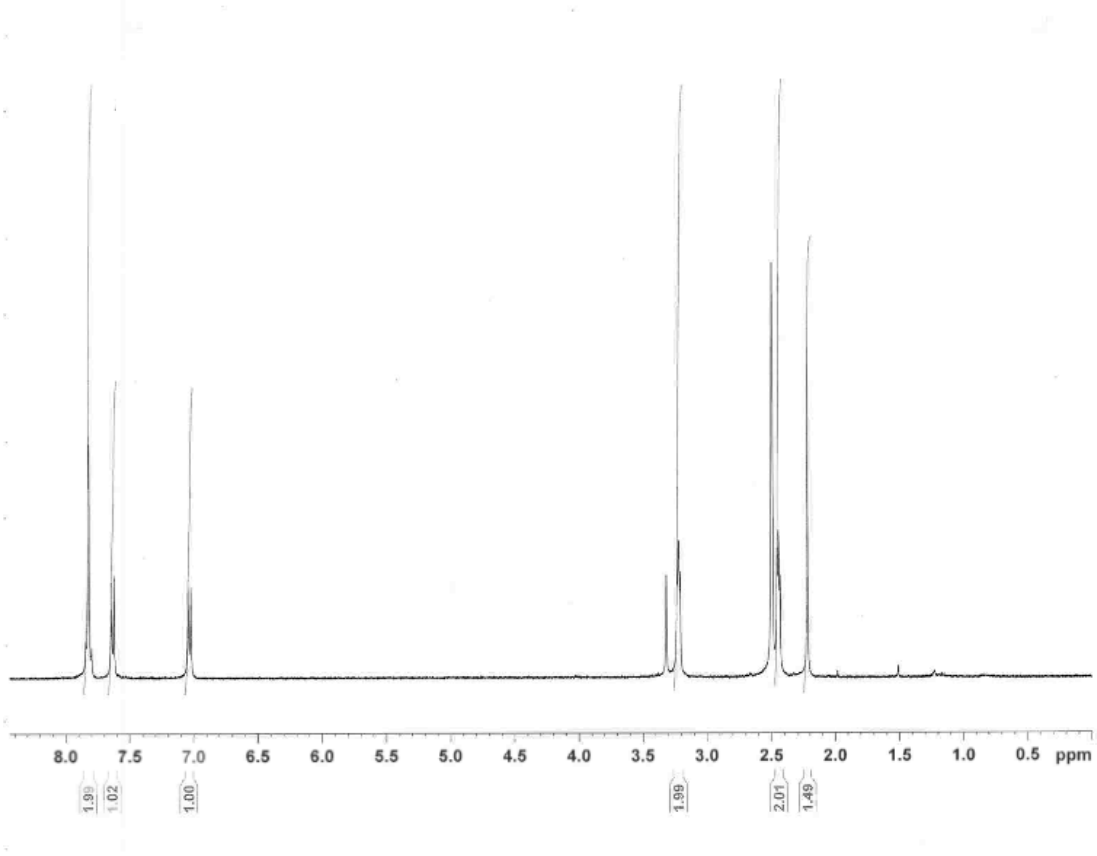

Figure S5. ^{1}H-NMR of **3**

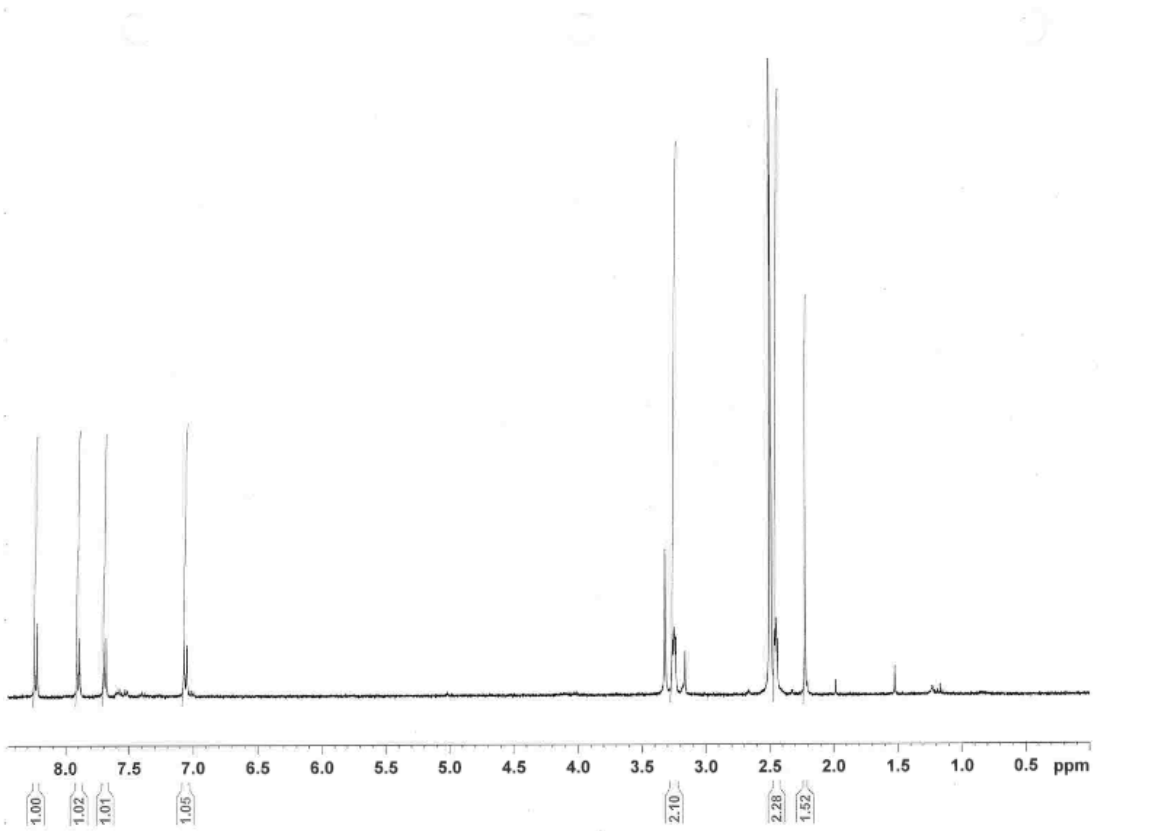

Figure S6. ^{1}H-NMR of **4**

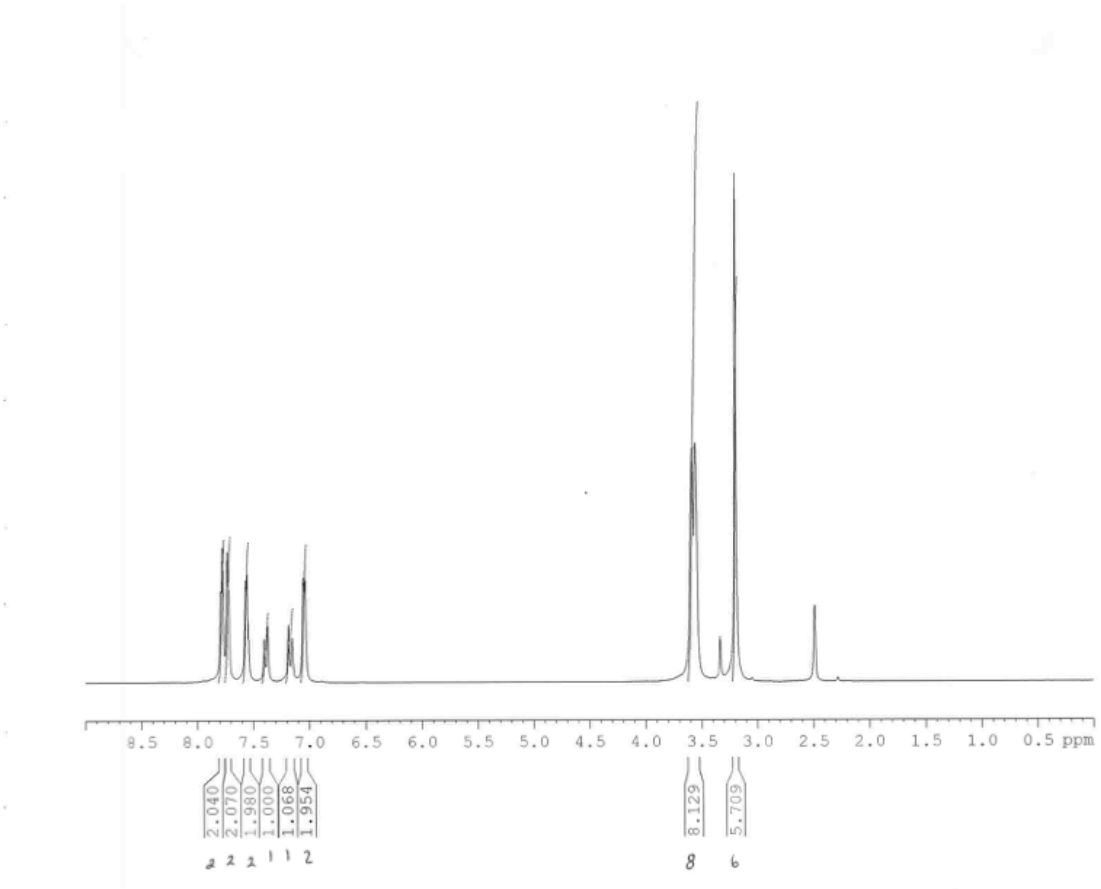

Figure S7. ^{1}H-NMR of **1m**

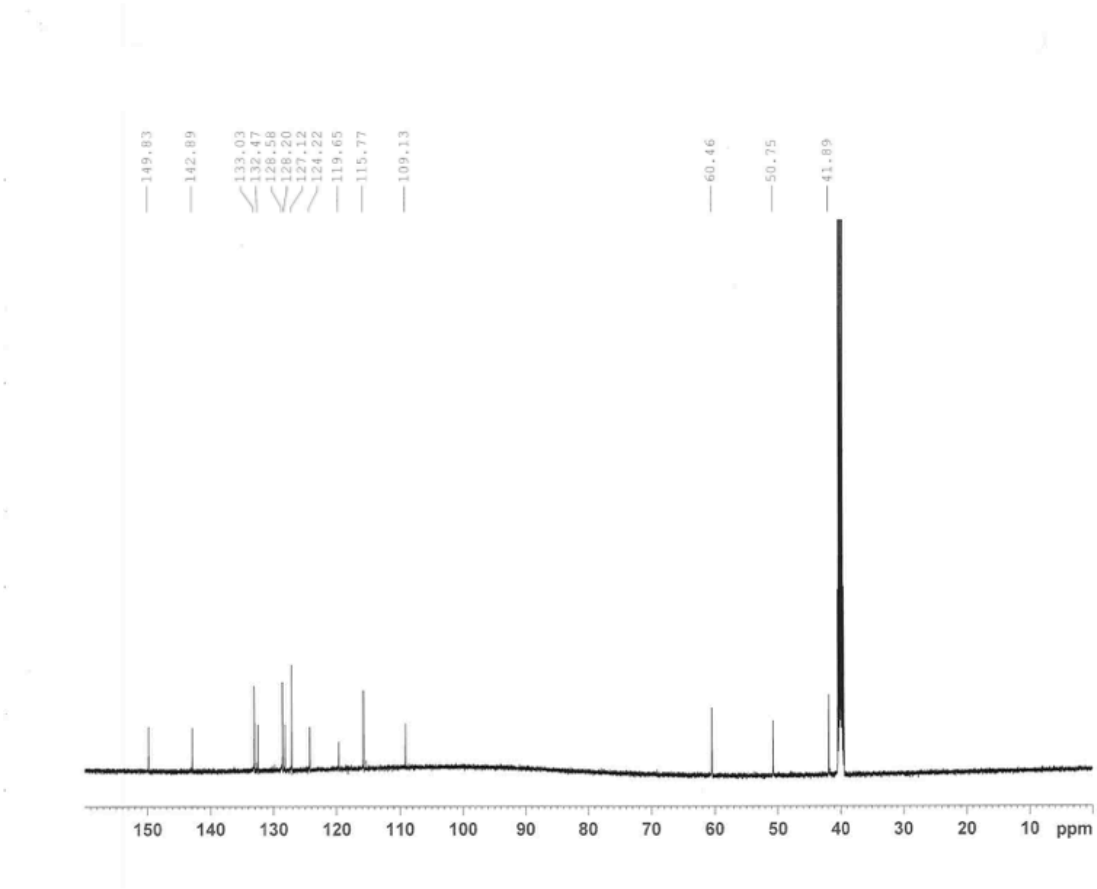

Figure S8. ^{13}C-NMR of **1m**

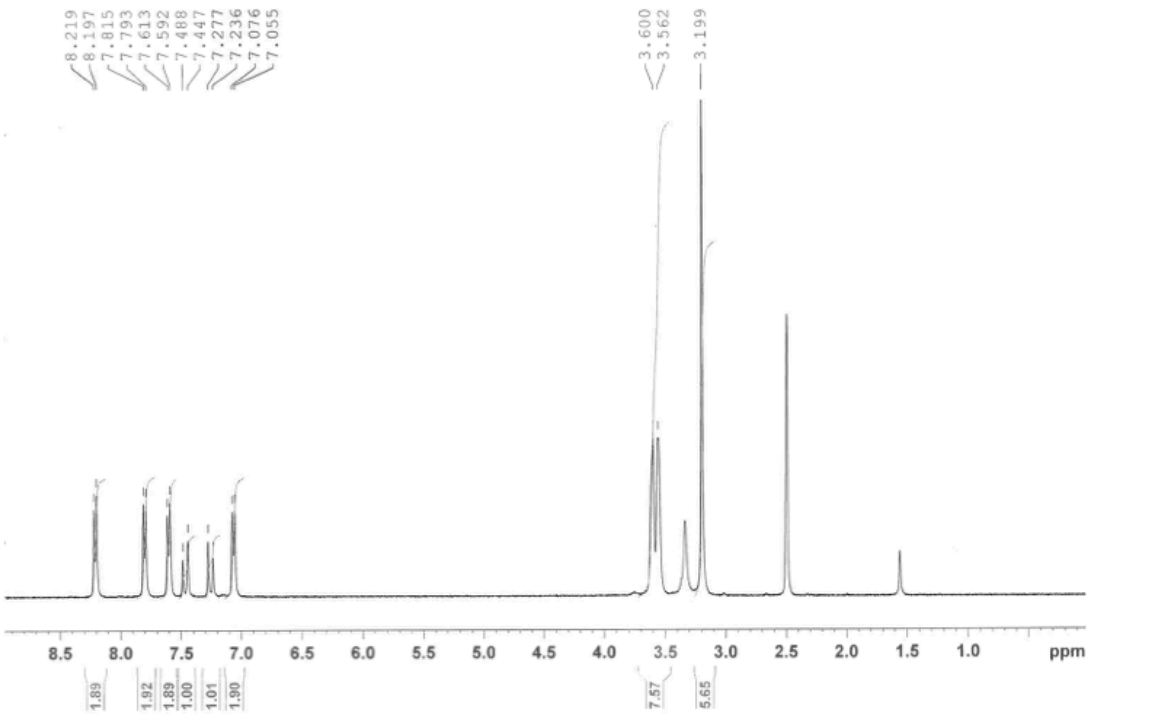

Figure S9. ^{1}H-NMR of **2m**

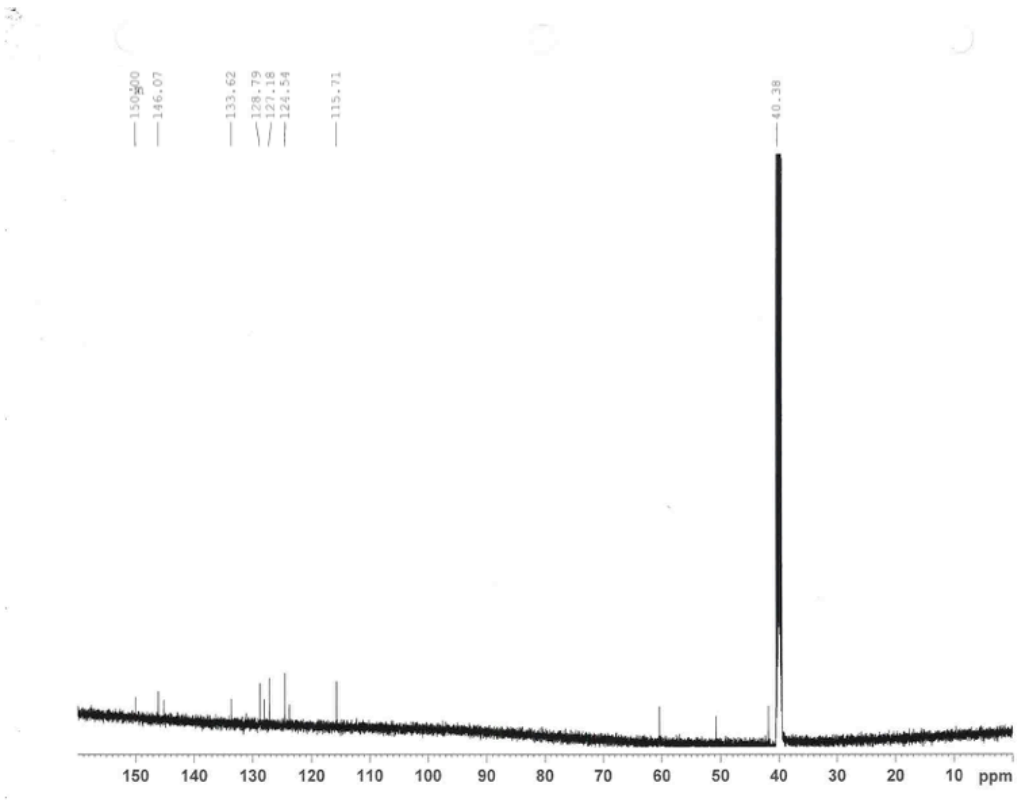

Figure S10. ^{13}C-NMR of **2m**

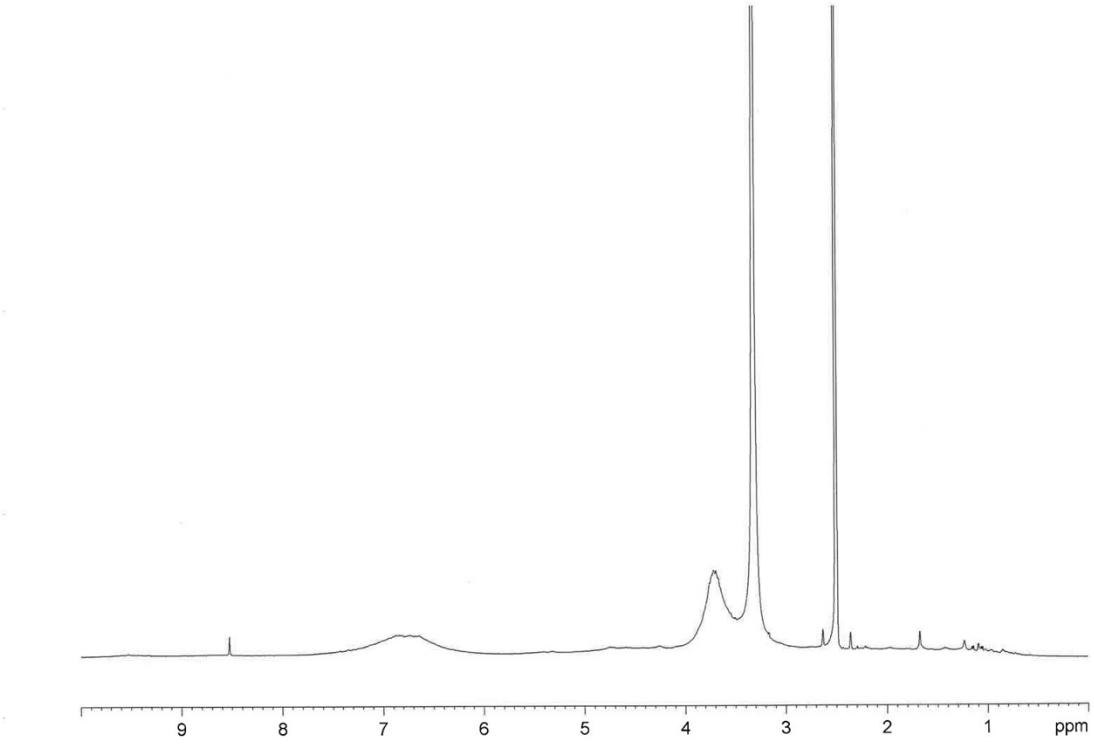

Figure S11. ^{1}H-NMR of lignin

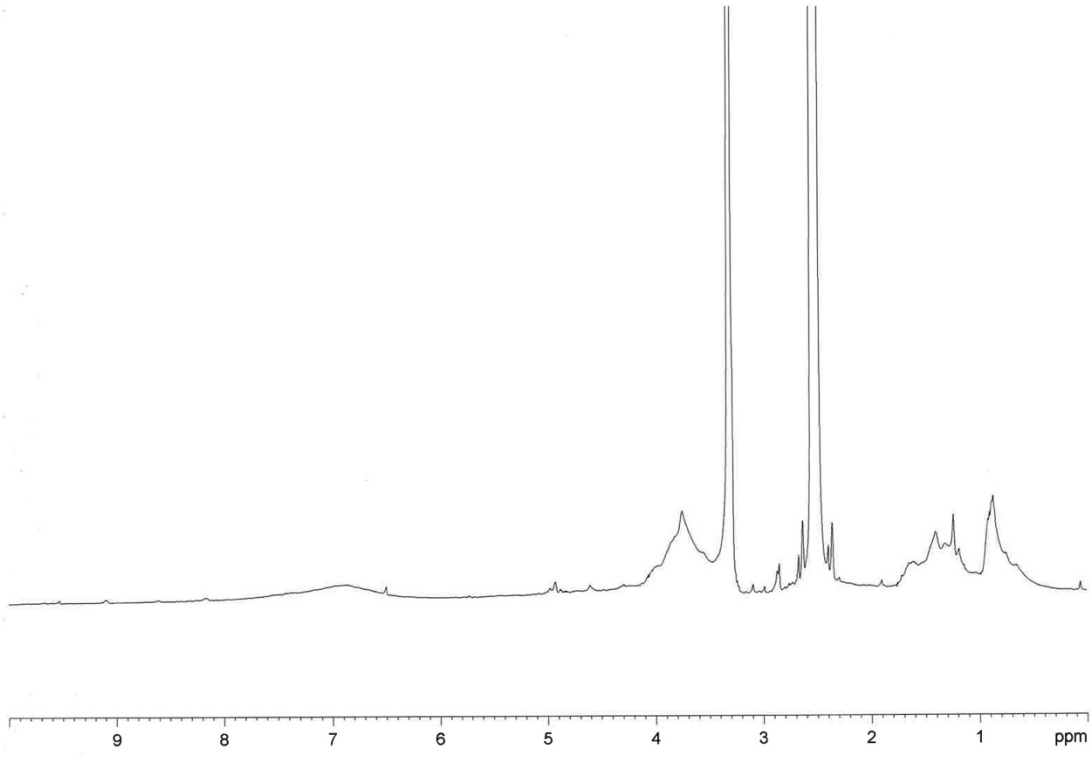

Figure S12. ^{1}H-NMR of L-Bu

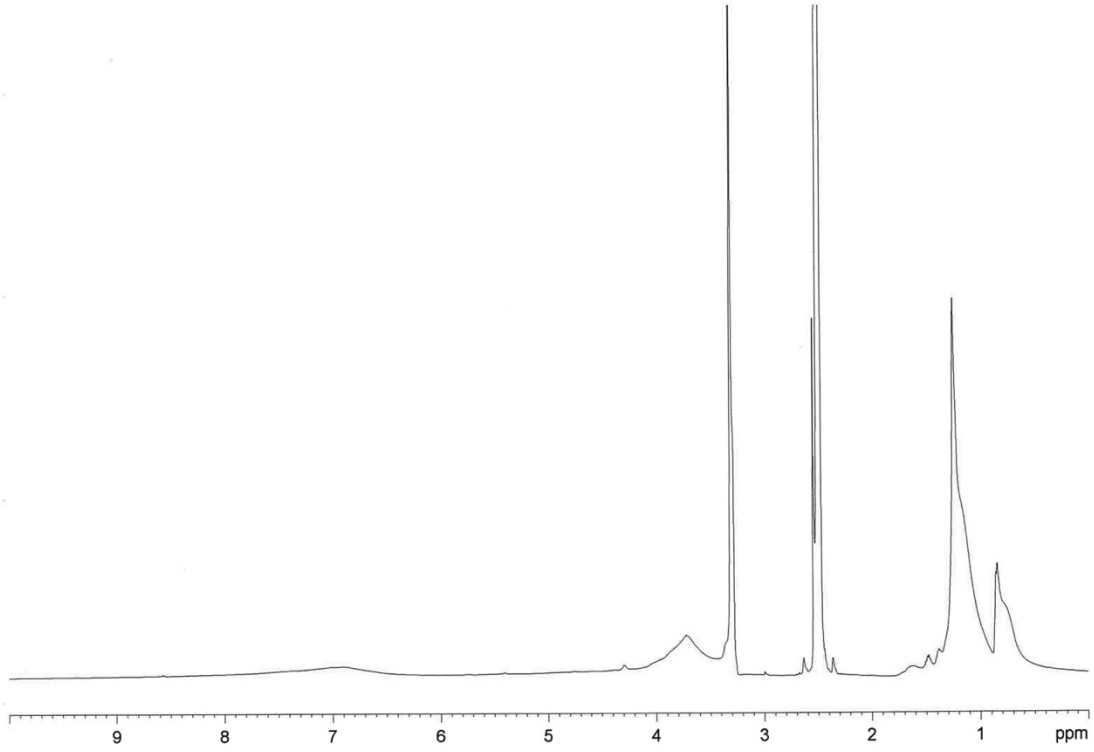

Figure S13. ^{1}H-NMR of L-Dec

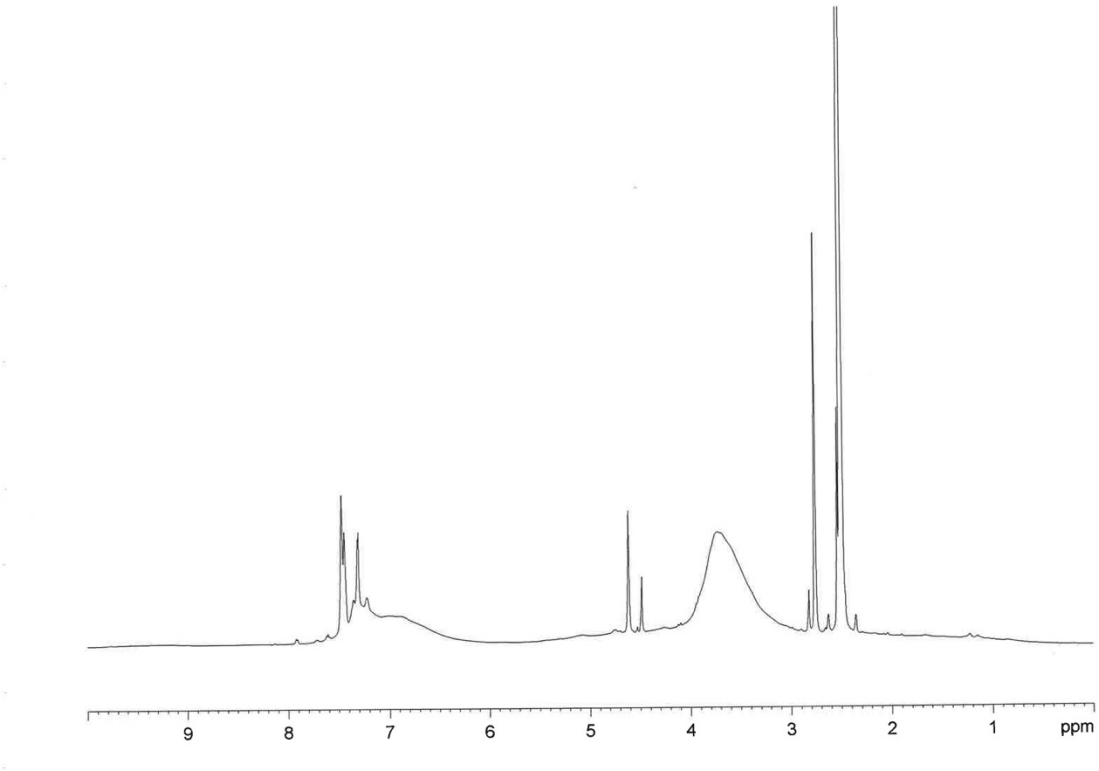

Figure S14. ^{1}H-NMR of L-Bn

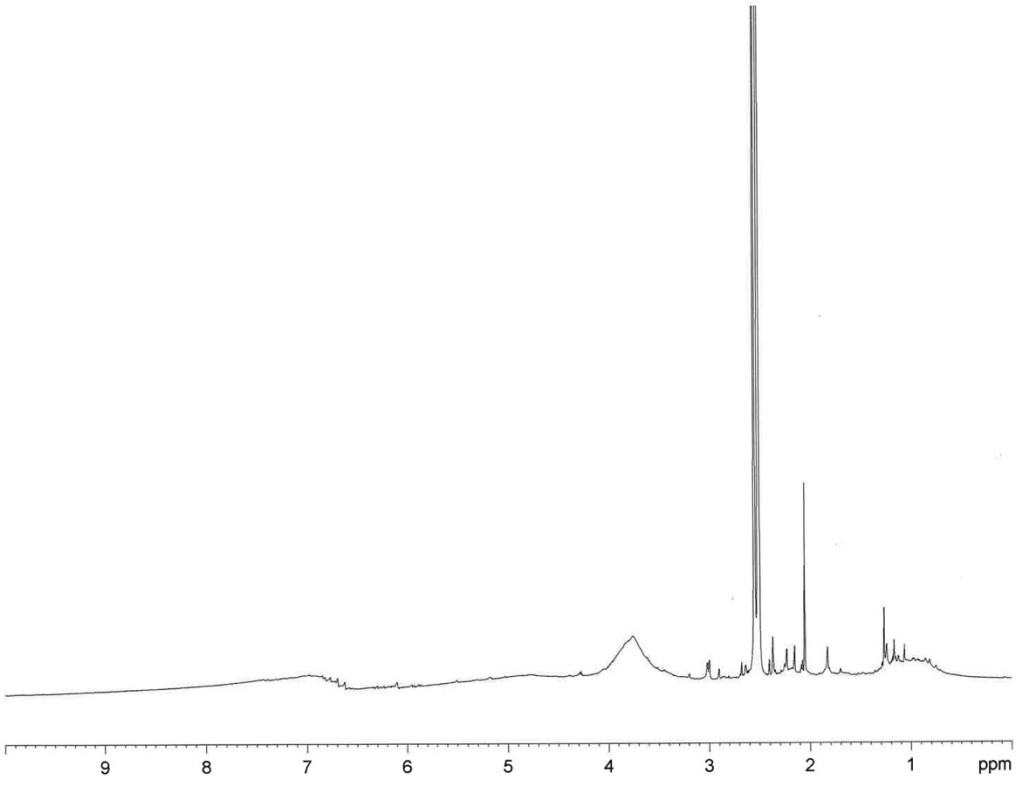

Figure S15. ^{1}H-NMR of L-PA

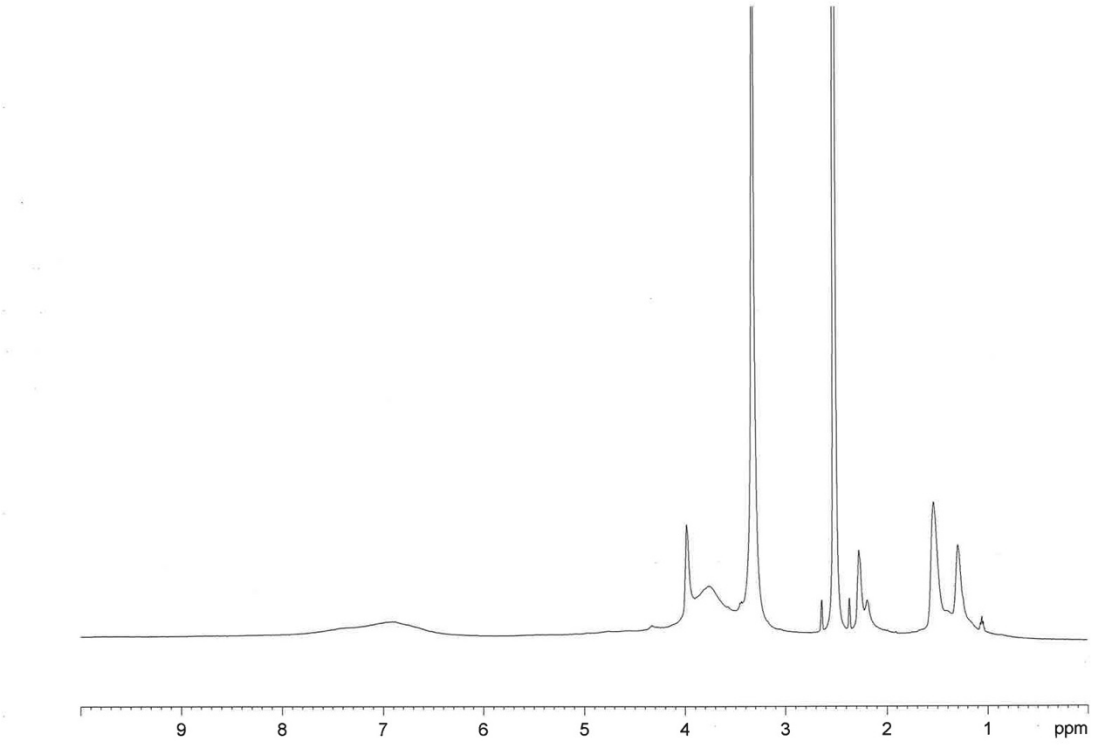

Figure S16. ^{1}H-NMR of L-HA

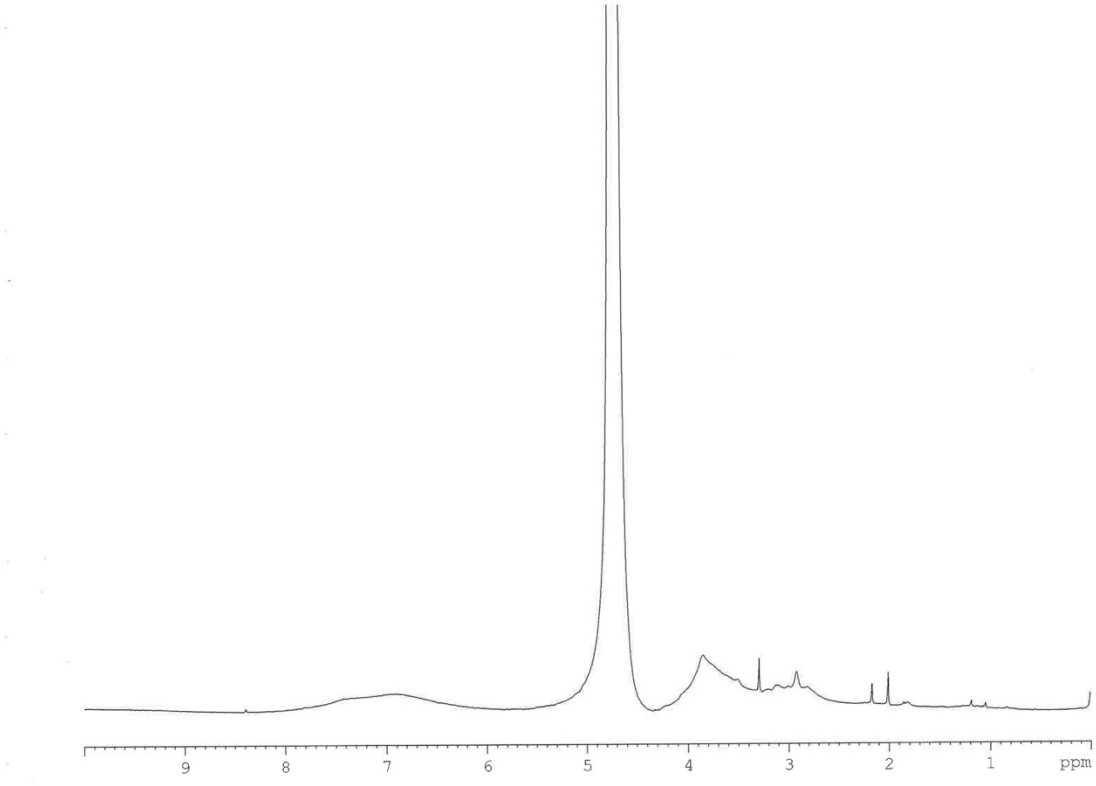

Figure S17. ^{1}H-NMR of L-PTMA

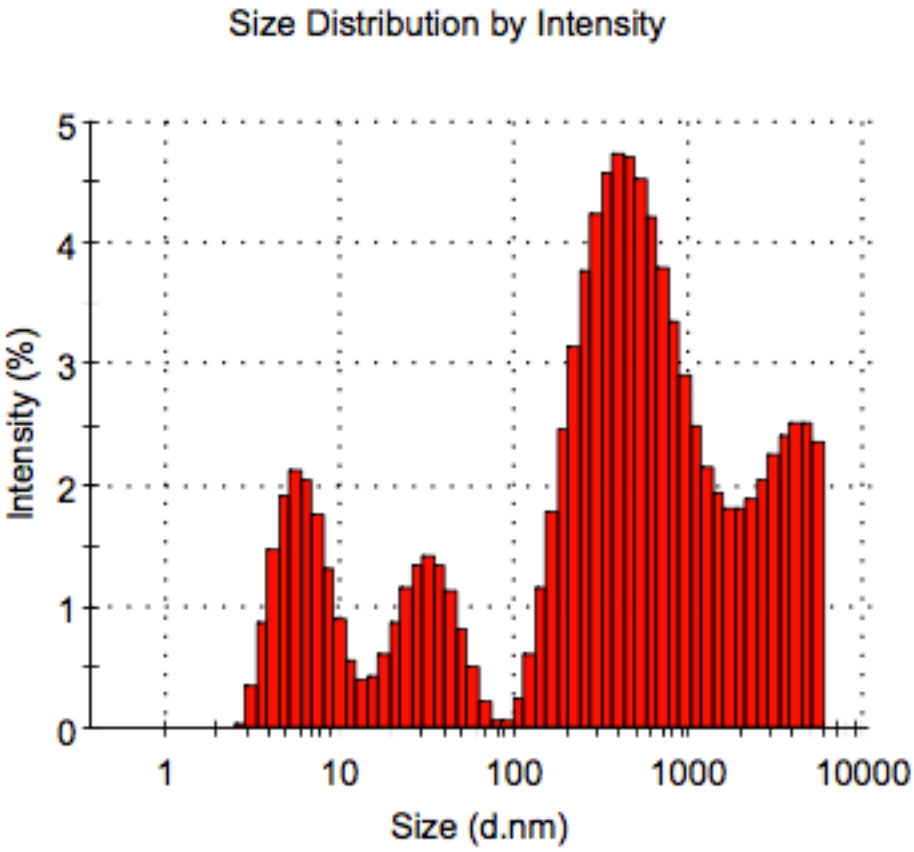

Figure S18. DLS Histogram of lignin

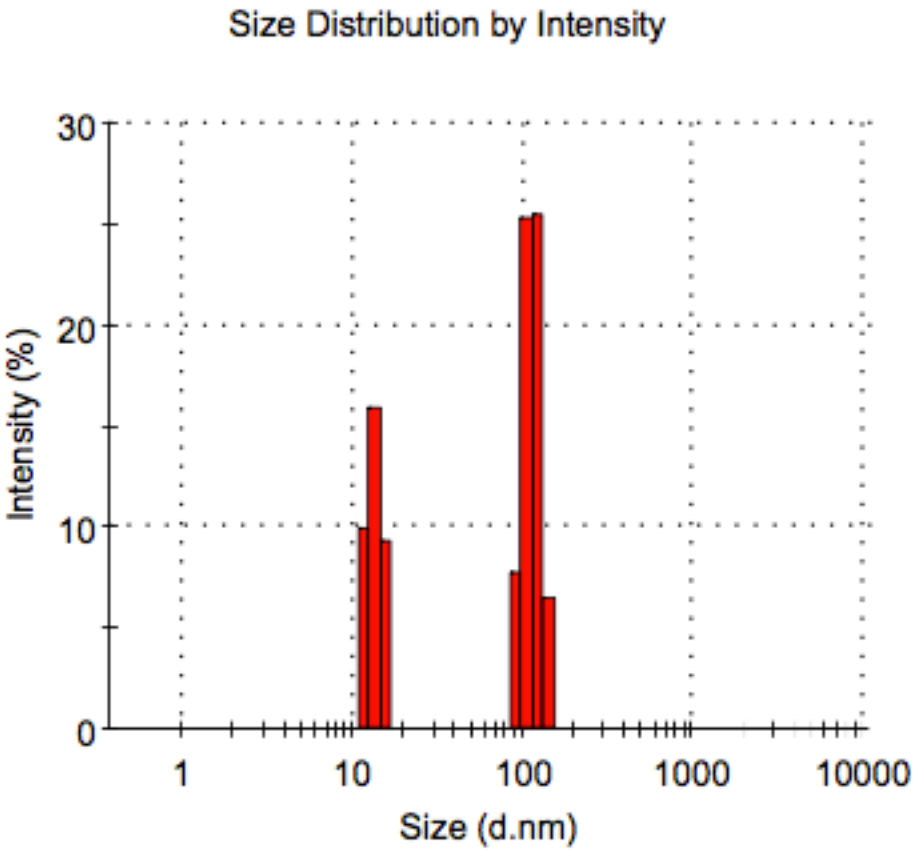

Figure S19. DLS Histogram of L-Bu

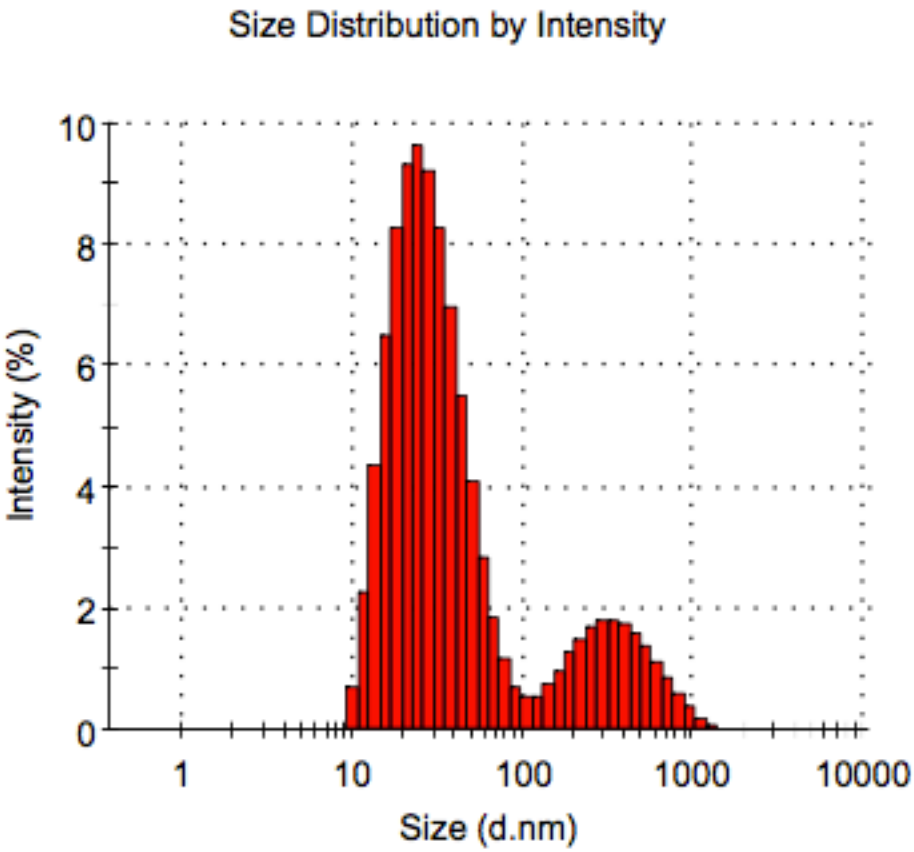

Figure S20. DLS Histogram of L-Dec

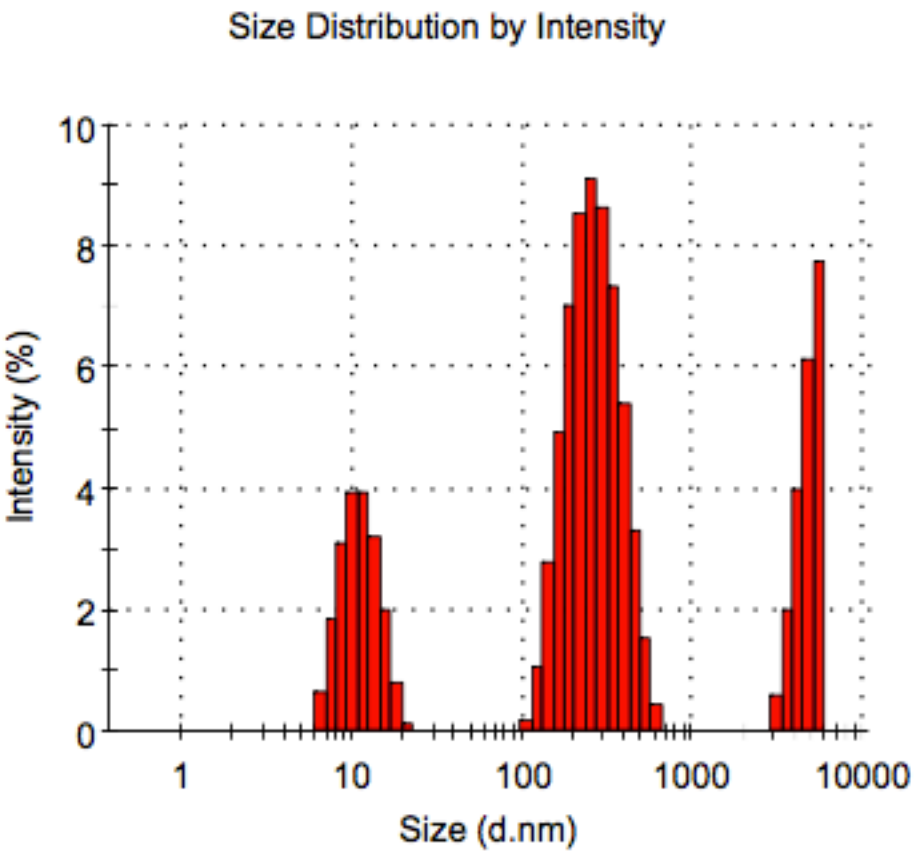

Figure S21. DLS Histogram of L-Bn

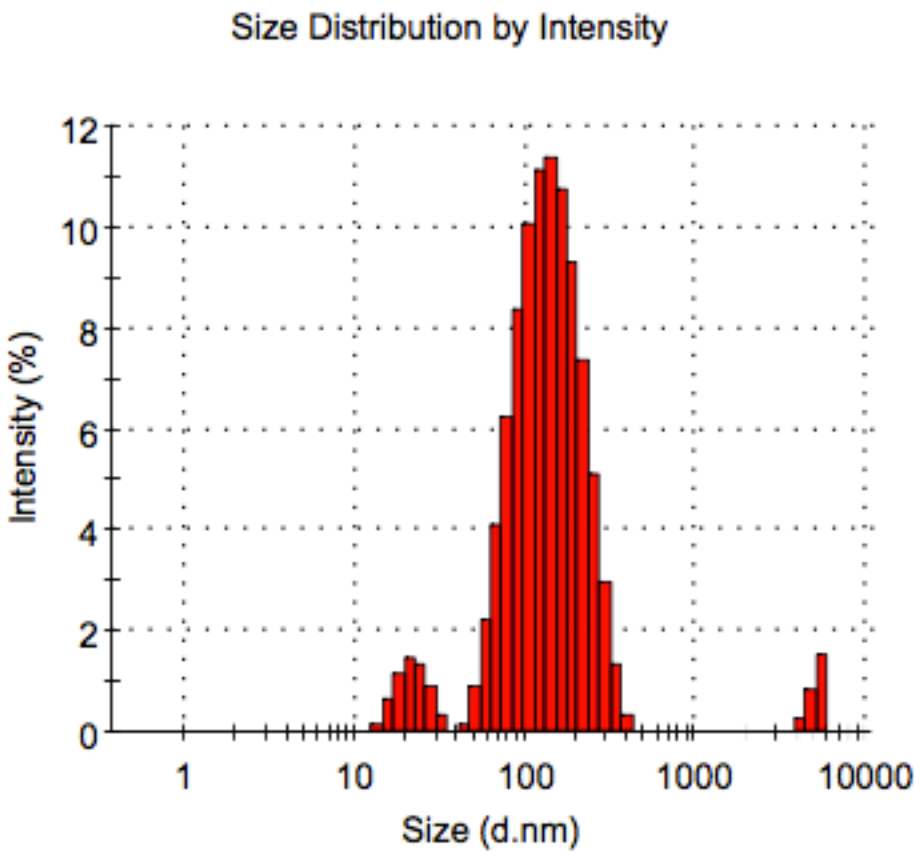

Figure S22. DLS Histogram of L-PA

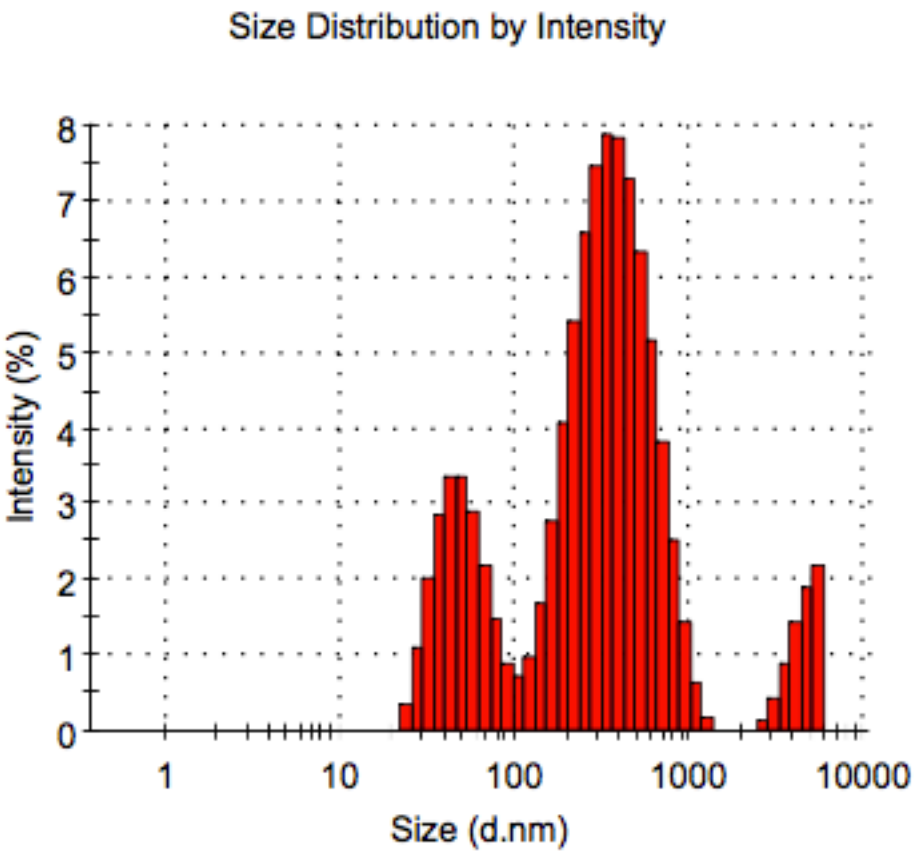

Figure S23. DLS Histogram of L-HA

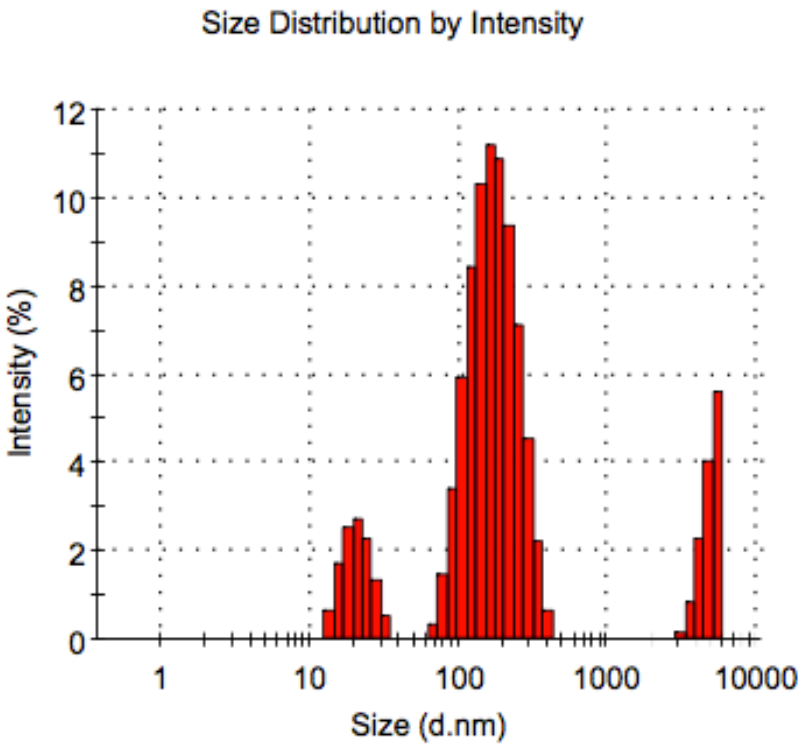

Figure S24. DLS Histogram of L-PTMA

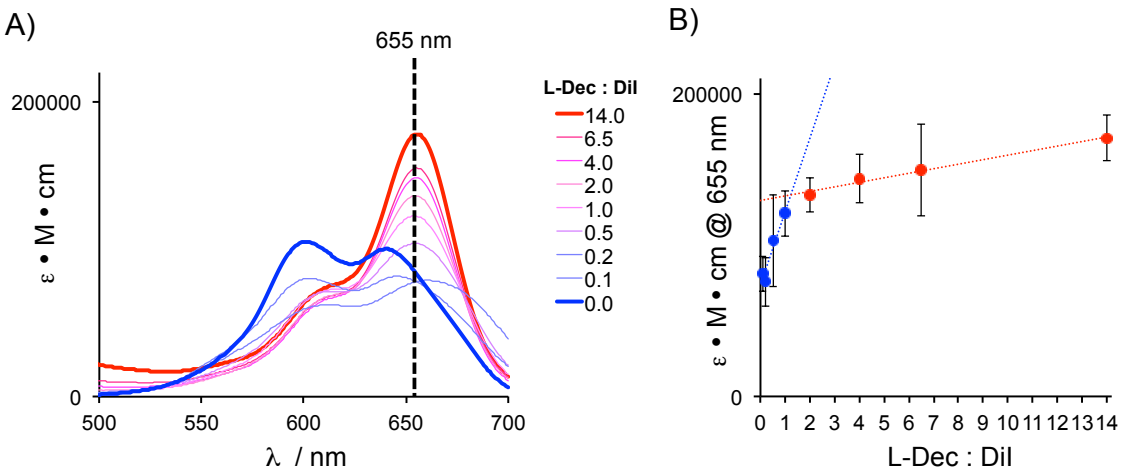

Figure S25. UV-vis analysis of L-Dec:DiI binding ratios. A) At low L-Dec (i.e. high DiI) concentrations, pronounced hypochromicity is observed as the dyes electronically couple. B) This is clearly seen in the analysis of the λ_{max} at 655 nm, as below a 1:1 ratio, i.e. lower L-Dec concentrations, there is a marked drop-off in ε (blue data points). Optimal dye loading is therefore kept at one dye molecule per lignin macromolecule, although these may be assembled into larger structures containing more dyes as seen in SEM images.

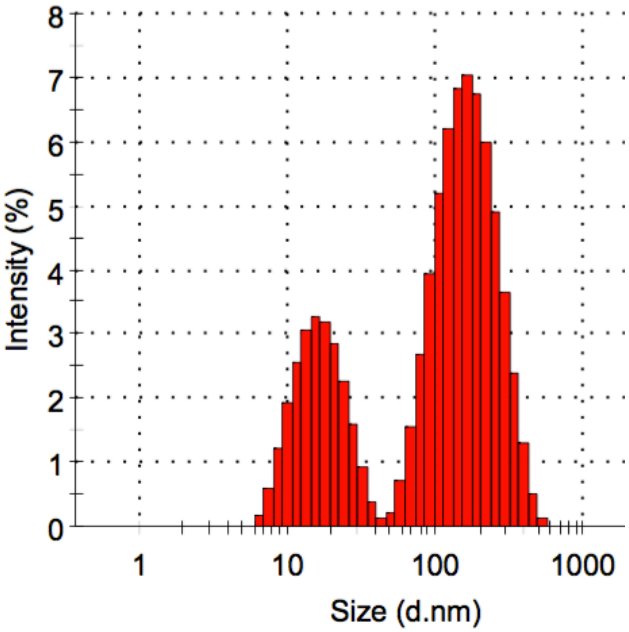

Figure S26. DLS Histogram of propargyl lignin

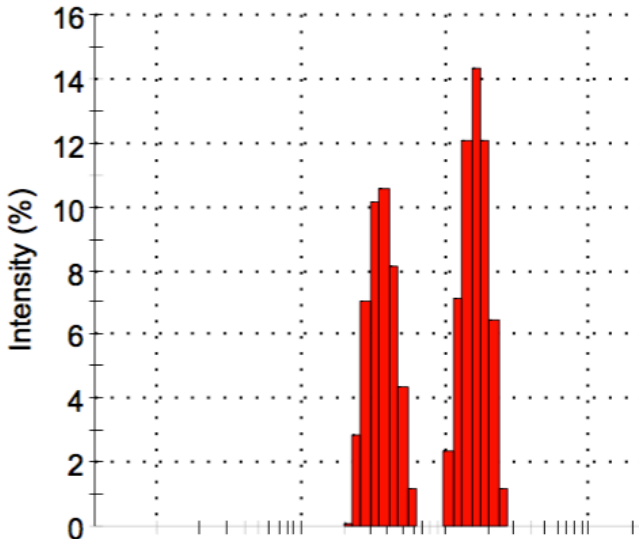

Figure S27. DLS Histogram of azido-PEG3-amine click product